UNIVERSIDADE FEDERAL DE SANTA CATARINA

DEPARTAMENTO DE ENGENHARIA ELÉTRICA

PROGRAMA DE PÓS-GRADUAÇÃO EM ENGENHARIA ELÉTRICA

Dimas Irion Alves

Change Detection Methods for Wavelength-Resolution SAR Images

Florianópolis, 17 de Abril de 2020.

DIMAS IRION ALVES

CHANGE DETECTION METHODS FOR WAVELENGTH-RESOLUTION SAR IMAGES

Tese submetida à Universidade Federal de Santa Catarina como parte dos requisitos para a obtenção do grau de Doutor em Engenharia Elétrica.

Orientador: Bartolomeu Ferreira Uchôa Filho

Coorientador: Renato Machado

FLORIANÓPOLIS

2020

Ficha de identificação da obra elaborada pelo autor,
através do Programa de Geração Automática da Biblioteca Universitária da UFSC.

Alves, Dimas Irion
Change Detection Methods for Wavelength-Resolution SAR Images / Dimas Irion Alves ; orientador, Bartolomeu Ferreira Uchôa-Filho, coorientador, Renato Machado, 2020.
117 p.

Tese (doutorado) - Universidade Federal de Santa Catarina, Centro Tecnológico, Programa de Pós-Graduação em Engenharia Elétrica, Florianópolis, 2020.

Inclui referências.

1. Engenharia Elétrica. 2. Change Detection Methods. 3. Wavelength-Resolution SAR images. 4. Image Stacks. 5. Bayes' Theorem. I. Uchôa-Filho, Bartolomeu Ferreira. II. Machado, Renato. III. Universidade Federal de Santa Catarina. Programa de Pós-Graduação em Engenharia Elétrica. IV. Título.

Dimas Irion Alves

CHANGE DETECTION METHODS FOR WAVELENGTH-RESOLUTION SAR IMAGES

O presente trabalho em nível de doutorado foi avaliado e aprovado pela banca examinadora composta pelos seguintes membros:

Prof. Renato Machado, Dr.

Instituto Tecnológico de Aeronáutica

Prof. Felix Dieter Antreich, Dr.

Instituto Tecnológico de Aeronáutica

Prof. Mats I. Pettersson, Dr.

Blekinge Institute of Technology

Prof. Natanael Rodrigues Gomes, Dr.

Universidade Federal de Santa Maria

Certificamos que esta é a **versão original e final** da tese de doutorado que foi julgada adequada para obtenção do título de Doutor em Engenharia Elétrica.

Bartolomeu Ferreira Uchoa Filho:47636211491
Assinado de forma digital por Bartolomeu Ferreira Uchoa Filho:47636211491
Dados: 2020.05.19 10:47:29 -03'00'

Bartolomeu Ferreira Uchôa Filho, Dr.

Coordenador do Programa de Pós-Graduação em Engenharia Elétrica

Universidade Federal de Santa Catarina

Bartolomeu Ferreira Uchoa Filho:47636211491
Assinado de forma digital por Bartolomeu Ferreira Uchoa Filho:47636211491
Dados: 2020.05.18 16:32:25 -03'00'

Orientador: Prof. Bartolomeu Ferreira Uchôa Filho, Dr.

Universidade Federal de Santa Catarina

Renato Machado: SIAPE 1492370
Assinado de forma digital por Renato Machado: SIAPE 1492370
DN: cn=Renato Machado: SIAPE 1492370, o=Instituto Tecnológico de Aeronáutica, ou=ITA, email=rmachado@ita.br, c=BR
Dados: 2020.05.18 16:42:17 -03'00'

Coorientador: Prof. Renato Machado, Dr.

Instituto Tecnológico de Aeronáutica

Florianópolis, 17 de Abril de 2020.

Para minha mãe,

Maria do Carmo Oliveira Irion.

Agradecimentos

Gostaria de agradecer a todos que contribuíram de alguma forma para a realização deste trabalho de doutorado. Dentre estes, alguns merecem ser destacados.

Agradeço a minha mãe, Maria do Carmo Oliveira Irion, pelo amor, carinho e dedicação incondicional. Por todos os ensinamentos e desafios vivenciados, servindo de exemplo para moldar meu caráter e personalidade. Pela paciência, confiança e apoio que foram essenciais para que a conclusão deste trabalho fosse possível.

Agradeço a Bibiana Petri da Silveira por me acompanhar durante essa e outras muitas jornadas, por toda a dedicação, apoio, auxílio, carinho e amor. Pela ajuda nas decisões difíceis e pelas palavras de incetivo em momentos necessários. Tua parceria foi essencial para que eu tomasse as decisões que me fizeram chegar a conclusão do Doutorado.

Agradeço ao professor e orientador Bartolomeu F. Uchôa Filho, ou ao meu amigo Bart, especialmente pela confiança em mim depositada. Sou grato pelos sábios conselhos e por todo o tempo dedicado a minha formação pessoal e acadêmica. Pelas palavras de incentivos e pelos laços de amizade formados. A sua dedicação e as oportunidades a mim dadas pelo senhor foram únicas, sendo essenciais para a realização desse trabalho de doutorado. Me sinto honrado de ter sido orientado pelo senhor, tanto no mestrado como no doutorado.

Agradeço ao professor, coorientador e amigo Renato Machado, pelo companheirismo, pela confiança depositada e por todas as oportunidades a mim confiadas. Pelos sábios conselhos, pelos momentos de descontração e pelos laços de amizade formados. Pelos mais de 8 anos de trabalho em conjunto e pela possibilidade de manter essa parceria. O senhor participou durante todos os momentos de minha formação como engenheiro e docente, desde minha graduação, servindo como exemplo de profissional, ao qual tenho como ideal e utilizo como modelo. Foi uma grande honra ser orientado pelo senhor durante todas estas etapas.

Agradeço a Blekinge Institute of Technology, a SAAB AB e aos colegas de departamento de TIMN pelo acolhimento, dedicação e oportunidades oferecidas durante o período de Doutorado Sanduíche. Vocês me proporcionaram uma experiência que contribuiu de maneira única para meu crescimento pessoal e profissional. Em especial, a Mats I. Pettersson e a Viet Thuy Vu pelo acolhimento durante o período de Doutorado Sanduíche, pelo apoio, dedicação e colaboração no trabalho de doutorado. Agradeço pelos momentos de descontração e de amizade.

Agradeço a Universidade Federal do Pampa e aos colegas do Campus Alegrete, pelo apoio e pela oportunidade oferecida que tornou possível a conclusão deste trabalho. Em especial, ao colega Crístian Müller, por todo apoio durante o período de Doutorado Sanduíche e pela parceria de pesquisa formada.

Agradeço a todos os amigos e companheiros que ajudaram a tornar essa jornada mais branda e amena, além de terem estendido a mão em momentos de necessidade. Em especial, gostaria de agradecer a Vinicius Ludwig Barbosa, Thomas Sievert e a Bruna Gregory Palm, que foram fundamentais durante o período de Doutorado Sanduíche, pelas nossas conversas, experiências compartilhadas, pelos “Fikas” e pelo apoio nos momentos difíceis.

“Olhos abertos, o longe é perto, o que vale é o sonho.”

(Mario Barbará)

Resumo da Tese apresentada à UFSC como parte dos requisitos
necessários para obtenção do grau de Doutor em Engenharia Elétrica

MÉTODOS DE DETECÇÃO DE MUDANÇAS PARA IMAGENS SAR COM RESOLUÇÃO EM COMPRIMENTO DE ONDA

Dimas Irion Alves

17 de Abril de 2020

Orientador: Bartolomeu Ferreira Uchôa Filho
Coorientador: Renato Machado
Área de concentração: Comunicações e Processamento de Sinais
Palavras-chave: Métodos de detecção de mudanças, radares de abertura sintética (SAR), imagens SAR com resolução de comprimento de onda, CARABAS, pilha de imagens, Teorema de Bayes.
Número de páginas: 117

Radares de abertura sintética (SAR) são amplamente utilizados para aplicações que requerem o mapeamento ou monitoramento de uma determinada região de interesse. Dentre estas aplicações, a detecção de alvos camuflados em regiões florestais sempre despertou um grande interesse tanto para aplicação civil quanto para a Defesa. Os sistemas SAR convencionais operam na faixa de frequência de micro-ondas. Atualmente, há um grande interesse em se monitorar atividades que ocorrem sob o dossel de florestas. Na faixa de micro-ondas (e.g., banda X), o número de difusores associados à copa das árvores é bastante elevado, fazendo com que os algoritmos de detecção de alvos sejam ineficientes. Assim, sistemas SAR com resolução de comprimento de onda são, tradicionalmente, empregados nesse tipo de aplicação. Frequentemente, os métodos de detecção de mudanças são as técnicas utilizadas para a detecção de alvos camuflados em regiões florestais, utilizando-se imagens SAR de resolução de comprimento de onda. As contribuições desta tese estão inseridas nesse contexto e podem ser divididas principalmente em dois tópicos de estudo. O primeiro tópico estudado é o uso de pilha de imagens SAR com resolução no comprimento de onda. É apresentada uma análise de um teste estatístico para pilhas de imagens SAR com resolução no comprimento de onda e seus resultados são utilizados para a proposição de novos métodos de detecção de mudanças. O segundo tópico estudado foi a consideração do teorema de Bayes na proposição de um método de detecção de mudanças em imagens SAR, que é facilmente adequado para o uso de diferentes

modelos de distribuição de *clutter* mais ruído. Com base nesse método, foram propostos um algoritmo não iterativo e um iterativo. Todos os métodos de detecção de mudanças propostos nesta tese são avaliados com dados reais, com resolução de comprimento de onda, obtidos pelo sistema SAR sueco CARABAS II. Os resultados apresentados mostram que as técnicas propostas obtêm melhor desempenho, em termos de probabilidade de detecção e taxa de falsos alarmes, quando comparadas com outros métodos de detecção de mudanças da literatura.

Resumo Expandido

Introdução

Radares de Abertura Sintética (SAR) são dispositivos aptos a gerar imagens em duas e três dimensões, com a capacidade de obter melhores resoluções espaciais do que sistemas de radar convencionais. Devido a essas características, esses dispositivos são utilizados em diversos tipos de aplicações, especialmente nas relacionadas com monitoramento e vigilância. Dentre essas aplicações, pode-se destacar a detecção de alvos ocultos em regiões com alta densidade de vegetação, empregando-se radares do tipo *Foliage-Penetrating* (FOPEN). Esses dispositivos operam em frequências abaixo de 1 GHz.

Dentre os diversos tipos de radares FOPEN, pode-se citar os radares do sistema CARABAS II que operam na faixa de frequências de 20 a 90 MHz e são caracterizados por sua grande largura de banda fracionária e uma ampla largura de banda de antena. A resolução de sistemas SAR com essas características é da ordem do comprimento de onda do sinal do radar. Por essa razão, são frequentemente chamados de sistemas de resolução de comprimento de onda.

Nas baixas frequências, as principais contribuições do sinal eco são provenientes de grandes dispersores, por exemplo, árvores, troncos e estruturas feitas pelo homem. Esses objetos tendem a possuir características estatísticas estáveis no tempo entre diferentes medições. Além disso, as imagens geradas por estes sistemas tendem a não sofrer com o efeito de *speckle*.

Essas características facilitam a aplicação de técnicas de detecção de mudanças em imagens provenientes deste tipo de sistema. Deste modo, em aplicações do tipo FOPEN, podem-se utilizar técnicas de detecção de mudanças em imagens SAR de resolução do comprimento de onda, com a finalidade de detectar alvos camuflados pelas copas das árvores. De fato, a pesquisa de métodos de detecção neste tipo de imagem é um importante tópico de estudo, que tem sido estudado por mais de duas décadas.

Recentemente, novos métodos de detecção de mudanças, considerando imagens SAR de resolução de comprimento de onda, obtiveram resultados promissores através da utilização de pequenas pilhas de imagens, métodos considerando o teorema de Bayes ou o uso de distribuições mais adequadas para modelar o *clutter* mais ruído. Essas publicações motivaram os estudos e propostas que são detalhados nesta tese de doutorado

Objetivos

Esta tese de doutorado tem como objetivos o estudo e desenvolvimento de técnicas de detecção de mudanças com ênfase em imagens SAR de resolução de comprimento de onda. Deseja-se que as técnicas propostas sejam competitivas quando comparadas com os resultados mais recentes publicados na literatura, de modo a apresentarem bons desempenhos em termos de probabilidade de detecção e taxas de falsos alarmes.

Metodologia

Inicia-se a pesquisa a partir de um estudo teórico referente a imagens SAR de resolução de comprimento de onda do sinal e referente a métodos de detecção de mudanças aplicados a este tipo de imagem. Motivado por recentes descobertas, observadas no decorrer deste estudo, foram identificados dois tópicos de estudos principais para a proposição de novos métodos de detecção de mudanças: o uso de pilhas de imagens SAR e o uso do Teorema de Bayes.

O estudo do uso de pilhas de imagens foi baseado em uma análise estatística utilizando o teste de qualidade de ajuste de Anderson Darling. Para essa análise experimental foram considerados dados reais obtidos através de medições do sistema SAR de banda ultralarga (UWB, *Ultra-Wideband*) VHF (*Very High Frequency*) CARABAS II. O uso do Teorema de Bayes em métodos de detecção de mudanças foi apresentado e estudado de forma analítica. A partir dos resultados dessas duas investigações, foram propostos novos métodos de detecção de mudanças com ênfase em imagens SAR de resolução de comprimento de onda do sinal.

Os métodos de detecção de mudanças propostos nessa tese são avaliados, predominantemente, em termos da probabilidade de detecção de mudanças e da taxa de falsos alarmes. Por simplicidade, esses resultados são, frequentemente, expressos graficamente através de curvas de característica de operação do receptor, também chamadas de curvas ROC.

Essas avaliações são realizadas utilizando um conjunto de configurações padrão para todos os métodos propostos. Além disso, as avaliações são realizadas utilizando um único conjunto de 24 imagens SAR, obtidas pelo sistema CARABAS II.

A fim de avaliar os métodos propostos, comparações de desempenho são apresentadas, considerando métodos recentemente publicados na literatura. Com a finalidade de garantir um cenário de avaliação justo, buscou-se utilizar um conjunto de configurações similares para todas as técnicas avaliadas. Essas configurações são apresentadas e discutidas detalhadamente no decorrer da tese.

Resultados e Discussões

O primeiro estudo realizado na tese é uma análise de um teste estatístico de qualidade de ajuste em pilhas de imagens SAR UWB VHF. Baseado nesse estudo, verificou-se a partir de um grupo de distribuições testadas a existência de uma distribuição estatística que modela de maneira satisfatória a maioria dos conjuntos de amostras avaliadas da pilha de imagens. A partir dos resultados obtidos, foram propostos métodos de detecção de mudanças, os quais foram divididos em duas classes: os baseados no critério de decisão de Neyman-Pearson e os baseados no uso de máscaras.

Em seguida, foi apresentado um estudo sobre a implementação de métodos de detecção de mudanças baseados no uso do Teorema de Bayes. A partir desse estudo, foram propostas as versões não iterativa e iterativa de um novo método de detecção de mudanças para imagens SAR de resolução de comprimento de onda do sinal. Esse novo método tem como principal característica a exclusão da necessidade de um modelo estatístico para os alvos, sendo necessária apenas a seleção de uma distribuição adequada para o *clutter* mais ruído. A fim de validar os métodos propostos, duas distribuições diferentes são utilizadas e avaliadas.

A análise de desempenho dos métodos de detecção de mudanças propostos foi realizada utilizando-se dados reais, obtidos por medições realizadas com o sistema SAR CARABAS II. Através de comparações de desempenho com métodos recentemente publicados na literatura, é possível observar que, para a maioria dos casos avaliados, os métodos propostos apresentam ganhos em termos de probabilidade de detecção, e ou, de taxa de falsos alarmes.

Considerações Finais

Nessa tese são apresentados uma análise de um teste estatístico de qualidade de ajuste em pilhas de imagens SAR e um estudo analítico do uso do Teorema de Bayes em métodos de detecção de mudanças em imagens SAR. Ambos os estudos deram ênfase para imagens SAR de resolução de comprimento de onda do sinal.

A partir desses estudos, foram propostas diferentes técnicas de detecção de mudanças com ênfase em imagens SAR UWB VHF. Essas técnicas apresentaram desempenho competitivo quando comparadas com outros métodos recentemente publicados na literatura. Por fim, ressalta-se que ainda existem tópicos a serem estudados referentes ao uso de pilhas de imagens e ao uso do Teorema de Bayes em métodos de detecção de mudanças em imagens SAR de resolução de comprimento de onda, de modo que aprimoramentos para os métodos propostos nesta tese, e ou, novas técnicas de detecção de mudanças podem ser propostos em trabalhos futuros.

Palavras-chave: Métodos de detecção de mudanças, radares de abertura sintética (SAR), imagens SAR com resolução de comprimento de onda, CARABAS, pilha de imagens, Teorema de Bayes.

Abstract of Dissertation presented to UFSC as a partial fulfillment
of the requirements for the degree of Doctor in Electrical Engineering

CHANGE DETECTION METHODS FOR WAVELENGTH-RESOLUTION SAR IMAGES

Dimas Irion Alves

April 17th, 2020

Advisor: Bartolomeu Ferreira Uchôa Filho
Co-advisor: Renato Machado
Area of concentration: Communications and Signal Processing
Keywords: Change detection methods, synthetic aperture radar (SAR), wavelength-resolution SAR images, CARABAS, image stacks, Bayes' theorem.
Number of pages: 117

Synthetic Aperture Radars (SAR) are widely used in applications that require the mapping or monitoring of a certain interest ground area. Among these applications, the detection of concealed targets in forestry areas has always been of great interest for both civilian and defense purposes. Conventional SAR systems operate in the microwave frequency range. Currently, there is a strong interest in monitoring activities that occur under the forest canopy. In the microwave range (e.g., X-band), the number of treetop-associated scatterers is quite high, making target detection algorithms inefficient. Thus, wavelength-resolution SAR systems are traditionally employed in this type of application. Frequently, change detection methods are the techniques used for the detection of concealed targets in forestry areas using wavelength-resolution SAR images. The contributions of this dissertation are inserted in this context and can be mainly divided into two topics. The first topic studied is the use of wavelength-resolution SAR images stacks. A statistical test analysis of the wavelength-resolution SAR image stacks is presented, and its results are used in the proposition of new change detection methods. The second topic studied is the consideration of the Bayes theorem into the proposition of a SAR change detection, which is easily suitable for the use of different clutter-plus-noise distribution models. Based on this method, two algorithms, one non-iterative and the other iterative, are proposed. All change detection methods proposed in this dissertation are evaluated with real wavelength-resolution data obtained by the Swedish CARABAS II SAR system. The results presented show that the

proposed techniques provide better performance in terms of probability of detection and false alarms rate when compared with other change detection methods from the literature.

List of Figures

List of Tables

Acronyms

AD	Anderson-Darling
AFRL	Air Force Research Laboratory
ATD	Advanced Technology Demonstration
CARABAS	Coherent All Radio Band Sensing
CDF	Cumulative Distribution Function
CFAR	Constant False Alarm Rate
DARPA	Defense Advanced Research Projects Agency
EDF	Empirical Distribution Function
FAR	False Alarm Rate
FOI	Swedish Defence Research Agency
FOPEN	Foliage-Penetrating
GoF	Goodness-of-Fit
LORA	Low-frequency Radar
LRT	Likelihood-Ratio Test
MAP	Maximum a Posteriori Probability
MCMD	Multiple Concatenated Masking Detection
MLC	Multi-Look Complex
MLE	Maximum Likelihood Estimator
NP	Neyman-Pearson
NPC	Change Detection Method Based on NP-Criterion
NPSOC	Change Detection Method Based on NP using a Sub-optimal Criterion
NRL	Naval Research Laboratory
PDF	Probability Distribution Function
PSF	Point Spread Function
Radar	Radio Detection and Ranging
RFI	Radio Frequency Interference
RFN	Missile Test Area North
ROC	Receiver Operating Characteristic
SAR	Synthetic Aperture Radar
SLAR	Side-Looking Airborne Radar

SLC	Single-Look Complex
SMD	Simple Masking Detection
STAP	Space-Time Adaptive Processing
TRACER	Tactical Reconnaissance and Counter-Concealment Enabled Radar
UHF	Ultra High Frequency
UWB	Ultra-Wideband
VHF	Very High Frequency

Contents

1 Introduction

The first studies related to Radio Detection and Ranging (Radar) systems were documented in the late 19th century. In 1887 [1], Heinrich Hertz demonstrated that electromagnetic waves are reflected by both metallic objects and dielectric materials [2]. Later, in 1903 [3], Christian Hülsmeyer created a device called the telemobiloscope [4], which was capable of detecting ship-reflected radio waves, which can be considered the first radar in history. In 1922, researchers at the Naval Research Laboratory (NRL) performed wooden ship detections using a continuous wave radar. In 1930, another NRL researcher detected for the first time an aircraft using a continuous wave radar [3]. It is important to emphasize that experiments and the creation of radar systems were carried out in several countries simultaneously during the 1920s and 1930s [1]. However, the interest increase in radar-related research began during World War II [5]. The cause of this interest was the necessity of detecting enemy targets. The information obtained from the enemy side was used to optimize troop allocation and logistical resources in territory defense. According to [1], several war milestones are associated with radar systems, which contributed to the success of a large number of military operations, e.g., the use of the Chain Home radar in the Battle of Britain.

Even besides war applications, the interest of industry and academia in radar technologies continues to grow, which is motivated by the system's wide range set of applications, e.g., forest area imagery [6], weather monitoring [7], global ice sheets imaging [8, 9], vehicle traffic monitoring [10], imaging of other planets [11], air traffic control [12], military defense [13]. Due to this, radars have been diversifying, generating new configurations and types of systems, such as the Synthetic Aperture Radar (SAR), which are the radar type considered in this dissertation.

According to [14], the key observations that originated the SAR systems are attributed to C. A. Wiley in 1965 [15], who is considered the SAR system inventor [16]. These systems are based on the relative movement between the device antenna and the target, which enables

the collection of data similar to systems with a larger effective antenna aperture, resulting in images with enhanced spatial resolution. From this type of systems, it is also possible to obtain two-dimensional and three-dimensional images of a region of interest [17].

Due to the imaging capability, the small size of the device's antennas and finer spatial resolution, SAR systems are currently used for several applications, with emphasis on monitoring applications [18]–[20] and surveillance applications [21]–[23]. Among the various SAR systems applications, the detection of concealed targets in regions with high-density of vegetation can be highlighted. Systems used in this scenario are known as Foliage-Penetrating (FOPEN) radars, which usually operate at frequencies below 1 GHz. These systems are often used for military applications and monitoring of border areas [24].

In this context, the Swedish radars Coherent All Radio Band Sensing (CARABAS) are inserted, which have been used in various applications and scientific work since the first half of the 90s [25]–[28]. These studies were mainly promoted by the Swedish Defence Research Agency (FOI) and by the Swedish company SAAB. The CARABAS systems have versions I, II, and III. The data set used throughout this dissertation was obtained using the CARABAS II system.

The CARABAS II system operates in the 20 - 90 MHz frequency range and is characterized by its large fractional bandwidth and a wide antenna bandwidth [25]. Based on these characteristics, the CARABAS II system is classified as an Ultra-Wideband (UWB) Very High Frequency (VHF) radar. The resolution of SAR systems with these characteristics is on the order of radar signal wavelengths, so these systems are often referred to as wavelength-resolution systems [29]–[31]. Since the scattering process is only related to scatterers with dimensions in the order of the signal wavelengths, the CARABAS II is not sensitive to small scatterers present in the ground area of interest, e.g., forest canopy [31]. Thus, the CARABAS II system is an adequate selection for FOPEN applications and, therefore, it is frequently used for applications in forestry areas, e.g., retrieval of steam volume [32]–[34] and detection of concealed targets [35]–[37].

Traditionally, change detection methods are used for the detection of concealed targets, being a research topic for more than two decades [35]–[43]. Recently, wavelength-resolution SAR change detection methods achieved promising results by considering the use of image stacks [44], methods based on the use of the Bayes theorem [45, 46], or more accurate clutter-plus-noise distribution models [47, 48]. These proposals motivated the study presented in this dissertation.

Thus, motivated by the interest in the development of change detection techniques for wavelength-resolution SAR images and by the recent results obtained in [44]–[48], this

dissertation has as objectives the study and development of change detection methods for SAR, focusing on wavelength-resolution images. The proposed methods are divided into two classes, on the one hand methods based on SAR image stacks, and on the other hand methods that make use of the Bayes theorem. All proposed methods are evaluated using data from real measurements and present a competitive performance when compared with change detection methods from the literature.

1.1 Objectives

The main objectives of this dissertation are:

- To present a statistical test analysis of clutter-plus-noise distribution models of wavelength-resolution SAR image stacks;
- To present the analysis of the application of Bayes' theorem in SAR change detection based on the use of different clutter-plus-noise distribution models;
- To propose change detection methods based on the statistical test analysis of wavelength-resolution SAR image stacks and the implementation considering the use of Bayes' theorem;
- To show that the proposed change detection methods present a competitive performance by comparing them with other existing methods in the literature, using data obtained from real measurements.

1.2 Document Organization

The remainder of this dissertation is organized as follows:

- Chapter 2 - This chapter presents a brief theoretical review of the basic principles of SAR systems, addressing their main characteristics, principles of operation, and the image information characteristics. Also, a study is presented regarding one baseline detection criterion commonly used in SAR target detection;
- Chapter 3 - The main features of the CARABAS II system and wavelength-resolution SAR images are presented and discussed in this chapter. Also, the data set used in the experimental evaluations of this dissertation is detailed. Finally, some change detection methods for this same data set are presented;

- Chapter 4 - This chapter presents a statistical test analysis for SAR wavelength-resolution image stacks. Based on this statistical test analysis, change detection methods are proposed. The proposed change detection methods are divided into two classes: Neyman-Pearson (NP) criterion based and masking techniques based. The proposals are discussed and evaluated using CARABAS II data;

- Chapter 5 - An analysis of the application of Bayes' theorem in SAR change detection is presented considering the use of different statistical clutter-plus-noise models. Based on this analysis, a non-iterative version and an iterative version of the change detection method are proposed. As study cases, two distributions are discussed and evaluated using CARABAS II data, using both the non-iterative and the iterative techniques;

- Chapter 6 - This chapter presents the concluding remarks and emphasizes the main contributions of this dissertation. Also, a brief discussion about future studies is presented.

2 Principles of SAR Systems

SAR systems are a form of radar that is configured to exploit the motion between the antenna and the target region to generate a photograph-like image of the scene of interest [17]. These systems present advantages when compared with optical imaging systems, e.g., the possibility to emphasize human-made objects, lower performance susceptibility to weather conditions, and the possibility to mitigate undesirable vegetation aspects [17]. Moreover, SAR systems present better spatial resolution than conventional radar imaging systems, when similar aperture antennas are considered [49].

Motivated by the SAR system's advantages, studies have been carried out for extracting information from SAR images [18]–[50]. Among the existing techniques, it is possible to emphasize the change detection methods [35]–[43], which are the main studied topic in this dissertation.

This chapter presents a brief theoretical review of SAR system fundamentals, e.g., operation principles, resolution characteristics, and data collection modes. Additionally, topics related to SAR images, such as the image formation process, their characteristics, and their types, are also addressed. Finally, a baseline detection criterion, which is frequently used for SAR images, is discussed.

2.1 Principles of SAR Systems

SAR systems are a form of radar that uses the information of the relative motion between targets and sensors to obtain images from a ground area of interest. Unlike aerial optic imaging sensors, airborne SAR measurements are made using small grazing angles values, usually between 10° and 45°, i.e., the measurement is made in a side-looking perspective. For this

reason, SAR systems can be named as Side-Looking Airborne Radar (SLAR) systems. However, by convention, the designation SLAR is usually used only for real aperture radar [17].

The data collection in SAR systems is a procedure where the radar, located on a platform, either an airplane or a satellite, transmits pulses and collects echoes from the imaged region. The echoes associated with each one of these pulses provides the range dimension information, while the pulse repetition associated with the relative motion generates azimuth dimension information. The data from this process are organized as a two-dimensional array (range and azimuth dimensions), whose elements are samples that have amplitude and phase information [49].

Unlike SLAR systems, SAR radars are designed in a form that a specific location is visible in different measurement positions. These multiple positions provide the integration angle that is used to achieve finer azimuth resolutions, as further discussed throughout this section.

The major advantage of using SAR over SLAR systems is the achievable azimuth resolution gain, considering antennas with similar dimensions. In the following, an analysis based on [14, 51] is presented to justify this gain. The system geometry considered is the one shown in Figure 2.1.

It can be observed that the minimum separation between two resolvable points on the ground (ΔR_g) can be described as a function of their separation in the slant-range direction (ΔR_s). Thus, ΔR_g can be written as

$$\Delta R_g = \frac{\Delta R_s}{\sin(\eta)} = \frac{cT_p}{2\sin(\eta)}, \tag{2.1}$$

where η is the incidence angle, which is identical to the look angle γ for the considered geometry, T_p is the pulse duration, and c is the speed of light. Under the assumption that a pulse compression technique is employed, as the chirp signal compression described in [49], and considering an adequate processing of the received signal [14], the achievable range resolution can be written as

$$\delta R_g = \frac{c}{2B_\omega \sin(\eta)}, \tag{2.2}$$

where B_ω is the transmitted signal frequency bandwidth. Since δR_g depends only on B_ω and the processing employed on the received signal, it is possible to state that the SAR and SLAR systems present the same characteristics of range resolution. The resolution gains associated with the SAR systems are achieved in the azimuth dimension.

Similarly, azimuth resolution can be defined as the minimum distance in the along-track dimension between two points distinguishable by the system. Given that the transmitted signals have an angular spread θ_H in the azimuth region, it is possible to write the azimuth resolution

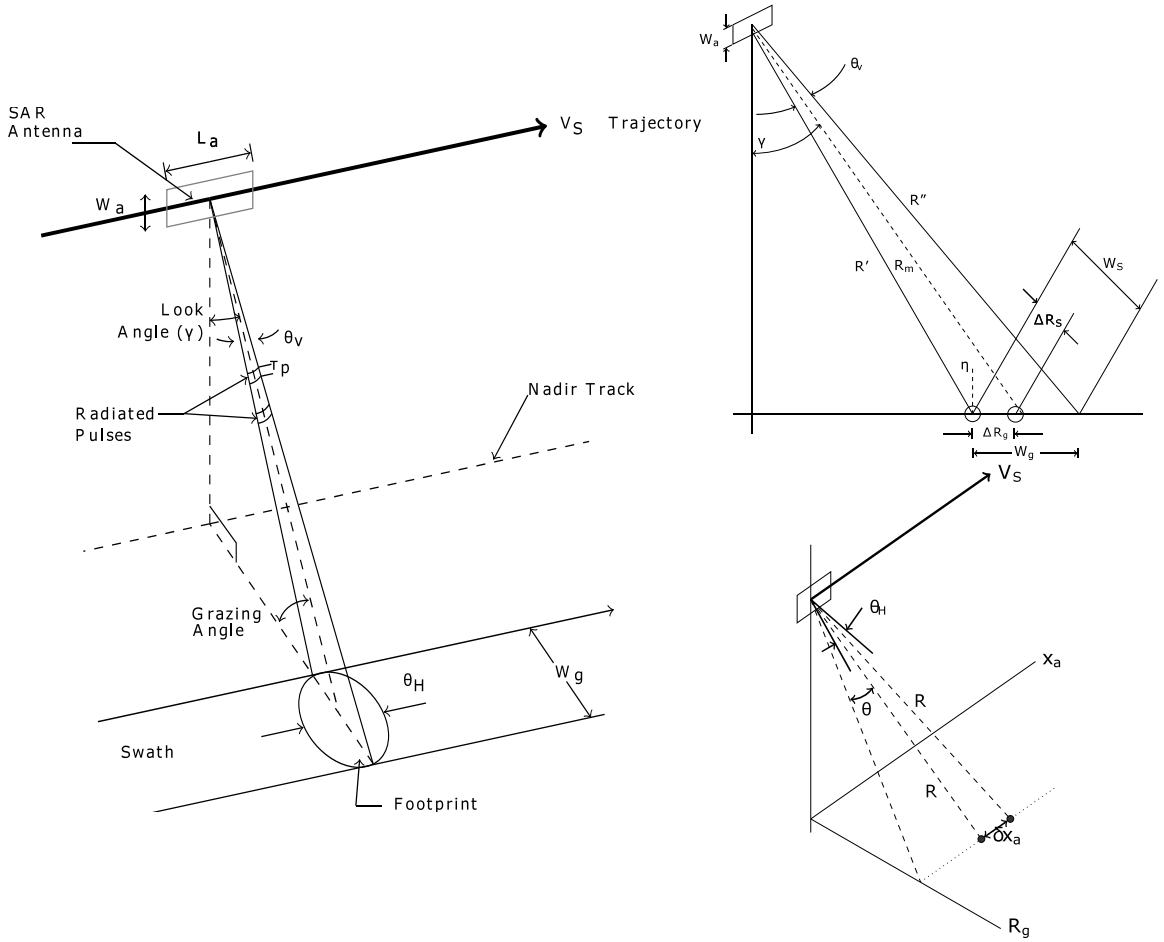

Source: Adapted from [14].

Figure 2.1: Basic geometry of a side-looking airborne radar.

for a SLAR system as

$$\delta x_a = R\theta_H = \frac{R\lambda}{L_a}, \tag{2.3}$$

where x_a is the variable associated with the azimuth dimension, R is the slant range, λ is the wavelength of the transmitted signal, and L_a is the antenna length in the along-track dimension. According to [14], (2.3) is the azimuth resolution limit for a SLAR system. Thus, to achieve finer azimuth resolutions, it is necessary to increase the antenna dimension, which tends to be not practical for mechanical reasons.

However, in a scenario with a mobile radar, it is expected that echoes relative to the azimuth direction from nearby targets tend to have different frequency deviations, which are caused by the instantaneous relative speed difference between them. This observation made by C. A. Wiley [15] is the basic principle of SAR technology. For the evaluated scenario, the Doppler shift can be approximated as

$$f_d = \frac{2V_{st}\sin(\theta)}{\lambda} \approx \frac{2V_{st}x_a}{\lambda R}, \tag{2.4}$$

where V_{st} is the relative speed between the target and the mobile station. For the sake of simplicity, the same consideration as in [14] is adopted, which is $V_{st} \approx V_s$, where V_s is the velocity of the mobile station. By simple algebraic manipulations, it is possible to write the system azimuth resolution as

$$\delta x_a = \frac{\lambda R}{2V_s}\delta f_d = \frac{\lambda R}{2V_s S_t}, \tag{2.5}$$

where S_t is the time that a target remains illuminated by the radar. According to the geometry presented in Figure 2.1, S_t is given by

$$S_t = \frac{\lambda R}{V_s L_a}. \tag{2.6}$$

Therefore, it is possible to rewrite (2.5) only as a function of the radar antenna length. Thus, the azimuth resolution for a SAR system is given by

$$\delta x_a = \frac{L_a}{2}. \tag{2.7}$$

The resolution limit presented in (2.7) indicates that finer resolutions can be achieved by reducing the antenna dimension in the azimuth dimension. However, this result requires some considerations that are not always feasible in all real applications [14]. Other practical aspects can interfere in the achievable azimuth resolution, e.g, pulse repetition frequency, received signal processing, SAR data collection mode [17, 49].

To better visualize the effect of other practical aspects, an azimuth resolution analysis is presented for two SAR data collection modes, named stripmap and spotlight. For the sake of simplicity, a straight line flight geometry is considered. The functioning of these two data collection modes is presented in Figure 2.2.

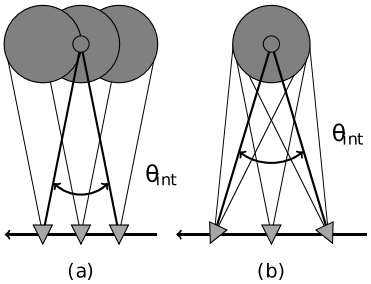

Source: Adapted from [17].

Figure 2.2: Data collection modes where (a) is the stripmap collection mode, and (b) is the linear flight spotlight.

By inspecting Figures 2.1 and 2.2, it is possible to relate the case under study with the stripmap operation mode. According to [17], the azimuth resolution for both data collection modes can be written as

$$\delta x_a = \frac{\lambda}{2\theta_{int}}, \tag{2.8}$$

where θ_{int} is the integration angle, which is related to the system measurements.

As can be observed, the evaluated spotlight mode can achieve finer resolutions by obtaining higher values of θ_{int} angles. However, this mode presents as a drawback the occurrence of gaps in coverage along the platform's ground track caused by the constraints of the system beam pointing. On the other hand, the stripmap mode provides a worse resolution performance than the spotlight mode but it enables the obtaining of an image for the whole flight path.

Additionally, from Figures 2.1 and 2.2, it is possible to establish the relation $\theta_{int} \leq \theta_H$. Thus, the azimuth resolution for a system operating in the stripmap mode can be written as

$$\delta x_a \geq \frac{\lambda}{2\theta_H}, \tag{2.9}$$

where the equality results in (2.7).

Thus, it is possible to state that different implementation aspects can be related to the SAR system azimuth resolution. The resolution of the SAR system considered in this dissertation is further discussed in Chapter 3.

2.2 SAR images

As previously mentioned, the data obtained during the SAR collection process results in a raw image, which can be described as a matrix composed of complex-valued elements. However, unlike other traditional imaging sensors, this raw image does not provide useful information [49].

To obtain a SAR image with useful information, signal processing techniques are employed. According to [49], this processing procedure can be simplified in the form of two matched filters operations, for the range and azimuth dimensions. These filters are frequently called compression filters. According to [52], the processed image can be represented as

$$\mathscr{E}(x_a, R_g) = C(R_g)S(x_a, R_g) * h_r(R_g) * h_a(x_a), \tag{2.10}$$

where R_g and x_a are the variables associated with the range and the azimuth dimensions, respectively, $C(R_g)$ is an attenuation factor associated with device losses and signal propagation

losses, $S(x_a, R_g)$ is the complex reflectivity of the scene of interest, $h_r(R_g)$ and $h_a(x_a)$ are, respectively, the azimuth and the range compression filters, and $*$ denotes convolution operation.

According to [52], the compression filters can be represented using the respective dimension Point Spread Function (PSF). The PSF can be defined as the system response to a point object source. The definition of PSFs can be done by theoretical analysis, such as the one presented in [52], or empirically. The SAR image formation process is an important research topic [53]–[57]. However, the study and analysis of SAR imaging algorithms are beyond the scope of this dissertation.

The previous discussions in this section are mainly related to image resolution characteristics and the image formation process. However, most of the applications where SAR images are applied tend to require to turn the resulting images into useful information about the scene of interest. Frequently, this procedure is performed considering two distinct analysis modes [52]. The first mode is based on the local scattering processes and by the electromagnetic properties of the earth's surface. In this mode, all information is associated with the electromagnetic theory. The second analysis mode is associated with the information obtained with the application of interest, to find specific patterns and characteristics in the images. Usually, this mode is associated with statistical theory.

It is important to emphasize that the previously mentioned analysis modes are not mutually exclusive. Their joint use tends to enhance the extraction of information from SAR images and should be evaluated according to the desired application. To better understand the interpretation process of SAR images according to its applications, the procedure described in [52] is considered. This interpretation process was used during the development of this dissertation's proposals. The blocks in Figure 2.3 can be described as:

- Image - Represents the initial information of the analysis process. Input data characteristics directly interfere with the information that can be extracted;
- Data feature - Understands the essential characteristics of the scene of interest, based on the chosen data model;
- Phenomenological description - Describes the physical phenomena associated with measurement, which is based on the desired information and the obtained image. The choice of the data model is based on this block;

- Data model - Block responsible for providing a model to be used in the image interpretation techniques, as well as providing the necessary information for the Data features block;
- Global model - Block with generic considerations about the interest region that can be used for a better data interpretation;
- Image interpretation techniques - Block that performs the interpretation of the image using algorithms, which extract the desired information from the image;
- Information - It is the block that contains the raw results from the image interpretation block;
- Applications - This block processes the raw information given by the image processing interpretation technique, providing the required information by the system operator.

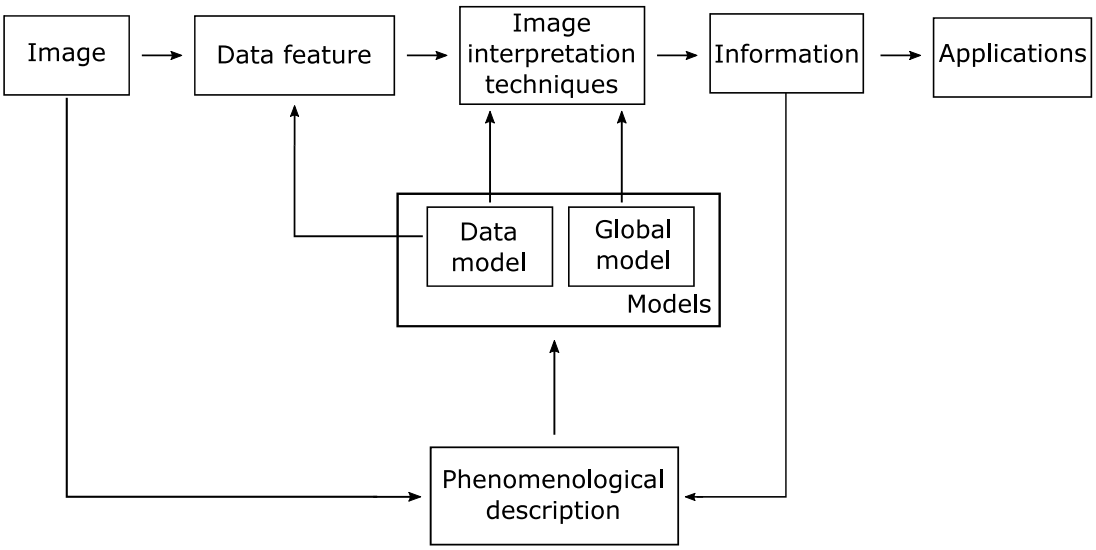

Source: Adapted from [52].

Figure 2.3: Simplified block diagram showing an interpretation process of SAR images.

Thus, based on Figure 2.3, it is possible to state that the selection of the image types, models, and SAR system characteristics should be based on the required information associated with the considered application. So, the image type used has a direct influence on the information that can be extracted from it. Some examples of existing SAR image types are given below [58]:

- Single-Look Complex (SLC) images - These images are produced from the processing of raw data of only one measure. For traditional microwave SAR systems, they tend to contain a speckle contribution, which is an inherent phenomenon of SAR systems and has a noise-like behavior [52]. The speckle phenomenon is further discussed in Section 3.1;

- Multi-Look Complex (MLC) Images - These images are produced from the processing of raw data of multiple measurements. This type of image is used in situations where the speckle effect is not desired, with a drawback of loosing some information;
- Polarimetric Images - This type of image can be either MLC or SLC. These images are generated by using polarimetric data, which are obtained from channels with different polarizations resulting in more information from the interest regions.

The images considered in this dissertation are incoherent wavelength-resolution SAR images obtained from SLC complex images. The features and characteristics of this type of image are discussed in Chapter 3.

2.3 Baseline Criterion for Target Detection in SAR Images

Traditionally, target detection in SAR images is performed considering binary hypothesis tests. A commonly evaluated hypothesis scenario for this kind of application can be written as

$$H_0\text{: x is background-related,}$$
$$H_1\text{: x is target-related,}$$

where x is the evaluated sample from a set of image pixels. For the sake of simplicity, x is considered as an amplitude value. Under this scenario, it is possible to define the error probability for a given detection criterion as

$$\begin{aligned} P_e &= \Pr\{\text{decide on } H_0,\, H_1 \text{ true}\} + \Pr\{\text{decide on } H_1,\, H_0 \text{ true}\} \\ &= P(H_0|H_1)P(H_1) + P(H_1|H_0)P(H_0), \end{aligned} \tag{2.11}$$

where $P(H_0)$ is the probability of hypothesis H_0 to be true, $P(H_1)$ is the probability of hypothesis H_1 to be true, $P(H_0|H_1)$ is the conditional probability of deciding on H_0 when H_1 is true, and $P(H_1|H_0)$ is the conditional probability of deciding on H_1 when H_0 is true. Thus, based on these observations, it is possible to state that $P(H_0|H_1)$ is the probability of missing the detection of a target, which is complementary to the probability of detection, whereas $P(H_1|H_0)$ is the probability of occurrence of a false alarm.

A possible detection criterion would be one that minimizes (2.11). Before analyzing this minimization process, it is convenient to define the evaluated critical regions as

$$R_0\text{: x decide on } H_0 \text{ or reject } H_1,$$
$$R_1\text{: x decide on } H_1 \text{ or reject } H_0,$$

where R_0 and R_1 partition the entire space R of x possible values. Thus, according to [59], (2.11) can be rewritten as

$$P_e = P(H_0)\int_{R_1} p(x|H_0)dx + P(H_1)\int_{R_0} p(x|H_1)dx, \tag{2.12}$$

where $p(x|H_0)$ is the conditional Probability Distribution Function (PDF) given the hypothesis H_0, and $p(x|H_1)$ is the conditional PDF given the hypothesis H_1. Under the consideration that R_0 and R_1 partition the entire space, it is possible to state that

$$\int_{R_0} p(x|H_i)dx = 1 - \int_{R_1} p(x|H_i)dx. \tag{2.13}$$

Then, (2.12) can be rewritten as

$$\begin{aligned} P_e &= P(H_0)\int_{R_1} p(x|H_0)dx + P(H_1) - P(H_1)\int_{R_1} p(x|H_1)dx \\ &= P(H_1) + \int_{R_1} \left[P(H_0)p(x|H_0) - P(H_1)p(x|H_1)\right] dx. \end{aligned} \tag{2.14}$$

Thus, to minimize P_e, H_1 is only decided on if the integrand in (2.14) is negative. Thus,

$$\begin{aligned} P(H_0)p(x|H_0) &< P(H_1)p(x|H_1) \\ \frac{p(x|H_1)}{p(x|H_0)} &> \frac{P(H_0)}{P(H_1)} = \tau, \end{aligned} \tag{2.15}$$

where τ is the threshold. The detector defined in (2.15) is known as the Maximum a Posteriori Probability (MAP) criterion [59]. However, for the majority of the cases, this decision criterion is not practical for target detection in SAR images, due to the requirement of the knowledge of the probabilities P(H_0) and P(H_1).

It is important to emphasize that the left term of (2.15) is not dependent on P(H_0) and P(H_1). Additionally, it is possible to correlate the conditional probabilities $p(x|H_1)$ and $p(x|H_0)$,

respectively, with the probability of detection (P_d) and the probability of false alarms (P_{FA}). In this way, P_d and P_{FA} can be written as

$$P_d = 1 - P_m = 1 - \int_{R_0} p(x|H_1)dx = \int_{R_1} p(x|H_1)dx, \tag{2.16}$$

$$P_{FA} = \int_{R_1} p(x|H_0)dx \tag{2.17}$$

where P_m is the probability of missing a target detection, and $p(x|H_i)$ is the conditional distribution of x without the knowledge of $p(H_i)$. Throughout this dissertation, the notation $p(x|H_i)$ is used instead of $p(x;H_i)$, as indicated in [59]. This notation was selected to be in accordance with the majority of the radar detection-related literature, e.g., [52, 58].

Similar to the MAP criterion analysis, another detection criterion can be obtained by maximizing P_d for a given P_{FA}. Considering the optimization process based on Lagrangian multipliers presented in [59], it is possible to write this optimization problem as

$$\begin{aligned} F &= P_d + \kappa(P_{FA} - \alpha), \\ &= \int_{R_1} \left[p(x|H_1) + \kappa p(x|H_0)\right] dx - \kappa\alpha, \end{aligned} \tag{2.18}$$

where F is the variable to be maximized, α is the significance level, and κ is the new variable associated with the Lagrangian multipliers optimization. To maximizes F, H_1 is only decided on if the integrand in (2.18) is positive. Thus,

$$p(x|H_1) + \kappa p(x|H_0) > 0. \tag{2.19}$$

It is possible to rewrite (2.19) as

$$\frac{p(x|H_1)}{p(x|H_0)} > \tau, \tag{2.20}$$

where $\tau = -\kappa$ and $\tau > 0$. Finally, the value of τ can be found from $P_{FA} = \alpha$. The detector defined in (2.20) is known as the NP Lemma [60]. To better visualize the characteristics of the NP detection criterion, one example of the hypothesis test is presented in Figure 2.4, where the critical regions and the probabilities P_d and P_{FA} are highlighted.

Finally, several other detection criteria can be used for target detection in SAR images. A list of detection criteria and its common employments is presented in [59]. However, for target

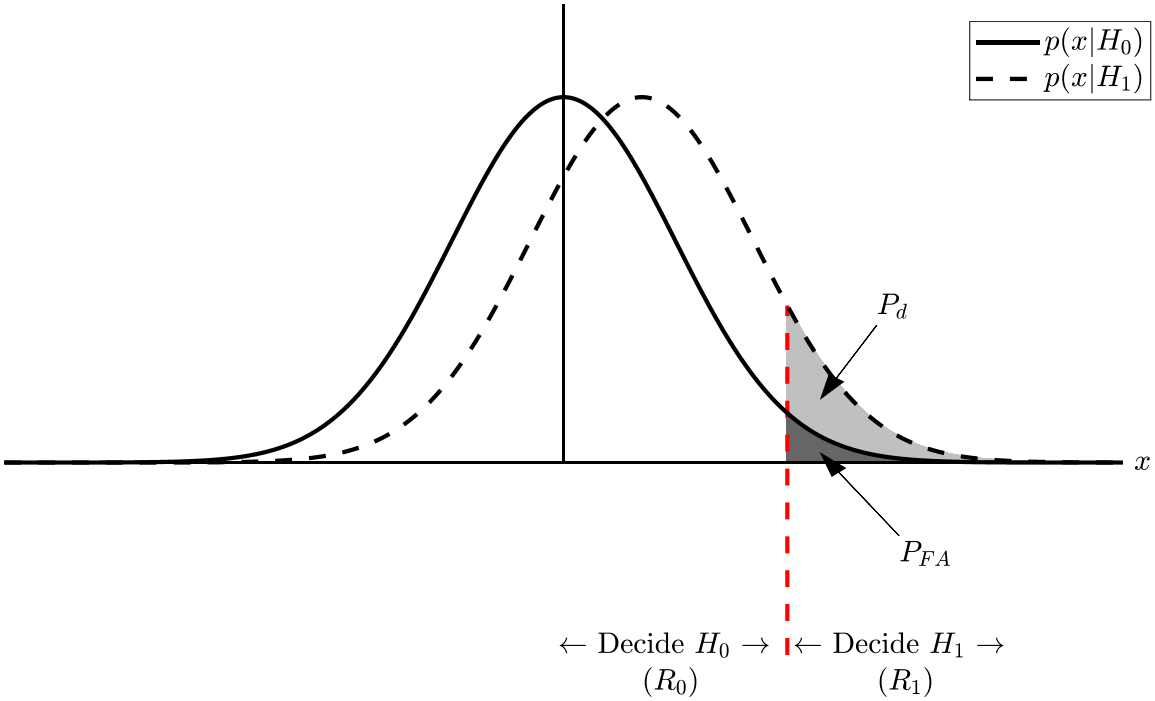

Source: Adapted from [59].

Figure 2.4: Example of the application of the NP criteriom, where the probabilities of detection and false alarm are highlighted.

detection in SAR images, the NP detection criterion is considered in the majority of the cases, being frequently addressed as the baseline target detection criterion in the literature [52, 58]. Moreover, the NP criterion is the adopted detection criterion for the majority of the proposed change detection methods used in FOPEN SAR applications [31, 43, 44, 47, 48, 61], which is the main research topic addressed in this dissertation.

2.4 Concluding Remarks

This chapter presented a brief theoretical review of SAR system fundamentals and a baseline change detection method for SAR images. Section 2.1 addressed topics related to SAR systems, such as its operational principles, resolution characteristics, and some data acquisition modes. Similarly, Section 2.2 presented a discussion about SAR images information. Aspects related to SAR images characteristics, the image formation, and types of SAR images were also addressed.

Additionally, Section 2.3 presented a baseline criterion for target detection, which is commonly used in SAR images. This detection criterion is the one considered for the proposed change detection method in Section 4.2 and for several detection techniques from the literature, such as the methods proposed in [44, 47, 61], which are used throughout this dissertation for performance comparison and evaluation.

3

Wavelength-Resolution SAR Images and CARABAS II System

Historically, the detection of concealed targets in FOPEN applications has, for a long time, been of great interest, especially for military purposes [24]. For FOPEN applications, when conventional microwave frequency SAR systems are employed, a large number of false alarms are observed caused by the abundance of small scatterers associated with the forest canopy. To avoid this problem, Ultra High Frequency (UHF) and VHF SAR systems are employed in this type of application [24].

Both UHF and VHF FOPEN SAR systems are characterized by their large fractional bandwidth and a wide antenna bandwidth, yielding adequate system resolutions. These characteristics result in systems with resolutions in the order of the radar signal wavelengths. The images obtained by these systems are often called wavelength-resolution images.

This chapter presents a study regarding the main properties and characteristics of wavelength-resolution SAR images. Also, the CARABAS II radar, which is the VHF UWB system used to obtain the images data set used in this dissertation, is presented. Finally, a brief state of the art of change detection in wavelength-resolution SAR images is presented.

3.1 Wavelength-Resolution SAR Images

Wavelength-resolution SAR Images are characterized by a system resolution in the order of radar signal wavelengths. According to [62], the resolution cell area of a SAR system can be written as

$$\delta A = \frac{\lambda_c c}{4\theta_H B_\omega}, \tag{3.1}$$

where λ_c is the wavelength corresponding to the system center frequency, θ_H is the aperture angle, i.e., the angle at which the antenna is moved and radiates as seen from the imaged ground, c is the speed of light, and B_ω is the system bandwidth. Thus, based on (3.1), it is possible to classify VHF and UHF UWB SAR systems as wavelength-resolution SAR systems.

Besides, the backscattering phenomenology for wavelength-resolution SAR systems is different from traditional microwave SAR. For wavelength-resolution systems, target-size elements present the characteristic of a resonance scattering regime, whereas small objects present the characteristic of a Rayleigh scattering regime [63]. Based on the backscattering phenomenology characteristics [17], it is possible to state that wavelength-resolution SAR systems are not very sensitive to small scatterers present in the ground area of interest., i.e., objects with dimensions significantly smaller than the signal wavelength. Thus, the scattering process is only related to scatterers with dimensions in the order of the signal wavelengths. For instance, considering the use of a SAR system operating with frequencies below 100 MHz in forestry areas, the foliage backscatter is dominated by the direct and ground-reflected backscattering from tree stems [64].

Therefore, there might be only a single scatter in the resolution cell. As a consequence, the image will not suffer from the speckle noise, which is a strong disturbance in non-wavelength-resolution SAR images. To better visualize the difference between the scattering process of traditional microwave and wavelength-resolution SAR systems, a schematic representation is presented in Figure 3.1.

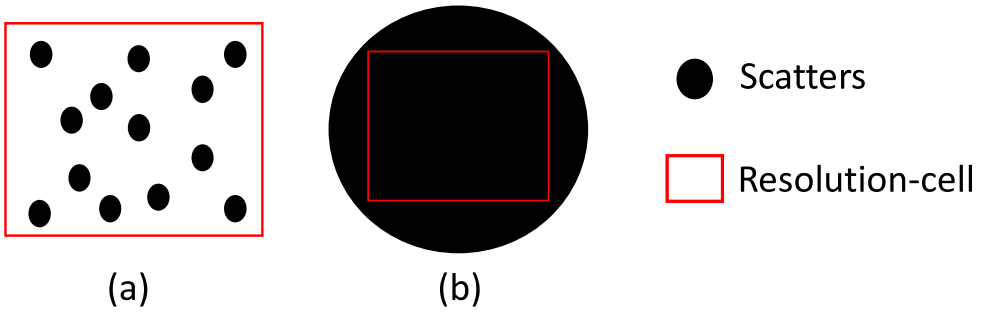

Figure 3.1: Schematic representation of distributed scatters in a resolution cell for two different types of SAR images: (a) non-wavelength resolution SAR image, e.g., a microwave frequency SAR system; (b) Wavelength-resolution SAR image.

Moreover, large scatterers in a ground area of interest tend to be static objects that are less sensitive to weather conditions than small ones. Furthermore, large scatterers tend to be stable in time, especially when low-frequency systems are considered. Hence, it is possible to obtain high similarity images of a determined ground area by measuring with multi-passes [65]. Thus,

it is possible to perform change detection methods in wavelength-resolution images without using clutter reduction techniques [44, 61].

Another important aspect to differentiate traditional microwave and low-frequency wavelength-resolution SAR systems is the signal attenuation due to foliage. Several tests have been carried out to evaluate the signal attenuation for different types of forest regions [24, 66]. For frequencies below 1 GHz, its effects are not significant, and it can get as low as less than 3 dB for frequencies below 100 MHz in specific scenarios [63].

Based on all these observations, it is suitable to state that low-frequency wavelength-resolution SAR images are a good choice for change detection methods, especially for FOPEN applications. A similar observation was made in [63] where the author states that the VHF-band is the optimum radar wavelength for detection in FOPEN applications for vehicle-sized targets. However, designing UWB VHF SAR is a challenging problem due to the required characteristics of integration angle, motion compensation, and range resolution [24]. Indeed, there is only a few UWB VHF SAR systems [50, 67], e.g., CARABAS, Low-frequency Radar (LORA) [68], Tactical Reconnaissance and Counter-Concealment Enabled Radar (TRACER) [69], and FOPEN SAR involved in an Advanced Technology Demonstration (ATD) [70] from the Defense Advanced Research Projects Agency (DARPA). The experimental evaluations presented in this dissertation considered the available public data set, which was obtained by the CARABAS II system and made public in [71]. The CARABAS II system is briefly discussed in Section 3.2.

3.2 The CARABAS II System

The Swedish radars CARABAS are SAR systems designed for FOPEN applications. Currently, they are in their third generation. CARABAS I was the first generation of the Swedish low-frequency radar systems [28], developed and operated by the FOI in the early nineties [72, 73]. CARABAS II is the second generation designed by the FOI. Developed in the mid-nineties [25], it is still in operation by FOI. Finally, CARABAS III was recently designed and built by the Swedish company SAAB AB [28].

Among the three radars generations, CARABAS II is the one that has participated in numerous military and civilian campaigns throughout four continents [74], and whose data have been used for research purposes for more than twenty years. CARABAS II is a VLF UWB SAR system which is usually hosted in a Sabreliner aircraft [75]. The radar transmits HH-polarized radio waves between 20-90 MHz, resulting in a wavelength range of 15 m - 3.3 m [76]. The CARABAS II radar can be classified as a wavelength-resolution SAR system.

For instance, in a scenario of full signal bandwidth using an azimuth integration angle of about 70°, a resolution cell of 2.5 m × 2.5 m is obtained in the slant range image plane [76]. Therefore, it is possible to approximate the system resolution to 3 m.

Table 3.1 presents some common parameters used during flight campaigns of the CARABAS II radar [76]. It is possible to observe that all the requirements for FOPEN SAR systems presented in [24] are accomplished by the CARABAS II, e.g., aperture angle and frequency fractional bandwidth requisites.

Table 3.1: Common CARABAS II system parameters.

System parameters	Values
Nominal flight altitude	3 - 9 km
Nominal flight speed	127 m/s
Frequency band	20 - 86 MHz
Aperture angle	90°
Transmitted power (peak)	500 W
Pulse modulation	Non-linear frequency modulation
Radio Frequency Interference (RFI) sniff	On
Frequency sub-bands	35 (36 with RFI-sniff)
Frequency step	1.875 MHz
Center frequencies	21.25 - 85 MHz
Pulse repetition	frequency 5000 Hz
Pulse length	15 μs
Maximum range	26.4 km

Source: Modified table from [76].

3.2.1 CARABAS II Data Set

To promote research on change detection methods for wavelength-resolution images, a CARABAS II data set is provided by the FOI and has been made publicly available by the Air Force Research Laboratory (AFRL) in [71]. This SAR image data set is the one used to evaluate the proposed change detection methods in this dissertation.

The data set is composed of 24 incoherent SAR images from a set of 150 SAR images obtained during a flight campaign. Each image covers the same ground area of 6 km^2 (2 km × 3 km) and is given in the form of a 3000 × 2000 matrix [76], where the pixel size is 1 m × 1 m. It is important to emphasize that the given images are already calibrated [77], pre-processed [62], and geocoded [78]. A basic block diagram of the processing chain used in the available data set is presented in Figure 3.2.

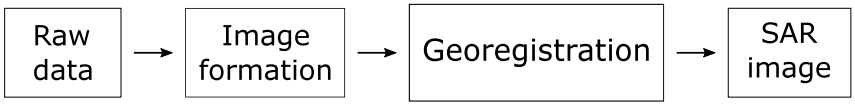

Figure 3.2: Simplified pre-processing block diagram of the available CARABAS II data set.

The flight campaigns were held in the military base station Missile Test Area North (RFN) Vidsel in northern Sweden in 2002 [75]. The selected test sites were a region close to an abandoned village known as Nausta [75]. The region is dominated by small/medium-sized trees, in which the dominant species is the Scots pine [76]. Additionally, the tested ground area contains lakes, roads, and fields [75].

Due to logistics reasons [75], two forest areas were selected for the evaluated target deployments. Each target deployment contain 25 testing targets arranged in different configurations. The tested targets consist of ten TGB11 model vehicles, eight TGB30 model vehicles, and seven TGB40 model vehicles. The dimensions of each vehicle model are presented in Table 3.2. Moreover, the location of Forest 1 and Forest 2 test sites are presented in Figure 3.3. Additionally, the targets present in each image are highlighted.

Table 3.2: Targets dimensions characteristics.

Terrain vehicles	Length	Width	Height	Quantity
TGB11	4.4 m	1.9 m	2.2 m	10
TGB30	6.8 m	2.5 m	3.0 m	8
TGB40	7.8 m	2.5 m	3.0 m	7

The 24 images are divided considering four different targets deployments (Missions), which are measured using different flight geometries (Passes). All measurements adopted an incidence angle of 58°, for a range of 12 km to a common aim point, and used the strip map SAR mode [76]. Also, the flights were conducted with the radar looking left [75]. For the sake of simplicity, the same mission nomenclature used in [76] is adopted in this dissertation.

The target deployments are composed of 25 targets pointing in the same direction and separated by approximately 50 m [76]. According to [76], the targets in Mission 2 are located in Forest 2 and have a heading angle of 225° pointing to the south-west direction; targets in Mission 3 are located in Forest 2 and have a heading angle of 315° pointing to the north-west direction; targets in Mission 4 are located in Forest 1 and have the same heading angle like the ones in Mission 2. Finally, the targets in Mission 5 are located in Forest 1 and have a heading angle of 270° pointing to the west direction. Figure 3.4 presents one example of an image of each mission.

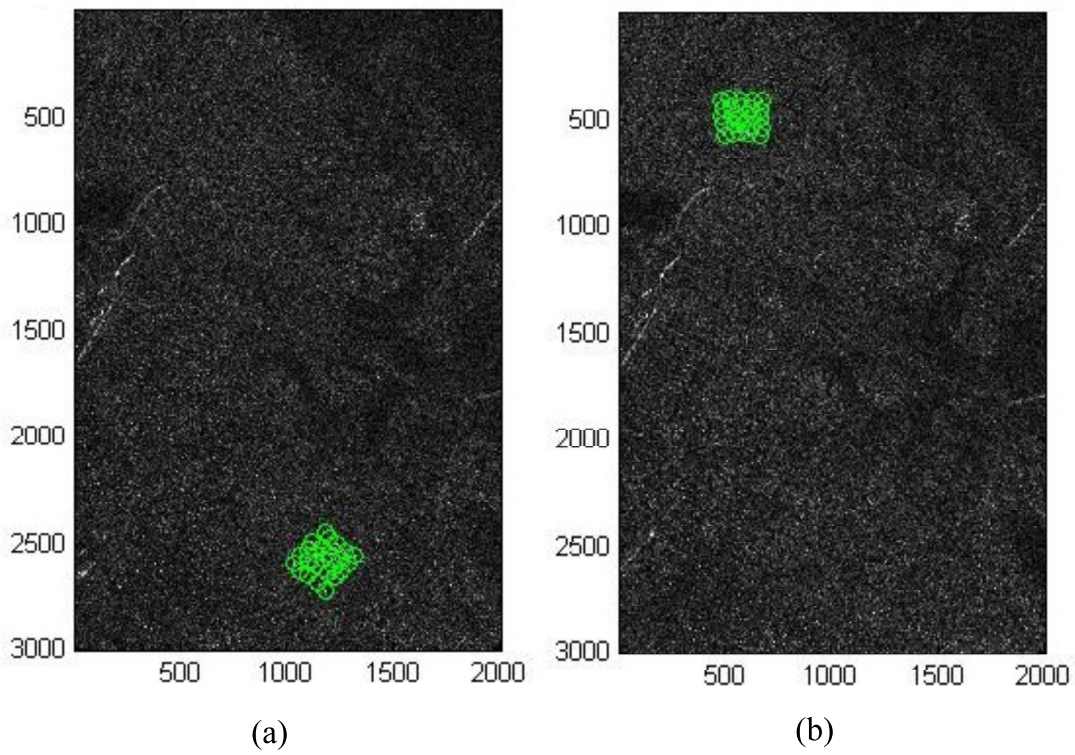

Figure 3.3: Location of forest test sites where (a) is Forest 1 and (b) is Forest 2. The targets present in each image are highlighted.

Each mission was measured considering six different passes, in which three different flight geometries were adopted. The flight heading angles were selected for passes pairs to obtaining different levels of RFI. The main RFI source close to the testing area was a low VHF-band TV broadcasting antenna located in the south-east direction [75]. As demonstrated by [75], higher RFI was obtained in situations where the radar antenna's main lobe was pointed to the main RFI source.

Based on the demonstration in [75] and according to the classification in [76], the passes were divided in the following form: Passes 1 and 3 had a flight heading angle of 225°, thus the radar antenna's main lobe was pointed to the south-east direction, which resulted in high RFI; Passes 2 and 4 had a flight heading angle of 135°, thus the radar antenna's main lobe was pointed to the north-east direction, which resulted in low RFI; Passes 5 and 6 had a flight heading angle of 230°, thus the radar antenna's main lobe was pointed to the south-east direction, which resulted in high RFI. Table 3.3 summarizes the information of each image in the data set.

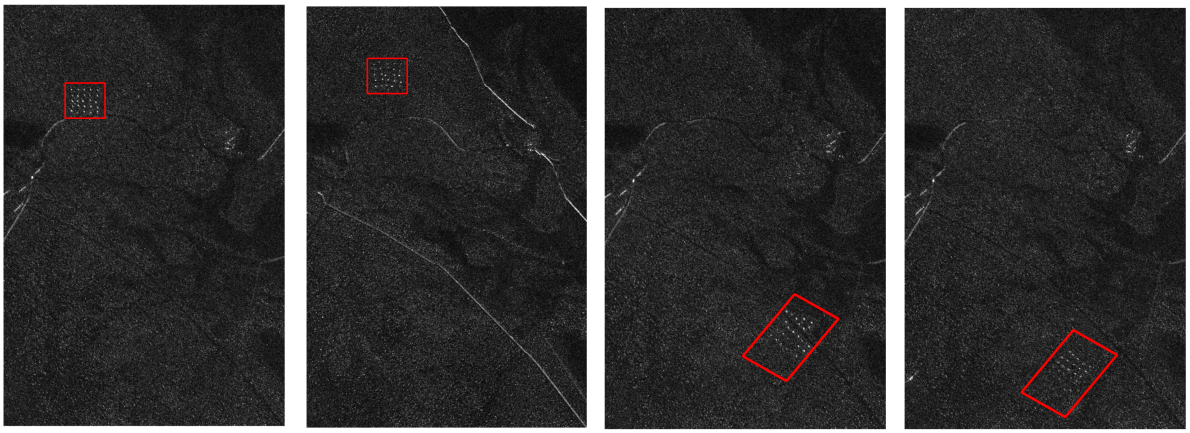

Figure 3.4: Examples of CARABAS II SAR images where (a) is Mission 2, (b) is Mission 3, (c) is Mission 4, and (d) is Mission 5.

3.3 Change Detection in Wavelength-Resolution SAR Images

As previously mentioned, target detection in FOPEN applications considering wavelength-resolution SAR images is an important research topic and has been studied for more than twenty years considering systems operating in both VHF [25, 48] and UHF [79, 80] frequency bands. In this context, the CARABAS II system was considered in several target-detection related studies [39]–[45].

Traditionally, the target in detection in CARABAS II images is mainly carried out by change detection methods. By the best of the author's knowledge, the first detection method used for the CARABAS II system was based on a Bayes linear classification scheme [81]. The method consists of defining the target and background classes and defining the boundaries that maximize the separation between the two classes. This method was also used to evaluate the impact of the bandwidth in the change detection method performance in [75, 63].

Afterward, change detection methods based on Space-Time Adaptive Processing (STAP) used in conjunction with a Likelihood-Ratio Test (LRT) were presented in [61, 76]. The change detection methods presented in [61, 76] consist of exploiting the differences in the space-time characteristics of targets, clutter and interference signals, which are formulated as an LRT to obtain the maximum probability of detection for a fixed false alarm probability. Until the publication of [61, 76], the study of change detection methods for wavelength-resolution SAR systems using CARABAS data was mainly carried out by FOI researchers. Since then, the CARABAS II data have been used in a large number of studies from researches of different institutions [39]–[45].

Table 3.3: Measurements parameters for each image.

Image Number	Mission	Pass	Flight Heading	RFI	Target heading
1	2	1	225°	High	225°
2	2	2	135°	Low	225°
3	2	3	225°	High	225°
4	2	4	135°	Low	225°
5	2	5	230°	High	225°
6	2	6	230°	High	225°
7	3	1	225°	High	315°
8	3	2	135°	Low	315°
9	3	3	225°	High	315°
10	3	4	135°	Low	315°
11	3	5	230°	High	315°
12	3	6	230°	High	315°
13	4	1	225°	High	225°
14	4	2	135°	Low	225°
15	4	3	225°	High	225°
16	4	4	135°	Low	225°
17	4	5	230°	High	225°
18	4	6	230°	High	225°
19	5	1	225°	High	270°
20	5	2	135°	Low	270°
21	5	3	225°	High	270°
22	5	4	135°	Low	270°
23	5	5	230°	High	270°
24	5	6	230°	High	270°

Additionally, the proposals in [61, 76] were part of the motivation for several other studies. For instance, change detection methods based on the combination of the STAP technique and the LRT were proposed in [47, 48]. The main difference among these proposals lies in the selected statistical clutter-plus-noise model, in which [61, 76] uses Gaussian statistics, [47] considers a Bivariate Gamma distribution, and [48] evaluates both Bivariate Rayleigh and K-distributions. To the best of the author's knowledge, the method proposed in [47] has the best performance for the evaluated CARABAS II data set without considering a SAR image stack scenario.

Recently, the authors in [31, 44] considered the use of small image stacks in change detection applications for wavelength-resolution SAR images. In [31], the author proposes a method to reduce false alarms in change detection methods for wavelength-resolution SAR images by using an adaptive noise canceller method, which uses three SAR images. In [44], a change detection method that uses three input images, which are combined into two new ones by a

subtraction operation is proposed. The difference images are processed using the combination of one STAP technique and an LRT, considering a Bivariate Gaussian clutter-plus-noise model. The experimental results presented in [31, 44] show that the use of image stacks can provide a performance improvement of the change detection methods by reducing the occurrence of false alarms. To the best of the author's knowledge, the method proposed in [44] has the best performance for the CARABAS II data set so far.

Another recent novelty that was evaluated using CARABAS II data was the proposed iterative change detection method based on Bayes' theorem presented in [46]. Instead of presenting a binary decision, as the majority of the methods discussed in this section, the method in [46] provides the probability of a candidate region containing a target. This non-binary information can be used by the system operator to achieve more adequate decisions. It is important to emphasize that a change detection method based on Bayes' theorem was the first technique used for CARABAS III data [82].

Based on the discussion presented in this section, it is possible to state that the change detection methods for wavelength-resolution SAR images are an important topic that continues to instigate studies in diverse research institutions in the world. Also, this interest is expected to increase, due to the recently developed CARABAS III system.

3.4 Concluding Remarks

This chapter presented the main properties and characteristics of wavelength-resolution SAR images, the CARABAS II system, the data set used to evaluate the proposals of this dissertation, and the state of art of the change detection methods for wavelength-resolution SAR images. Section 3.1 presented the main characteristics of wavelength-resolution SAR systems, which make them the optimal choice for change detection in FOPEN applications, i.e., large-fractional bandwidth, backscattering phenomenology, absence of speckle noise, relative time stability, and low signal attenuation by the foliage. Additionally, according to the information presented in the section and to other authors' observations, it is stated that the VLF frequency band is optimal for FOPEN change detection applications.

Based on the observations of Section 3.1, the CARABAS II data set was selected to be used in this dissertation. Section 3.2 briefly presents the CARABAS II system and details the available data set of 24 incoherent SAR images. Finally, Section 3.3 presents the wavelength-resolution SAR change detection state of the art, focusing on methods that used CARABAS II data in their evaluation.

4 Change Detection Based on Wavelength-Resolution Image Stacks

Change detection methods are used in several applications for SAR systems and have been studied for many decades [47, 83]. Recently, the authors in [31, 44] considered the use of small image stacks in change detection applications for wavelength-resolution SAR images. The experimental results presented in [31, 44] show that the use of image stacks can provide a performance improvement of the change detection methods by reducing the occurrence of false alarms. It is important to highlight that the use of image stacks in SAR high-resolution applications is a well studied topic [84, 85]. However, the use of image stacks in change detection applications using wavelength-resolution SAR images has not yet been well explored.

Motivated by the promising results presented in [31, 44], this chapter presents a statistical test analysis for SAR wavelength-resolution image stacks. Also, this chapter presents the proposal of change detection methods based on the statistical test analysis results. The proposed change detection methods are divided into two classes: Neyman-Pearson criterion-based, and masking techniques based.

4.1 Statistical Test Analysis

The data set used in the statistical test analysis is the open challenge data presented in Chapter 3. The data set contains 24 SAR incoherent wavelength-resolution images, which are divided into four missions and six passes. The images are equally divided into three stacks according to the flight geometry used during the data acquisitions, which means that the images belonging to the same stack have similar scattering properties. In particular, the images obtained with Passes 1 and 3 form Stack 1, while Stack 2 is formed with the images obtained with Passes

2 and 4; the rest builds Stack 3. Figure 4.1 provides image samples selected from Stacks 1, 2, and 3.

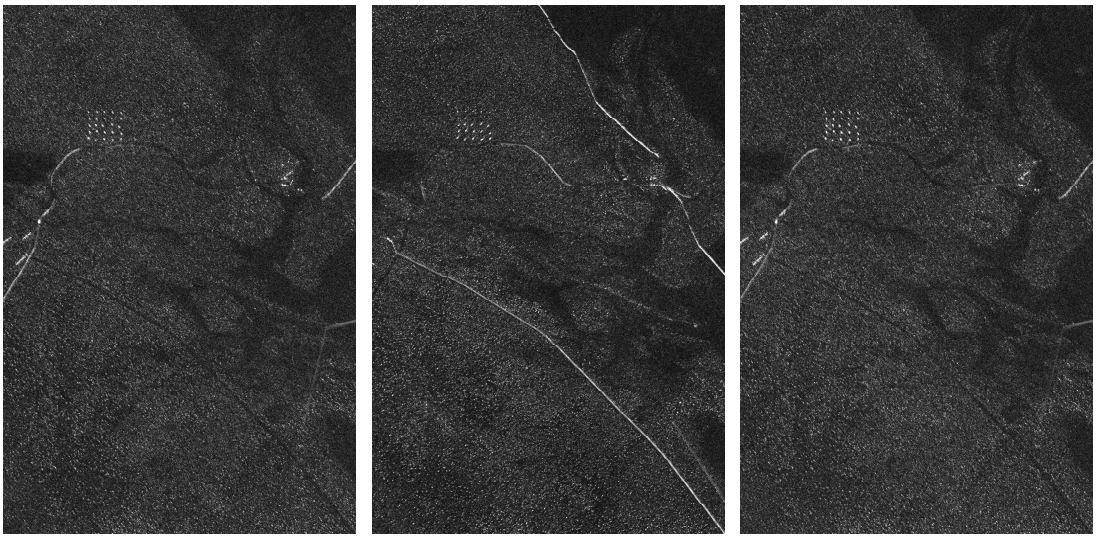

(a) (b) (c)

Figure 4.1: CARABAS II images obtained for (a) Stack 1, (b) Stack 2, and (c) Stack 3.

Based on the data set characteristics mentioned in Chapter 3, these images can be considered stable in time, and amplitude changes between them are mainly driven by thermal noise [65]. Considering the stack division and the properties of the images, a statistical test analysis is made between pixels in the "stack dimension," i.e., the same flight geometry time dimension.

The statistical test analysis is performed in each pixel position of one stack composed of 8 images with 6 million pixels per image. However, performing the test with only 8 pixels samples is inappropriate. Since the spatial resolution of the images is about 3 m $\times$ 3 m, 8 pixels surrounding the pixel of interest are also considered in the statistical test analysis. Thus, each assessed SAR data sample consists of 8 $\times$ 9 pixels. Figure 4.2 gives an illustrative example of how a tested pixel and its neighbors are chosen for the statistical test analysis, marked with blue and red colors, respectively.

The statistical test analysis aims to obtain well-fitted distribution models for the SAR data samples based on the "stack dimension." A possible approach to reach this goal is to evaluate candidate distributions in SAR data samples by the use of Goodness-of-Fit (GoF) tests [86, 87]. For the present analysis, the Anderson-Darling (AD) GoF test, which is one of the most frequently used GoF tests in the literature [88], is considered. The AD test and the evaluated candidates' distributions are presented in Sections 4.1.1 and 4.1.2, respectively.

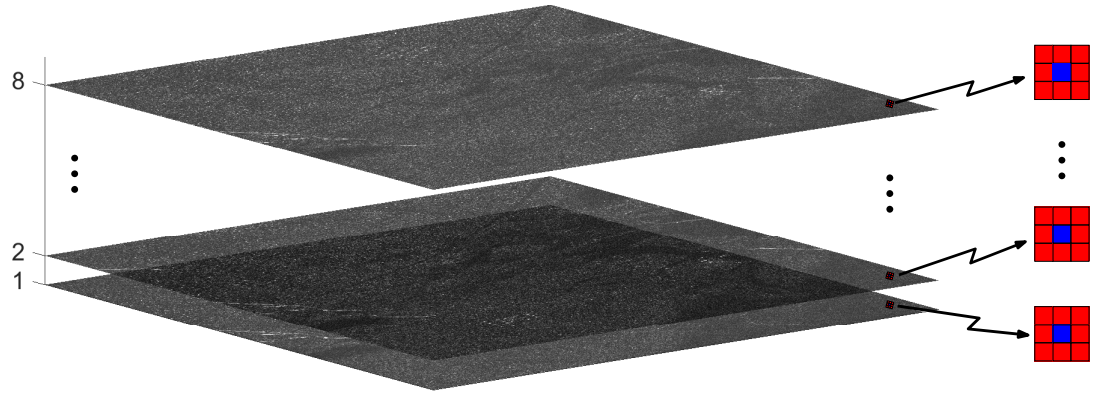

Figure 4.2: Sample of an image stack where an arbitrary pixel and the closest eight neighbors are highlighted in blue and red, respectively.

4.1.1 Anderson-Darling GoF Test

The use of the AD GoF test is motivated by the fact that it is well suited for the analysis of tailed distributions than other GoF tests [89], which are frequently associated to wavelength-resolution SAR images [47, 48] and SAR change detection applications, given that the target samples amplitudes are often stronger than the close surrounding pixels. Moreover, the AD test is considered the most powerful test based on the Empirical Distribution Function (EDF) [90].

The AD test consists of one statistical nonparametric hypothesis test, which aims to determine if a given null hypothesis (H_0) should be rejected, or not [91, 92]. Traditionally, the AD test is used to investigate if a given probability distribution null hypothesis yields a good fit for a given data sample [93, 94]. This GoF test consists of evaluating the distance A_n between $F_Y(y)$ and $F_0(y)$, which are, respectively, the EDF and the Cumulative Distribution Function (CDF) of H_0. According to [89], the distance A_n can be defined as

$$A_n \triangleq n \int_{-\infty}^{\infty} (F_Y(y) - F_0(y))^2 \phi(F_0(y)) dF_0(y), \tag{4.1}$$

where $Y = \{Y_i\}_{i=1}^n$ denotes the n tested samples and $\phi(t) = \frac{1}{t(1-t)}$ is a weight function defined for $0 \leq t \leq 1$.

By sorting in ascending order the observations $Y_1, Y_2 \ldots Y_i$ and by breaking the integral in (1) into n parts, it is possible to rewrite A_n as

$$A_n = -\sum_{i=1}^{n} \frac{(2i-1)[\ln Z_i + \ln(1 - Z_{n+1-i})]}{n} - n, \tag{4.2}$$

where $Z_i = F_0(Y_i)$.

The hypothesis test in the AD GoF test consists of a comparison between A_n and a critical value z. If $A_n > z$ the AD will reject the null hypothesis H_0; otherwise, the AD test fails to reject the hypothesis H_0 [89]. The selection criterion of z can be written as

$$Pr(A_n \geq z|H_0) = 1 - Pr(A_n < z|H_0) = \alpha, \tag{4.3}$$

where α is the significance level.

The distribution $Pr(A_n < z|H_0)$ is unknown [95]. However, the asymptotic solution presented in [95] for A_n given H_0 is a good approximation for the conditional probability. Thus, according to [95], this approximation can be written as

$$\begin{aligned}\lim_{n\to\infty} Pr(A_n < z|H_0) = \frac{\sqrt{2\pi}}{z}\sum_{j=0}^{\infty}\binom{-\frac{1}{2}}{j}(4j+1) \\ \times e^{\frac{-(4j+1)^2\pi^2}{8z}}\int_0^{\infty} e^{\frac{z}{8(1+w^2)}-\frac{w^2(4j+1)^2\pi^2}{8z}}dw.\end{aligned} \tag{4.4}$$

The number of operations required in the previously presented AD test equations (4.1)–(4.3) is very high. Thus, performing this method in the presented form would require a lot of computational resources. However by the numerical approximation presented in [95] for (4.4), the AD test becomes feasible in this statistical test analysis.

4.1.2 Candidate Distributions

As previously mentioned, the statistical test analysis considered in this chapter consists of the evaluation of SAR data samples based on the "stack dimension" using the AD GoF test for different candidate distributions. The three candidate distributions considered in this dissertation are:

i) Rayleigh – This distribution is suitable for modeling scattering regions composed of a large number of scatterers with similar strength. Thus, this distribution is traditionally used for statistically modeling the amplitude of SAR data [52]. Besides, the Rayleigh distribution is also suitable for modeling the amplitude of scattering regions in which the main contributions come from additive noise, as the evaluated wavelength-resolution images. Based on this knowledge, the pixel positions from an image stack related to areas with the absence of a strong scatter can

be modeled as Rayleigh distributed. The PDF of a Rayleigh distribution can be written as

$$p(x) = \frac{x}{\sigma^2} e^{-\frac{x^2}{2\sigma^2}}, \tag{4.5}$$

where σ is a scale parameter and x is a non-negative real number ($x \geq 0$).

ii) Rician – This distribution is suitable for a scattering medium composed of a large number of scatterers and with a dominant one [96]. In addition, the Rayleigh distribution is a special case of the Rician distribution, which also makes this distribution indicated for low backscattering areas and regions without the dominance of one scatterer. Thus, the Rician distribution is suitable for modeling scenarios with a possible scatterer presence in the tested pixel position. The PDF of a Rician distribution is expressed by

$$p(x) = \frac{x}{\sigma^2} e^{-\frac{(x^2+\nu^2)}{2\sigma^2}} I_0\left(\frac{x\nu}{\sigma^2}\right), \tag{4.6}$$

where σ is a scale parameter, ν is a parameter related to the dominant scatterer, x is a non-negative real number ($x \geq 0$), and I_0 is the modified Bessel function of the first kind with order zero.

iii) Log-normal – This distribution is suitable to model land clutter over built-up areas [97]. Its long-tail patterns provide an acceptable match for the statistics of the CARABAS II images in the spatial domain. Even being more empirical than the others, the log-normal distribution can be suitable to model changes between images from the stack. The PDF of a log-normal distribution is given by

$$p(x) = \frac{1}{\sqrt{2\pi}\sigma_t x} e^{-\frac{\ln(x-\mu_t)^2}{2\sigma_t^2}}, \tag{4.7}$$

where x is a positive real number ($x > 0$), σ_t and μ_t are, respectively, the standard deviation and the mean value of the natural logarithm of the random variable.

4.1.3 Experimental Results

This section presents the experimental results for the statistical test analysis considering the three distributions hypotheses: Rayleigh, Rician, and Log-normal. The AD GoF test is performed for all the pixel sets, i.e., all pixels in all three image stacks where each stack consists of 8 CARABAS II images. The test is performed for $\alpha = 0.05$, which is a typical significance level value considered for this kind of test [98]. All parameters needed in the distributions

(4.5)–(4.7) are estimated by using the Maximum Likelihood Estimator (MLE), applying the necessary numerical considerations to respect the restrictions of the parameters.

The presented statistical analysis is related to a multi-comparison scenario. Thus, an increase in the occurrence of false positives (Type I errors) is expected [99]. To alleviate this problem, Type I error control techniques are usually applied, such as Bonferroni correction; Family-wise error rate control; and false discovery rate [99, 100]. However, it is not possible to control Type I errors and false-negative occurrences (Type II errors) simultaneously [59]. Furthermore, trying to control Type I errors could be statistically too conservative considering the number of multiple tests performed, resulting in a significant increase in the number of Type II errors [101]. Thus, to avoid the possible increase of Type II errors, which could lead to loss of information related to targets, this kind of control technique will not be used in this dissertation.

The experimental results of the AD GoF test are presented in Figure 4.3, for Stacks 1, 2, and 3. The metric used in Figure 4.3 is defined as the percentage of times that the AD test fails to reject the tested null hypothesis. The experimental results show that the Rician distribution is the best fit among the tested distributions. The output of the AD GoF test for the Rician distribution was positive in 98.59% of the samples (pixel and its neighbors) for Stack 1, 98.42% for Stack 2, and 98.17% for Stack 3.

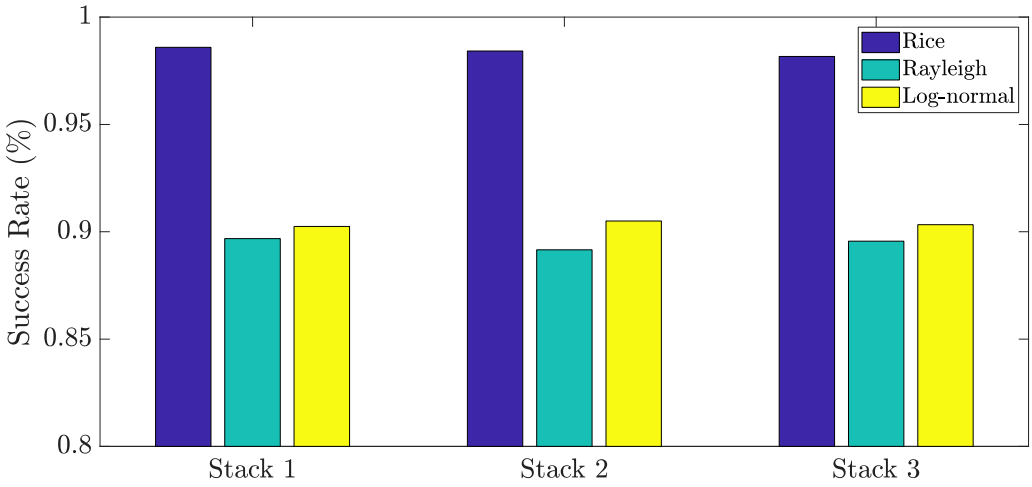

Figure 4.3: Anderson Darling GoF test for the candidate distributions considering Stacks 1, 2, and 3.

To further evaluate the GoF of the Rician distribution for the image stacks, the images are divided into three different scattering regions. The evaluation was based on the estimation of the Rician parameters of three random pixel-sets samples of each region. The set of pixels was obtained in the same way as described in Section 4.1.1. The scattering regions were classified as:

1) The first region is related to a lake, which is characterized by sets that contain only low amplitude pixels. At VHF band frequencies, the surface of the lake does not have substantial backscattering due to the long wavelength of the radar wave. This behavior is also expected in open areas and corresponds to the most common type of scenario for those SAR stacks. It is expected that Rayleigh and Rician distributions could yield a good fit for this kind of region.
2) The second region is related to areas that have a dominant scatterer. This region can be characterized by human-made objects, e.g., power lines, fences. This group contains only pixels with strong amplitudes. Thus, it is expected that the Rician distribution could yield a good fit for these sets.
3) The third region is related to areas that contain a real target (change) in at least one of the stack images. Since the database contemplates only four target deployments, there will be only two images with targets in this scenario per evaluated region. Thus, this region is characterized by a large number of pixels with low amplitude and a small number of pixels with high amplitude. It is expected that long-tail distributions could yield a better fit for this kind of scenario.

Table 4.1 presents this evaluation, where each line shows the estimated parameters for a random pixel position for each region. Also, each line presents the AD GoF test indication variable h, where $h = 0$ indicates a failure to reject the distribution hypothesis. Otherwise, $h = 1$ indicates an AD GoF test rejection of the null hypothesis.

Table 4.1: Rice estimated parameters and AD GoF test results for different groups of pixel-sets.

Groups	Stack 1		Stack 2		Stack 3		h
	$\hat{\sigma}$	$\hat{v}$	$\hat{\sigma}$	$\hat{v}$	$\hat{\sigma}$	$\hat{v}$	
1: Lakes	0.077	0.050	0.057	0.064	0.061	0.055	0
	0.056	0.072	0.045	0.077	0.066	0.063	0
	0.042	0.083	0.071	0.004	0.088	0.001	0
2: Strong scatterers	0.207	1.476	0.175	0.912	0.252	1.261	0
	0.275	0.535	0.352	1.231	0.347	0.453	0
	0.196	0.99	0.293	0.678	0.200	0.924	0
3: Targets	0.468	0.018	0.379	0.005	0.435	0.013	1
	0.497	0.014	0.39	0.01	0.399	0.009	1
	0.456	0.013	0.298	0.007	0.511	0.02	1

To correctly evaluate whether the rejection on the AD GoF test could characterize the presence of a change, the statistical test results for one image stack are presented in the form of binary images in Figure 4.4. These results are presented for the three candidate distributions, where each pixel is represented using the output h. It is possible to observe two different patterns in Figures. 4.4 (a) and (b); however, this pattern is not visible in Figure 4.4 (c). The first pattern

is characterized by the isolated pixels, which are mainly related to Type I errors and minor changes associated with the randomness present in the images that form the stacks. The second one is characterized by agglomerations of unitary pixels, which refer to changes present in the image(s) from the stack. For better visualization of the detected changes, they are highlighted by red rectangles.

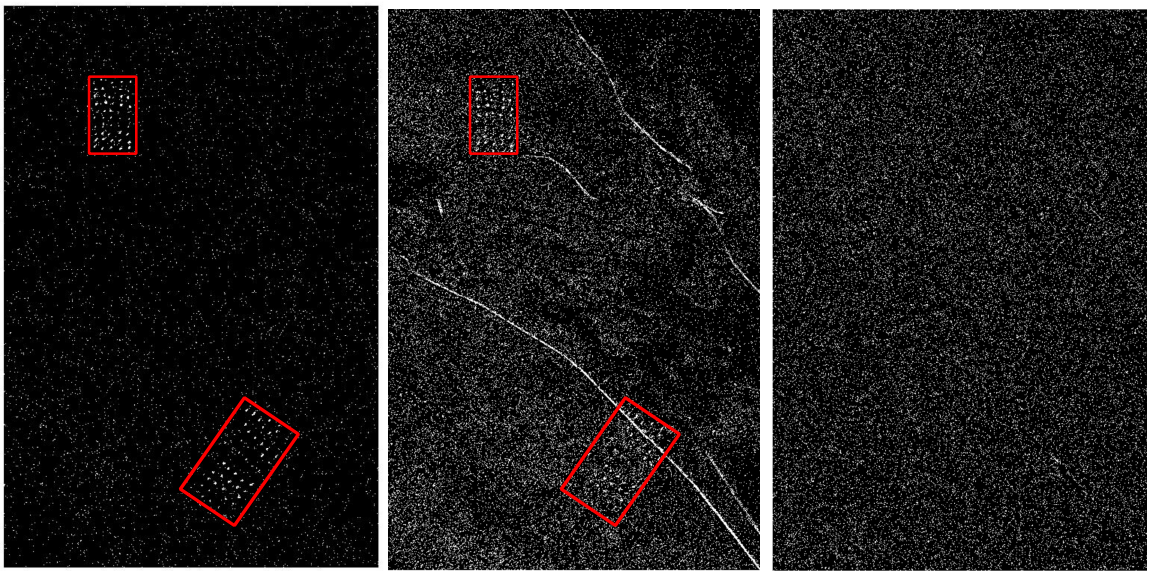

(a) (b) (c)

Figure 4.4: The AD GoF test results for an image stack considering the null hypotheses as (a) Rician, (b) Rayleigh, and (c) Log-normal, respectively. The target deployment areas are highlighted when the targets are visible.

Based on the scattering characteristics of the tested samples, the results presented in Figure 4.4 are theoretically consistent. It was expected that both the Rayleigh and the Rician distributions would not be able to provide a good fit for regions where real changes occur. Moreover, it was also not expected that the Rayleigh distribution would have a good fit for regions with the presence of a dominant scatterer, such as the visible elongated structures presented in Figure 4.4 (b). Finally, it is important to highlight that no pattern behavior could be detected in Figure 4.4 (c).

The tested scenario is not ideal, given the necessity of the use of the pixel neighbors, which are not truly independent when compared with the tested one. A more accurate scenario for the statistical test would require a higher number of images with the same flight geometries. A statistical test is used considering a SAR image stack with images from Stacks 1 and 3, which contains similar flight geometries, as presented in Chapter 3. For this analytical test, only the pixels from each tested position were considered, resulting in 16 data samples per test. The

results of the test are presented in the form of a binary image in Figure 4.5. Based on the results presented in Figures 4.3 and 4.4, only the Rician distribution was tested.

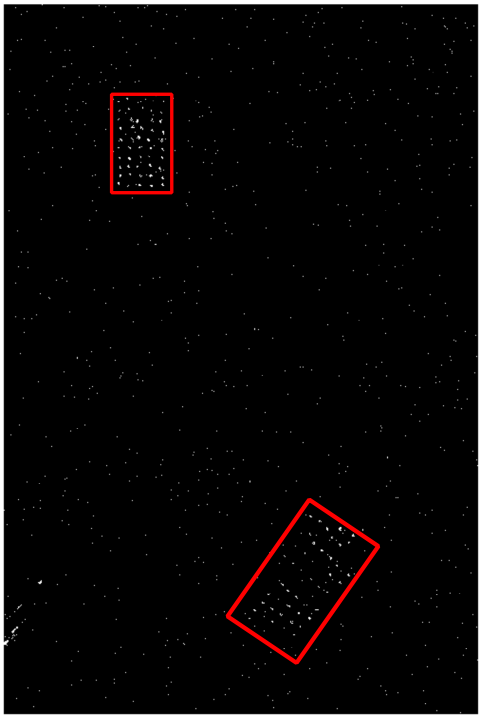

Figure 4.5: The AD GoF test results for the image stack with slight differences in the flight geometry, considering the Rician distribution hypothesis. The target deployment areas are highlighted when the targets are visible.

The experimental results show that the output of the AD GoF test for the Rician distribution was positive in 99.67% of the samples. This result is similar to the ones observed in Figure 4.4, from which the same conclusions about the analysis for the Rician distribution can be drawn. However, Stacks 1 and 3 have similar but not equal flight geometries, which usually results in different statistical properties for the stack data. The use of image stacks with images from different passes may result in totally unexpected observations, especially with the increase of flight geometries discrepancies.

Based on the results presented in Figure 4.4, a relation between the presence of changes in the image(s) of a stack and the rejection of the Rician and Rayleigh distribution null hypotheses in the AD GoF test can be established. Also, it is suitable to say that long-tail distributions, which are usually used to model SAR images, do not provide a good fit for stacks of wavelength-resolution SAR images. Finally, based on the results presented in Figures 4.4 and 4.5, it is suitable to say that the Rician distribution yields a good fit for most of the pixels in the wavelength-resolution SAR image stacks.

4.2 Neyman-Pearson Criterion-Based Change Detection Methods

This section presents the proposal and evaluation of two Neyman-Pearson criterion-based change detection methods for wavelength-resolution SAR image stacks. These techniques are named Change Detection Method Based on NP using a Sub-optimal Criterion (NPSOC) and Change Detection Method Based on NP-Criterion (NPC). A simplified block diagram for the processing of both change detection methods is presented in Figure 4.6. According to the processing scheme, the block diagram inputs are one surveillance image, the parameters of the background distribution, and, if available, information from the target statistics. The background distribution parameters are obtained from the image stack data.

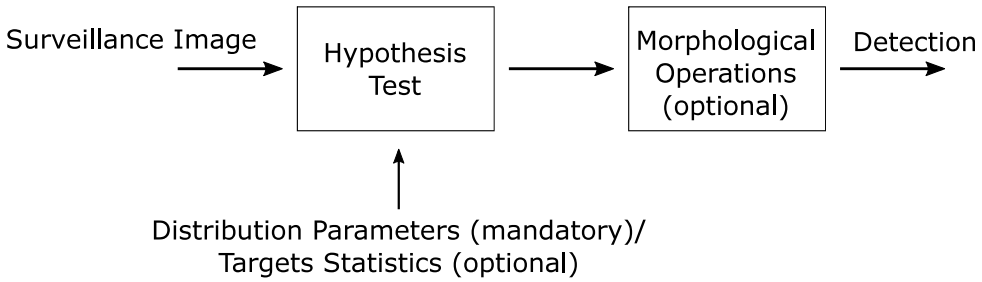

Figure 4.6: Simplified block diagram for the proposed change detection methods.

From the experimental results presented in Section 4.1.3, the background statistics for SAR wavelength-resolution image stacks are modeled as a Rician distribution in the course of Section 4.2. Based on the available CARABAS II data set and the images flight geometry, each stack could have a maximum of eight images. However, to extend the range of applications where the proposed methods could be applied, the use of images with the same target deployment as the surveillance image is not considered in the stack. So, the distribution parameters for each pixel position are obtained from data of six images with the same flight geometry, using the same setup presented and discussed in Section 4.1. Thus, each assessed sample consists of 6×9 pixels, and the background statistics are calculated, pixel-by-pixel, for all the 6 million-pixel positions.

The first block presented in Figure 4.6 consists of a hypothesis test applied to each pixel position. Both proposed change detection methods are based on the Neyman-Pearson hypothesis test. To facilitate the understanding of the proposed method, the NP criterion presented in (2.20)

can be rewritten as

$$\frac{p(z_s|H_1)}{p(z_s|H_0)} \underset{H_0}{\overset{H_1}{\gtrless}} \tau, \tag{4.8}$$

where z_s is the pixel amplitude of a particular pixel position in the surveillance image τ is a threshold, H_0 is the hypothesis that the evaluated pixel is background-related, and H_1 is the hypothesis that the evaluated pixel is target-related (change). For the sake of simplicity, in this chapter, the following denominations $p(z_s|H_0)$ as $p(z_s|B)$, and $p(z_s|H_1)$ as $p(z_s|T)$ are used.

Additionally, one optional morphological operations block is included as the final stage of the processing chain. Morphological operations are frequently used for this type of data set to avoid the appearance of isolated and fragmented objects. For a fair performance comparison in Section 4.2.3, similar morphological operations like the ones considered in [44, 47, 61] are adopted. These operations are one erosion with a structuring element with the size of the system resolution cell (3×3), followed by dilatations whose size enables the merging of detection pixels within a distance lower than 10 m.

The output of the processing scheme is a binary image that contains the detected targets and false alarm (if any). This type of binary image is the output standard for all change detection methods proposed in this dissertation. Figure 4.7 presents a final detection image example, where the detected targets and the false alarms are highlighted.

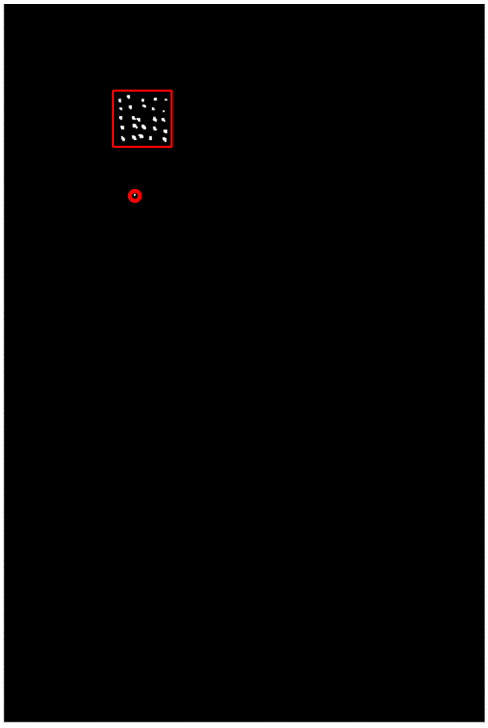

Figure 4.7: Example of a final detection image where the detected targets and the false alarms are highlighted.

Finally, the proposed change detection methods only differ from each other in the hypothesis test block. The hypothesis test of each method is discussed and detailed in Sections 4.2.1 and Section 4.2.2.

4.2.1 NPSOC

Most practical applications using change detection techniques do not have enough information on the target statistics. In general, only the background distribution can be characterized. A sub-optimal detection criterion can be used to avoid assumptions for the distribution $p(z_s|T)$, as the method presented in [52]. In this method, an image sample would be assigned as a target, i.e., not belonging to the background statistics, if

$$p(z_s|B) \leq \tau. \tag{4.9}$$

One example of this hypothesis test is presented in Figure 4.8. Considering the thresholds, t_1, t_2, presented in Figure 4.8, and a single background-pixel sample, the probability that this sample is considered a target (false alarm probability) is given by

$$P_{\text{FA}} = \int_0^{t_1} p(z_s|B)dz_s + \int_{t_2}^{\infty} p(z_s|B)dz_s. \tag{4.10}$$

Most change detection applications focus on targets present in the distribution tails, which is the case for the CARABAS II data set. Thus, the area over the interval $z_s < t_1$ can be disregarded. Besides, for the majority of distributions considered for this kind of application, this area will present a small value when compared with the area for $z_s > t_2$. Thus, (4.10) can be approximated as

$$P_{\text{FA}} \approx \int_{t_2}^{\infty} p(z_s|B)dz_s. \tag{4.11}$$

Based on (4.11), t_2 is defined for each sample given a fixed P_{FA}. Thus, it is possible to define the threshold τ as

$$\tau = p(t_2|B), \tag{4.12}$$

substituting (4.12) into (4.9)

$$p(z_s|B) \leq p(t_2|B), \tag{4.13}$$

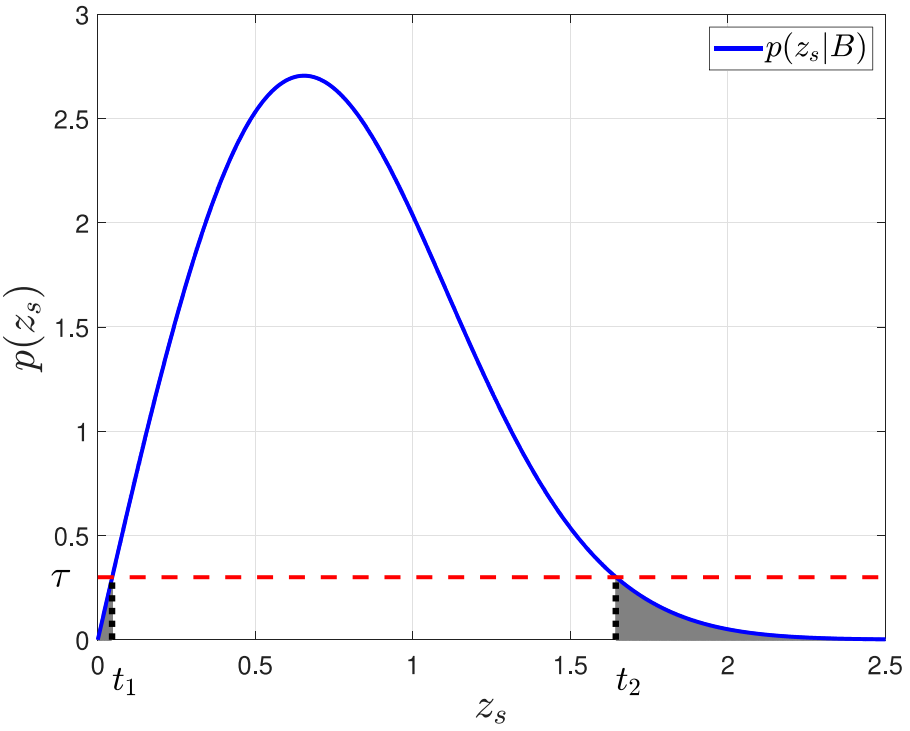

Figure 4.8: Hypothesis test for a given sample of $p(z_s|B)$ as a Rician distribution. The gray highlighted area is related to the false alarms region according to (4.10).

which results in the detection criterion $z_s \geq t_2$. It is possible to rewrite (4.11) in terms of the background CDF, which is given by

$$\begin{aligned} 1 - P_{\text{FA}} &\approx \int_{-\infty}^{t_2} p(z_s|B)dz_s \\ &\approx P_{\text{B}}(t_2), \end{aligned} \tag{4.14}$$

where $P_{\text{B}}(\cdot)$ is the background CDF. From (4.13), the detection criterion can be written as

$$P_{\text{B}}(z_s) \geq P_{\text{B}}(t_2), \tag{4.15}$$

substituting (4.14) into (4.15), we obtain the following detection criterion

$$P_{\text{B}}(z_s) \geq 1 - P_{\text{FA}}. \tag{4.16}$$

The detection criterion presented in (4.16) directly correlates the background CDF with a fixed false alarm probability. However, for traditional SAR change detection scenarios, which obtains the background statistics using the information of the whole image, this detection

criterion will detect as a target any sample that contains high amplitude. Thus, for these scenarios, the proposed criterion could result in a large number of false alarms.

To overcome this problem, the setup of the statistical test, discussed in Section 4.1, is considered to obtain the background statistics for a given pixel sample. Thus, without loss of generality, the constant τ can be converted into a function of the pixel position $\tau(z_s)$, for a fixed P_{FA}. This procedure can be performed using (4.12) and (4.13) for each pixel position, considering its Rician estimated parameters.

As previously observed in Section 4.1, the background statistics samples can be modeled as a Rician distribution, considering the distribution parameters σ and ν. Thus, the background samples related to strong scatterers tend to present high values of ν. For the Rician distribution, the higher is the ν value smoother will be the inclination of the sample CDF, as can be observed in Figure 4.9.

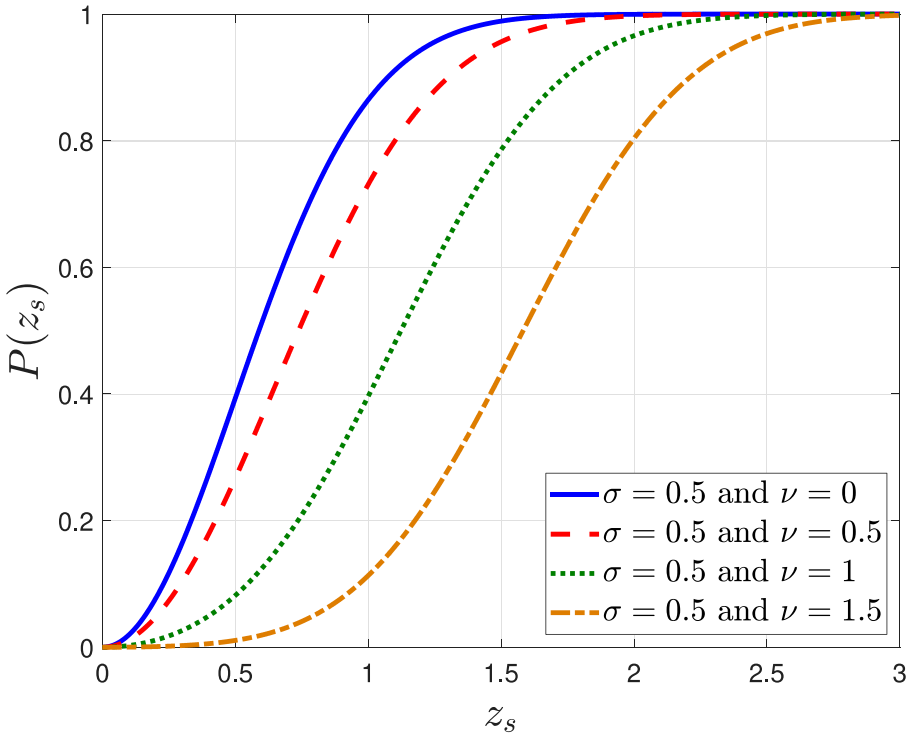

Figure 4.9: CDF for different values of ν.

As can be observed in Figure 4.9, for a fixed P_{FA}, the higher is the ν parameter, the higher will be the threshold $\tau(z_s)$. Thus, the detection criterion (4.16) applies different thresholds for each tested pixel, being able to avoid most of the false alarms related to the region that contains strong scatterers in the background. Based on that, the proposed change detection method consists of the processing scheme shown in Figure 4.6, considering the hypothesis test presented in (4.16) using the image stack background statistics.

4.2.2 NPC

The detection criterion presented in (4.16) used in the NPSOC method directly correlates the background CDF with a fixed false alarm probability and only requires information about the background statistics. However, for some change detection applications, there is some information available on the target statistics, which can be exploited to improve the method's performance. Under these conditions, the detection criterion of (4.8) can be considered.

For the considered CARABAS II data set and other similar ones, it is assumed that the targets have an amplitude signature that ranges from a minimum amplitude a_{min} to a maximum amplitude a_{max} as considered in [46, 82]. The assumption of an amplitude signature for targets is acceptable for change detection applications, as can be observed in [30, 61, 76]. Moreover, it is possible to state that the targets' statistics are similar, based on the stability of this type of image, and assuming a specific type of target. For the sake of simplicity, it is considered that the targets present a uniform distribution [46, 82].

Figure 4.10 presents one example of the hypothesis test (4.8) considering $p(z_s|B)$ as a Rician distribution using the stack statistics and $p(z_s|T)$ as a uniform distribution. Thus, the false alarm probability can be written as

$$P_{\mathrm{FA}} = \int_{t_2}^{a_{max}} p(z_s|B)dz_s, \tag{4.17}$$

where t_2 is the projection of the threshold τ in the x-axis. Based on the assumption of a uniform distribution for $p(z_s|T)$, an upper-bound for P_{FA} can be written as

$$P_{\mathrm{FA}} \leq \int_{t_2}^{\infty} p(z_s|B)dz_s. \tag{4.18}$$

It is possible to rewrite (4.18) in terms of the background CDF, which can be described as

$$1 - P_{\mathrm{FA}} \leq P_{\mathrm{B}}(t_2). \tag{4.19}$$

Thus, t_2 can be written as

$$t_2 = Q(1 - P_{\mathrm{FA}}), \tag{4.20}$$

where $Q(\cdot)$ is the Quantile function and t_2 is related to the threshold τ according to (4.12).

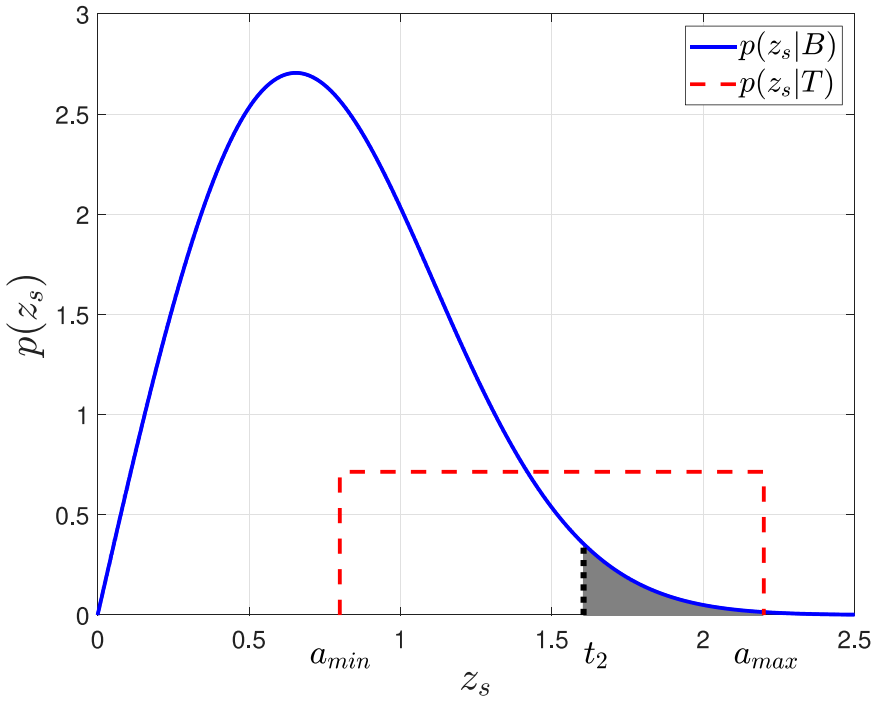

Figure 4.10: Hypothesis test for a given sample considering $p(z_s|B)$ as a Rician distribution and $p(z_s|T)$ as a uniform distribution. The gray highlighted area is related to the false alarms region according to (4.8).

4.2.3 Experimental Results

This section presents the experimental results for the performance evaluation of both NPSOC and NPC detection methods, considering the CARABAS II data set. The methods' performance is assessed in terms of the probability of detection, i.e., the ratio of the number of detected targets to the known number of targets, and the False Alarm Rate (FAR), i.e., the number of false alarms per square kilometer. For this analysis, every object detected by the methods was considered as a change, even knowing that some of them could be related to systems or image formation issues.

For the evaluation, as previously mentioned, the probability $p(z_s|B)$ is considered as Rician distributed and $p(z_s|T)$ as Uniform distributed. The parameters of the distribution $p(z_s|B)$ are obtained according to the previously described methodology, in the introduction of Section 4.2. The parameters of the distribution $p(z_s|T)$, a_{min} and a_{max}, are selected according to assumptions on the targets.

It is expected that target-related pixels, for data sets similar to the CARABAS II data set, will present higher amplitudes than background-related pixels. Also, no information regarding the maximum amplitude of target-related pixels is expected. Based on these assumptions, the set of

values $a_{min} \in [0.2; 0.3; 0.4]$ considered in [47] is used. Besides, for the sake of simplicity, we adopted a_{max} as the highest pixel amplitude value of the surveillance image.

It is important to emphasize that more information on the targets can be considered to enable the use of better-matched distributions for $p(z_s|T)$, which could lead to an increase in the proposed method performance. However, a bad choice of the distribution $p(z_s|T)$ or its parameters can result in worse performances in terms of P_d or even the failure to detect targets for some thresholds. It is noticeable that the methodology described in Section 4.2 only guarantees that the performance of the NPC method will be equal or better than the NPSOC in terms of false alarm probability.

The threshold selection for the NPSOC method is based on (4.16), under the selection of different constant values of $P_{\text{FA}} = 10^{-n}$, using $n \in [1, 2, 3...]$. For the NPC method, the threshold can be obtained by using (4.20) and (4.12). However, this selection requires a large number of mathematical operations due to the necessity to calculate the quantile function for every tested pixel. Based on the number of tested images and their sizes for the CARABAS II data set, this selection becomes unpractical. To simplify the threshold choice, $t = 10^{j}$ is considered, where $j \in [0, 1, 2, 3...]$, which guarantee $p(z_s|T) \geq p(z_s|B)$ and overcomes the computational complexity issue for this data set. However, for data sets or situations with less tested pixels, the threshold selection considering the derivation presented in Section 4.2 becomes more suitable.

Based on the previously described implementation aspects, a comparison between the NPSOC and NPC method is made in terms of their Receiver Operating Characteristic (ROC) curves. The results are presented in Figure 4.11.

By analyzing points with the same probability of detection, Figure 4.11 shows that, for the majority of cases, the NPC outperforms the NPSOC method in terms of FAR. Thus, the assumptions related to target statistics for the CARABAS II data set were sufficiently adequate to achieve performance gains, for the majority of the studied cases. However, a saturation in terms of detection probability is observable in the NPC curve with $a_{min} = 0.4$, which results in the NPSOC outperforming the NPC method with $a_{min} = 0.4$ for $P_d > 0.991$.

The combination of an imperfect selection of the a_{min} and the erosion morphological operation caused the observed saturation. This combination of not accurate selections fails to detect four targets for the evaluated scenario. This issue could be solved by pre-processing the surveillance image, e.g., using an average filter as in [61, 76]. However, usually, the use of pre-processing techniques would lead to variations in the target statistics. Also, the selection

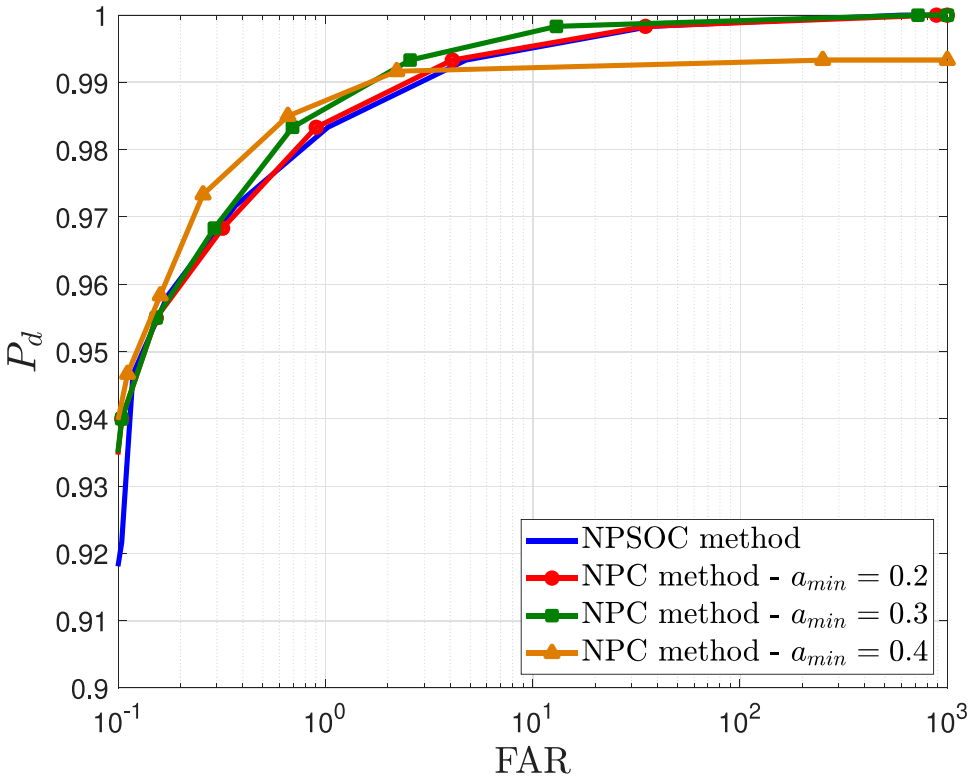

Figure 4.11: ROC performance for both proposed NP based methods.

of the pre-processing technique and its parameters should be made to each specific application resulting in very specific methods. Thus, to perform a fair comparison between the evaluated methods, the pre-processing of the surveillance image was not considered.

To validate the use of image stacks in change detection methods, a comparison analysis is presented. This analysis consists of the comparison between the proposed methods based on image stacks and others based on the use of only one reference image. For this analysis, two methods were selected. The first method is the one presented in [61], which was one of the firsts techniques used to perform change detection in CARABAS II images. The other one is the method proposed in [47], which has, to the best of the author's knowledge, the best performance for the CARABAS II data, without considering a SAR image stack scenario. This comparison is based on the results presented in Figure 4.12. For better visualization of the results, only the two best ROC curves presented in [47], and the best ROC curve presented in [61] are shown in Figure 4.12. Also, the curve for the NPC with a_{min} = 0.2 was omitted for the same reason. Finally, the original notation presented in [47] and [61] was kept for the sake of simplicity.

As can be observed in Figure 4.12, the proposed methods outperform the other evaluated ones both in terms of P_d and FAR, excluding the saturation region for the NPC method with a_{min} = 0.4. These results corroborate the use of image stacks to improve the performance of

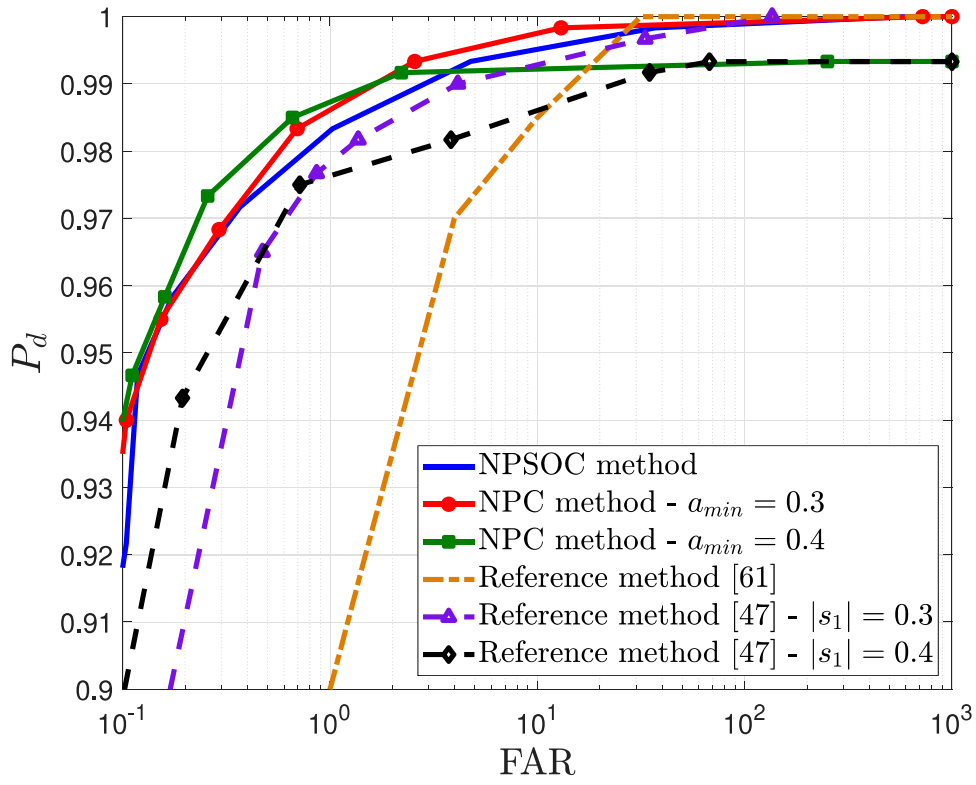

Figure 4.12: ROC performance comparison among the proposed methods and the selected curves of the reference methods.

change detection methods in terms of probability of detection and FAR. Also, comparing the NPC method with $a_{min} = 0.4$ and the reference method [47] with $|s_1| = 0.4$, both methods present an observable saturation in terms of the probability of detection. This phenomenon is caused by the use of a similar target amplitude consideration.

Another evaluation made in this section is a comparison between the proposed methods and the proposal presented in [44], which are all based on image stacks. To the best of the author's knowledge, the method presented in [44] has the best performance in terms of FAR and the probability of detection for the CARABAS II data set so far. This method considers the subtraction of two reference images with the same target deployment to be used in the hypothesis test associated with a surveillance image. This comparison is based on the results presented in Figure 4.13. For visualization purposes, the curve for the NPC with $a_{min} = 0.2$ was omitted, and only the best ROC curves of the reference method [44] are presented.

As can be observed in Figure 4.13, the proposed methods have similar performance when compared with the method of [44]. It is possible to state that the NPC method with $a_{min} = 0.4$ and the NPSOC presents better performance than the best ROC curve of the reference method for $P_d \leq 0.99$ and $P_d \leq 0.959$, respectively. Moreover, the NPSOC and NPC methods enable

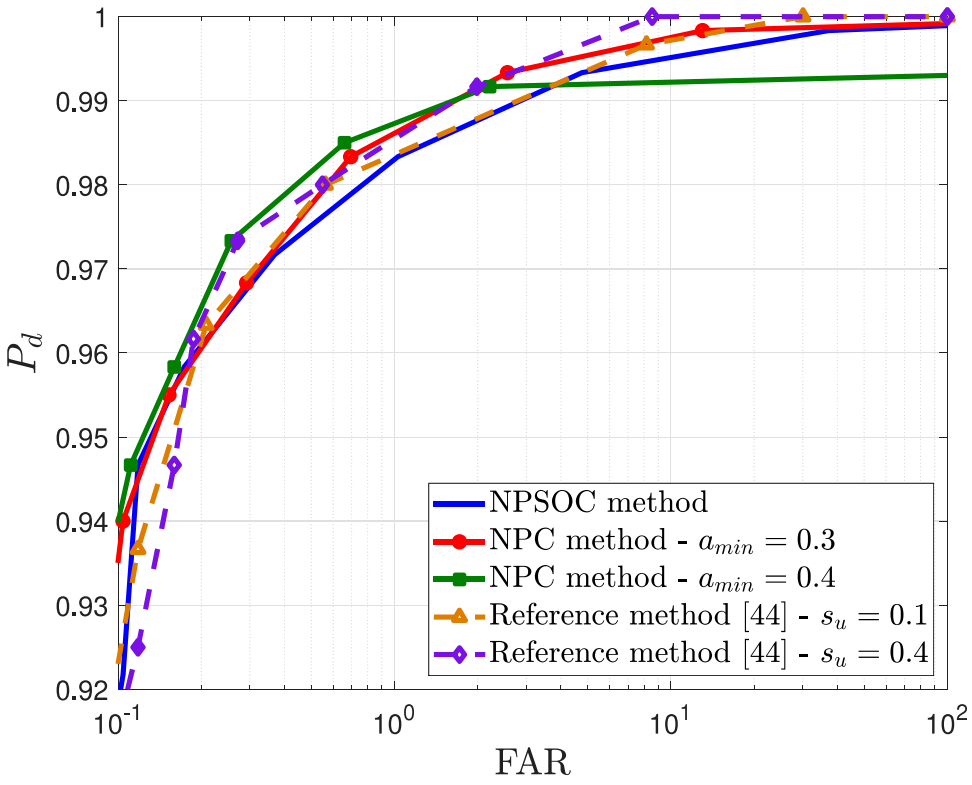

Figure 4.13: ROC performance comparison among the proposed method and the best curves of the reference method.

the use of more images in the stack, which can provide better estimations of $p(z_s|B)$ and often for $p(z_s|T)$. Also, the methods do not require that the reference images contain the same target deployment. These characteristics enable the use of the proposed method in a greater number of applications. Finally, the NPC performance can be further improved when more prior information about the targets is available or when the system enables the use of pre-processing techniques. However, as previously mentioned, these situations were omitted to guarantee a fair comparison between the evaluated techniques.

4.3 Change Detection Methods Based on Masking Techniques

According to the definition of masking presented in [102], this technique consists in to generate a binary image from a point operator applied in two images, i.e., the mask image and the image to be masked. Obtaining and using image masks more effectively is an important research topic from the image processing area, especially for segmentation applications [103]–[105].

The output of the statistical analysis presented in Section 4.1.3 is a binary image that can be used as a mask image in masking techniques. Also, according to the discussion presented

in Section 4.1.3, changes in one or more images of the stack will be characterized by an agglomeration of failures in the AD GoF, for a Rician distribution null hypothesis. Thus, based on the definition of masking techniques and the previous observation, two masking change detection methods are proposed and evaluated in the following sections. These techniques are named Simple Masking Detection (SMD) and Multiple Concatenated Masking Detection (MCMD).

Both proposed change detection methods consider the same processing scheme, which only differs in terms of the mask obtaining procedure. This processing scheme is presented in Figure 4.14. The masking procedure is the first block of the processing scheme and can be described as

$$I_u = I_s \circ M, \tag{4.21}$$

where, I_u represents the updated image, i.e., the output of the masking process, I_s is the surveillance image, M is the binary mask image generated by the same dimension as I_u, and the operation ($\circ$) represents the Hadamard product [106].

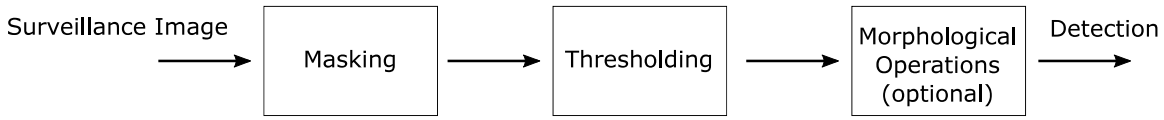

Figure 4.14: Simplified block diagram for the proposed change detection methods.

The second block presented in Figure 4.14 is a detection procedure based on a fixed threshold. The output of the block is a binary image where the evaluated pixels with amplitudes above the fixed threshold are represented by unitary amplitude pixels, whereas the other pixels are represented by pixels with null amplitude. Finally, the third block is an optional block composed of a series of morphological operations. These operations are selected according to the methods' application specificity.

4.3.1 SMD

As previously mentioned, the change detection methods using masking techniques proposed in Section 4.3 are based on the statistical analysis and in the observations presented in Section 4.1. In this way, the SMD technique consists of using as a mask the binary output image generated by the statistical analysis presented in Section 4.1. Thus, for the available CARABAS II data, three masks can be obtained, each one associated with the Stacks 1, 2, and 3, respectively. Figure 4.15 presents one example of an SMD mask where the target deployments are highlighted.

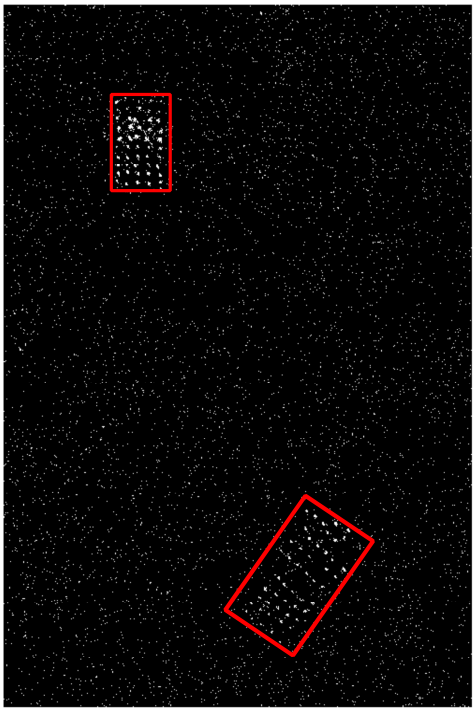

Figure 4.15: SMD mask where the target deployments are highlighted.

It is important to emphasize that, to the correct functioning of the SMD change detection method, the statistical analysis constraints must be respected, such as the use of an appropriate amount of tested pixel samples and the use same flight geometry images. Also, at least one image with the same target deployment as the surveillance image must compound the evaluated image stack. A simple way to fulfill this second requirement, without requiring any prior knowledge about the targets, is to include the surveillance image in the evaluated stack.

4.3.2 MCMD

The MCMD technique uses as a mask one binary image resulting from one concatenation procedure. This concatenation process is the result of the Hadamard product of all binary image masks obtained using the previously described SMD approach. This mask can be written as

$$M = M_1 \circ M_2 \circ \cdots \circ M_{NI}, \tag{4.22}$$

where M_i is the i-th mask from the SMD method, NI is the total number of SMD masks, and $i = 1 \ldots NI$. The MCMD mask for the available CARABAS II data is presented in Figure 4.16 where the target deployments are highlighted.

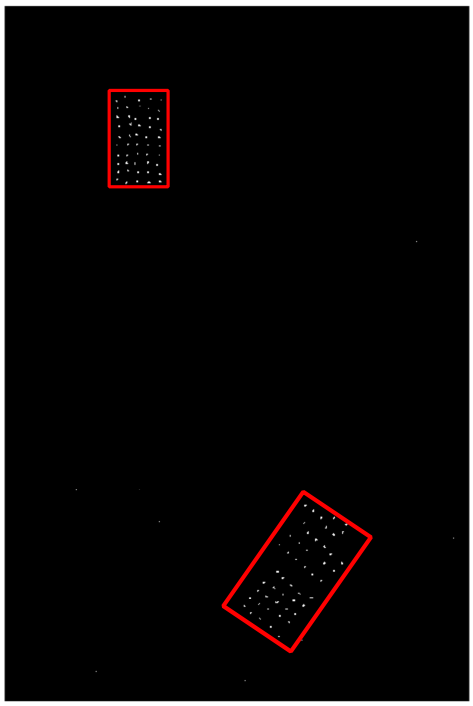

Figure 4.16: MCMD mask where the target deployments are highlighted.

Comparing the masks presented in Figures 4.15 and 4.16, the MCMD mask is more selective than the masks from the SMD method. This selectivity tends to lead to a lower occurrence of false alarms. However, it could also lead to a reduction in the target detection probability.

Besides of it, to correctly obtain the MCMD mask, the masks used in the concatenation process must contain the target deployment of interest. Thus, the target deployment of the surveillance image must be present in at least one image of each stack used in the masks of the concatenation process. This requirement reduces the number of applications where the method could be used. However, there are still applications where this method can apply, e.g.,

image stack applications focusing on fixed targets (concealed structures, land mines, and hidden objects), or image stacks applications using different flight geometry measurements obtained in short periods.

4.3.3 Experimental Results

The experimental evaluation of the proposed change detection methods based on image stacks considers all the 24 incoherent CARABAS II images from the data set presented in Chapter 3. Similarly, as Section 4.2.3, the methods' performance is assessed in terms of the P_d and FAR. Moreover, the same decision criterion is considered for any object detected.

For the studied data set, target-related pixels tend to present higher amplitudes than the clutter-related pixels. So, it would be suitable to selected threshold values similar to the ones used as the expected minimum target amplitudes $z_{s_{min}} \in [0.2; 0.3; 0.4]$ considered in [47], for the same data set. However, to obtain a higher range of P_d and FAR values, the set of possible thresholds is extrapolated to a set with a higher range of amplitude values. Thus, for this evaluation, the fixed threshold lies in the range of [0, 0.5]. Finally, the same morphological operations considered in Section 4.2 are applied to the evaluated images.

The combination of a very selective mask, like the one in the MCMD method, and the erosion operation could turn impossible to detect targets. This saturation phenomenon was already observed in Section 4.2.3. To better visualize this situation, a scenario with a pre-processing block in the block-diagram processing-chain input is considered. This pre-processing block consists of one average filter with a window size equal to the system resolution cell (3×3). It is important to emphasize that the use of the average filter result in different image statistics and change detection performances. Thus, the comparison between pre-processed and without pre-processing versions of the methods is not fair.

Figure 4.17 presents the ROC curves for both masking change detection methods with and without the pre-processing blocks. Due to the very low false alarms occurrences in the MCMD method, for visualization purposes, a linear scale in Figure 4.17 x-axis is used.

As can be observed in Figure 4.17, both SMD and MMCD can achieve high detection probabilities for considerably low values of FAR. This scenario is caused by the combination of the very selective mask and the erosion morphological operation. The MMCD can obtain a FAR = 0 for a detection probability value ($P_d \approx 0.967$), whereas the SMD obtains a FAR ≈ 0.126 for the same P_d. However, this combination also results in the impossibility of the MCMD detecting six targets resulting in a maximum $P_d = 0.99$, which tends to jeopardize its performance

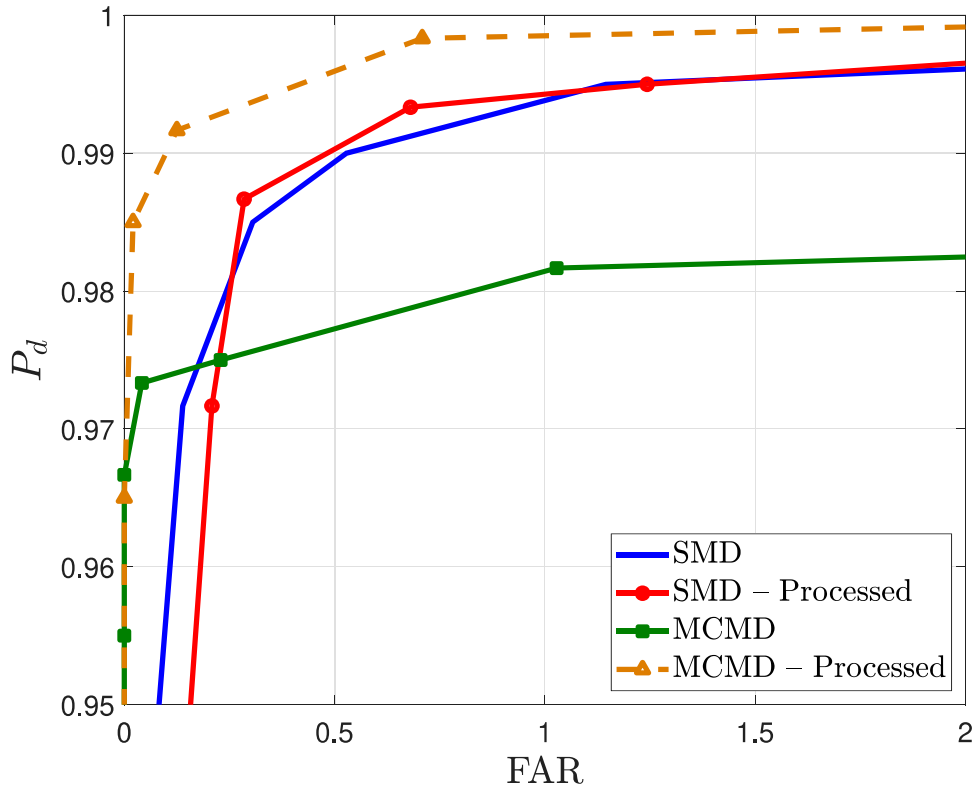

Figure 4.17: ROC curves for both proposed methods with/without the use of the pre-processing average filter.

for high detection probability values. In order to obtain this maximum number of detected targets, a threshold of 0 was considered resulting in a FAR $\approx$ 12.37. However, this point is omitted from the ROC for visualization purposes. Due to the saturation issue, the SMD presents a better performance when compared with the MCMD for $P_d > 0.974$.

By analyzing the scenario with the average filter, a performance increase in the MCMD is observable, which can not be observed in the SMD. This effect is directly related to the selectivity of their masks. In the studied scenario, the average filter acts as a blur filter in the input image. This blur effect tends to smooth differences of amplitude among neighboring pixels. Thus, target-related pixels tend to form a block of high-amplitude pixels which will be not removed by the erosion, whereas isolated pixels tend to form a block of low-amplitude pixels which will be removed by the morphological operation. Since the SMD filter does not have a very selective mask, the use of an average filter only tends to remove few false alarms. However, for the MCMD method, the filter effect results in the possibility of achievement of $P_d > 0.99$, besides removing some false alarms granting a performance increase in terms of both evaluated metrics.

Comparing the results presented in Figures 4.13 and 4.17, both SMD and MCMD, without the averaging filter, usually present a better performance than the proposed methods of Section 4.2.

For instance, considering $P_d \approx 0.967$ the SMD has FAR ≈ 0.126, the MCMD has FAR = 0, and the best ROC curve of Figures 4.13 has FAR ≈ 0.208. However, this comparison would only be possible for specific scenarios due to the masking techniques requirements of the application. Even so, both SMD and MCMD methods have a competitive performance when compared with other change detection methods from the literature, given that their requirements are fulfilled.

4.4 Concluding Remarks

This chapter presented a statistical test analysis for SAR wavelength-resolution image stacks and the proposal of change detection methods based on SAR wavelength-resolution image stacks. Section 4.1 showed the statistical test analysis for SAR wavelength-resolution image stacks detailing the adopted methodology. Based on the experimental results, the Rician distribution yields a good fit for samples composed of background pixels statistics obtained from the wavelength-resolution SAR image stack.

Sections 4.2 and 4.3 presented the proposed change detection methods for wavelength-resolution SAR image stacks, considering the observations from Section 4.1. The change detection methods of Sections 4.2 and 4.3 are based on statistical hypothesis tests and masking procedures, respectively. The experimental evaluation was carried out in terms of the detection probability and the false alarm rate, considering the CARABAS II available data set. The experimental results have shown that, usually, the use of image stack provides better performance than methods that do not consider the use of image stacks, in terms of both evaluated metrics. Moreover, the proposed change detection methods presented a competitive performance in terms of the evaluated metrics when compared to a recently proposed stack-based change detection method from the literature.

Finally, the results, discussions, and part of the text presented in Section 4.1 were published in [107]. Moreover, the contributions and part of the text presented in 4.2 were already submitted to a journal, and it is currently under review. Also, it is expected to submit for publication, shortly, the contributions presented in Section 4.3.

5

Change Detection Method Using the Bayes Theorem

Recently, change detection methods based on statistics and probability theory have been proposed, some of them are related to Bayes' theorem [46, 82, 108, 109]. In [46, 82], the authors present and evaluate a change detection method using the Bayes theorem, considering data obtained with the CARABAS system. This method considers the use of a data histogram from two images and a generic model for target distribution to obtain, iteratively, the probabilities of changes that can occur in a specific number of positions.

Another frequently studied topic in SAR change detection is the clutter-plus-noise statistical modeling, especially for wavelength-resolution images. Several change detection algorithms use the differences between targets, clutter, and noise to enable the detection of changes [47, 61]. More realistic clutter models, which use this kind of information, tend to provide a better performance, as suggested in [61], which can be observed by comparing the same likelihood ratio test under a simple clutter distribution model [61] and more realistic models such as in [47, 48].

Motivated by the method and results presented in [46, 82], and the possibility of obtaining better performance in change detection methods using more realistic clutter-plus-noise distributions models [47, 48], this chapter presents an analysis of the Bayes' theorem application in SAR change detection based on the use of different clutter-plus-noise statistical models. A non-iterative and iterative version of a change detection method is presented using the Bayes theorem, which enables the use of different clutter-plus-noise distribution models. Finally,two distributions are studied and evaluated using CARABAS II data, using both the non-iterative and the iterative approach. The distributions considered in the study cases are the bivariate Rayleigh distribution and the bivariate Gaussian distribution.

5.1 Interpretation of Bayes' Theorem in SAR Change Detection

Bayes' theorem is used to describe the probability of an event, given some prior knowledge of conditions that could be related to this event [110]. Based on this definition, a common SAR change detection scenario is studied. The scenario is characterized by the use of two complex images, where one is the surveillance image, and the other is the reference image. Using Bayes' theorem, the probability of detecting a change in one test sample, given the amplitude of the tested pixel in the surveillance and reference images, can be expressed as

$$P\left(s \equiv s_T|\tilde{z}_s, \tilde{z}_r\right) = \frac{P\left(\tilde{z}_s|s \equiv s_T, \tilde{z}_r\right) P\left(s \equiv s_T|\tilde{z}_r\right)}{P\left(\tilde{z}_s|\tilde{z}_r\right)}, \tag{5.1}$$

where s represents the tested image sample, $\tilde{z}_s$ and $\tilde{z}_r$ are the amplitude of the tested pixel in the surveillance and reference image, respectively, and $s \equiv s_T$ is the statement that the given image sample contains a change. Thus, a change detection method based on (5.1) requires this test to be performed in each image pixel, resulting in a matrix of probabilities with the same dimensions as the input images.

Under the same assumption as in [46, 82], that the reference image magnitudes are independent of the change statement, the conditional probability $P\left(s \equiv s_T|\tilde{z}_r\right)$ can be approximated as

$$P\left(s \equiv s_T|\tilde{z}_r\right) \approx P\left(s \equiv s_T\right) = \frac{VK}{N}, \tag{5.2}$$

where K is the number of detected changes, V is the number of samples that a change occupies, N is the number of image samples, and $N \gg VK$.

The conditional probability $P\left(\tilde{z}_s|\tilde{z}_r\right)$ can be described by two mutually exclusive events, which are based on a presence or absence of a change. According to [46], the probability $P\left(\tilde{z}_s|\tilde{z}_r\right)$ can be written as

$$\begin{aligned} P\left(\tilde{z}_s|\tilde{z}_r\right) \quad = \quad & P\left(\tilde{z}_s|s \equiv s_T, \tilde{z}_r\right) P\left(s \equiv s_T|\tilde{z}_r\right) \\ & + P\left(\tilde{z}_s|s \not\equiv s_T, \tilde{z}_r\right) \left[1 - P\left(s \equiv s_T|\tilde{z}_r\right)\right], \end{aligned} \tag{5.3}$$

where $s \not\equiv s_T$ is the statement that the given image sample does not contain a change.

The studied scenario analysis, considering (5.1), was firstly introduced in [46]. This analysis focused on a target geometry analysis. Unlike [46], the analysis motivation of this chapter is to consider the clutter-plus-noise statistical model information into the studied SAR scenario. To enable the use of this information, (5.3) can be rewritten as

$$P\left(\tilde{z}_s|s \equiv s_T, \tilde{z}_r\right) = \frac{P\left(\tilde{z}_s|\tilde{z}_r\right) - P\left(\tilde{z}_s|s \not\equiv s_T, \tilde{z}_s\right)\left[1 - P\left(s \equiv s_T|\tilde{z}_r\right)\right]}{P\left(s \equiv s_T|\tilde{z}_r\right)}. \tag{5.4}$$

Substituting (5.2) and (5.4) into (5.1) results in

$$P\left(s \equiv s_T|\tilde{z}_s, \tilde{z}_r\right) = 1 - \frac{P\left(\tilde{z}_s|s \not\equiv s_T, \tilde{z}_r\right)}{P\left(\tilde{z}_s|\tilde{z}_r\right)}\left[1 - \frac{VK}{N}\right]. \tag{5.5}$$

Applying Bayes' theorem to (5.5), and considering (5.2), the expression for (5.1) is given by

$$P\left(s \equiv s_T|\tilde{z}_s, \tilde{z}_r\right) = 1 - \frac{P\left(\tilde{z}_s, \tilde{z}_r|s \not\equiv s_T\right)}{P\left(\tilde{z}_s, \tilde{z}_r\right)}\left[1 - \frac{VK}{N}\right]. \tag{5.6}$$

The conditional probability $P\left(\tilde{z}_s, \tilde{z}_r|s \not\equiv s_T\right)$ can be calculated by using an appropriate statistical distribution for the clutter-plus-noise of the tested images, while the joint probability $P\left(\tilde{z}_s, \tilde{z}_r\right)$ can be calculated from the SAR images histogram.

Under the assumption of a correct statistical model choice for the clutter and noise in (5.6), the occurrence of a change in the scene tend to lead to $P\left(\tilde{z}_s, \tilde{z}_r\right) \gg P\left(\tilde{z}_s, \tilde{z}_r|s \not\equiv s_T\right)$, resulting in $P\left(s \equiv s_T|\tilde{z}_s, \tilde{z}_r\right) \approx 1$. Conversely, a situation with absence of changes will lead to $P\left(\tilde{z}_s, \tilde{z}_r\right) \approx P\left(\tilde{z}_s, \tilde{z}_r|s \not\equiv s_T\right)$, resulting in $P\left(s \equiv s_T|\tilde{z}_s, \tilde{z}_r\right) \approx 0$.

The same analysis and interpretation can be used for an incoherent change detection scenario, considering the absolute values $z_s = |\tilde{z}_s|$ and $z_r = |\tilde{z}_r|$. In this case, the following expression replaces (5.6)

$$P\left(s \equiv s_T|z_s, z_r\right) = 1 - \frac{P\left(z_s, z_r|s \not\equiv s_T\right)}{P\left(z_s, z_r\right)}\left[1 - \frac{VK}{N}\right]. \tag{5.7}$$

5.1.1 Non-Iterative Change Detection Method

The proposed change detection method is based on (5.7). Thus, to ensure its correct operation, some considerations about the probabilities $P\left(s \equiv s_T\right)$ and $P\left(z_s, z_r|s \not\equiv s_T\right)$ are required. Since the number of pixels the targets occupy in an image is much smaller than the total number of pixels in the image, $VK \ll N$, the last term in (5.7) can be approximated

as $1 - VK/N \approx 1$. So, (5.7) is further simplified to

$$P\left(s \equiv s_T | z_s, z_r\right) \approx 1 - \frac{P\left(z_s, z_r | s \not\equiv s_T\right)}{P\left(z_s, z_r\right)}. \tag{5.8}$$

Based on the clutter-plus-noise statistical model selection required in (5.8), situations where the mismatch between the selected distribution and the histogram could lead to values below 0 are possible. Given that the detection method focuses on situations where changes are present, i.e., $P\left(s \equiv s_T | z_s, z_r\right) \approx 1$, this issue can be overcome by rewriting (5.8) as

$$P\left(s \equiv s_T | z_s, z_r\right) = \max\left(0, 1 - \frac{P\left(z_s, z_r | s \not\equiv s_T\right)}{P\left(z_s, z_r\right)}\right). \tag{5.9}$$

Based on (5.8), a processing scheme for the change detection method is proposed and presented in Figure 5.1. The technique uses as inputs one surveillance image and one reference image.

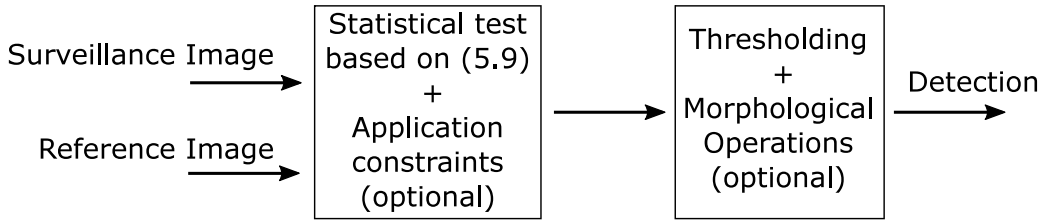

Figure 5.1: Simplified diagram block for the proposed non-iterative change detection method.

The first block of the diagram consists of the statistical test based on (5.9). This block consists of the statistical test based on (5.9). The test is applied to every image pixel position and the probabilities $P\left(z_s, z_r | s \not\equiv s_T\right)$, and $P\left(z_s, z_r\right)$ are calculated from the selected clutter-plus-noise distribution and the data histogram, respectively. Also, optional application constraints and pre-processing techniques can be applied. These optional operations are usually related to a priori knowledge of the data and the application and the selected clutter-plus-noise distribution.

To avoid the detection of $P\left(s \equiv s_T | z_s, z_r\right)$ related to isolated instances, an averaging filter is applied as the last operation of the first diagram block. This operation is performed by using an averaging filter for a window with the same size as the system resolution-cell. Thus, the output of the first diagram block is a matrix of average probabilities with the same dimensions as the surveillance image where each position value is represented by $\overline{P\left(s \equiv s_T | z_s, z_r\right)}$, and $\overline{(\cdot)}$ is the mean operation.

The first diagram block output is sufficient to establish possible target-related candidate pixel positions. This information can be further explored to set the top priority candidates in situations

where multiple high probability changes are detected. However, to better evaluated the proposed method and to enable its comparison with other already proposed ones, a second block in the processing scheme is used.

The second block of the diagram is composed of the thresholding operation and the application of some morphological operations. This thresholding operation consists of obtaining a binary image by setting as one the amplitude of pixels related to average probabilities higher or equal than a probability threshold (τ_p) and setting as zero the others. Finally, some optional morphological operations, selected according to the methods' application specificity, are applied to the binary image. As an example for a correct execution of the proposed method, Figure 5.2 presents one example of an input image and its resulting detection binary image.

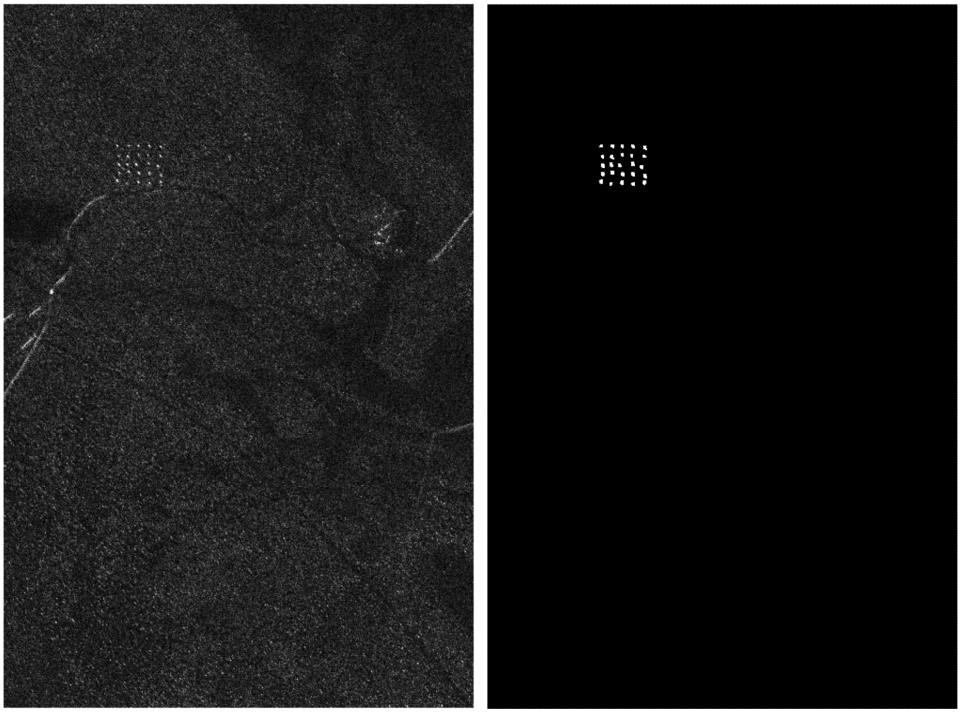

(a) (b)

Figure 5.2: Example of a detection using the proposed non-iterative method where (a) is the input surveillance image and (b) is the output image.

5.1.2 Iterative Change Detection Method

The proposed iterative change detection method is based on the proposals of [46, 82], and in (5.7). Based on the same analysis of the mismatch between the selected distribution and the histogram, presented in Section 5.1.1, (5.7) can be rewritten as

$$P\left(s \equiv s_T | z_s, z_r\right) = \max\left(0, 1 - \frac{P\left(z_s, z_r | s \not\equiv s_T\right)}{P\left(z_s, z_r\right)}\left[1 - \frac{VK}{N}\right]\right). \tag{5.10}$$

The approximation $1 - VK/N \approx 1$ is not considered in the iterative scenario, given that the number of target candidates (V) is equal to the number of iterations already completed. Finally, similarly to the analysis presented in Section 5.1.1, to avoid scenarios where isolated pixels are associated with high probabilities of being considered as a target, the iterative method only evaluates average probabilities. These average probabilities are obtained using the same filter considered in Section 5.1.1. Based on the iterative approach presented in [46, 82], and in (5.10), a simplified flowchart for the proposed iterative method is presented in Figure 5.3.

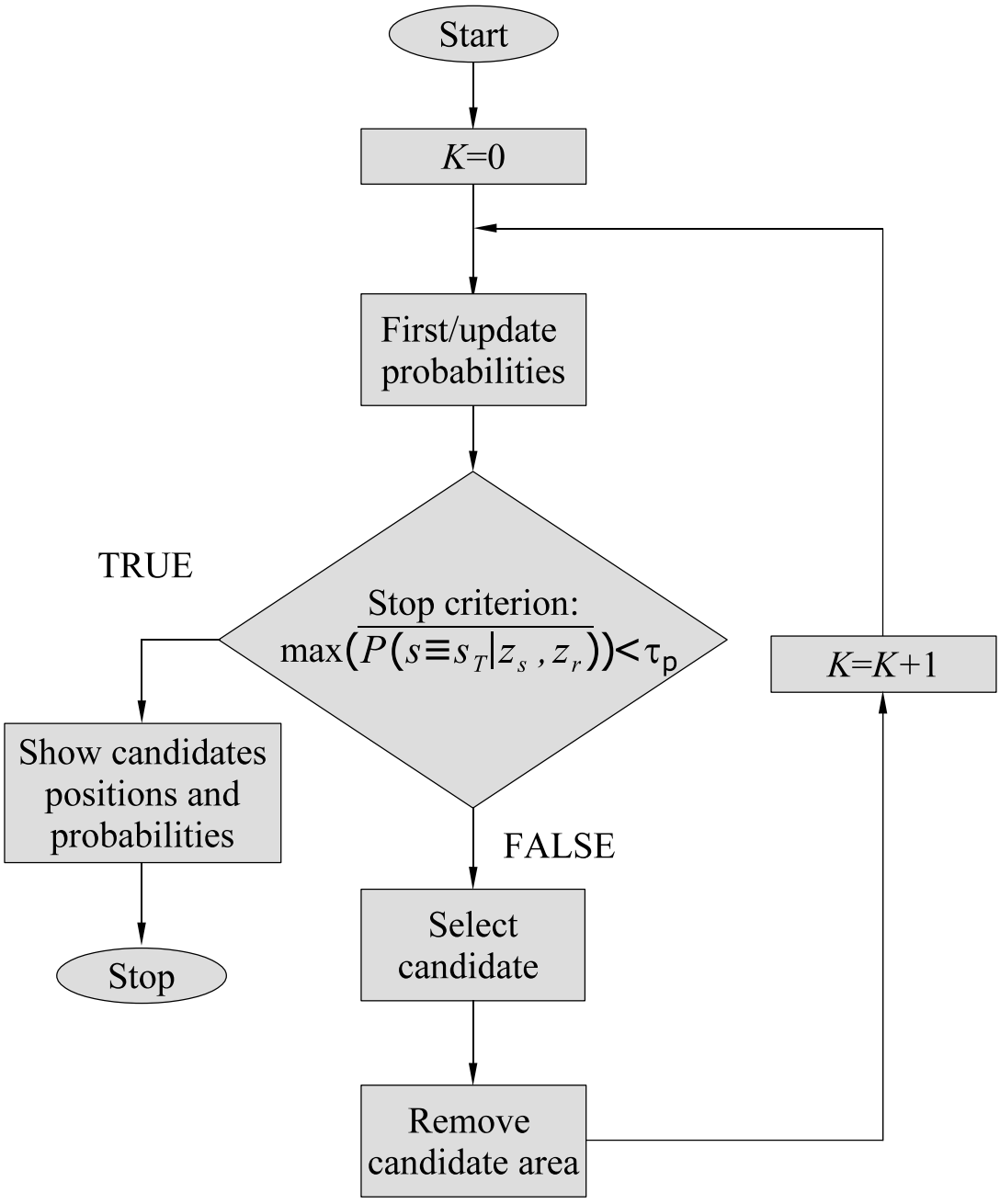

Figure 5.3: Simplified flowchart of the proposed iterative change detection method.

The reference and surveillance images are the inputs to the iterative algorithm, which starts with $K = 0$, as presented in Figure 5.3. The iterative approach consists of calculating the average probabilities $\overline{P\left(s \equiv s_T | z_s, z_r\right)}$ for every pixel position, verifying if the highest probability in the test image is higher than a threshold probability τ_p, which lies in the range (0,1). The pixel candidate with the highest probability of being a target is selected. Next, a guard area around the candidate pixel is removed. Finally, the values of the probabilities and K are updated iteratively until the stop criterion is satisfied. Thus, each iteration result is used to update the histogram and the parameters of the selected distribution model, providing a better match between the distribution model and the data, if the pixel removal is truly related to targets.

Four parameters can be modified according to the application of the proposed method. The first one is the parameter V, which is related to the expected target size. The guard window size should be selected to avoid multiple detections of the same target. The threshold, τ_p, is chosen according to the acceptable (or desirable) trade-off between probability of detection and false alarm rate per square kilometer. Finally, the stop criterion in this method can be defined either as a maximum number of iterations or by the probability threshold. This second stop criterion is the one adopted in this document, as presented in Figure 5.3.

Considering that the parameters were appropriately selected, the proposed iterative method overcomes the problems related to detection of isolated targets and multiple detections of the same target. Thus, there is no necessity of performing morphological operations, which are traditionally used for solving these issues [44, 47, 61]. Since no morphological application is performed, there is no need to transform the detection image into a binary image. Thus, the output of the proposed iterative method is a set of regions centered at their respective selected pixel candidate, which has a probability of being a target higher than τ_p. Finally, the probabilities are also available for the system operator, who can exploit this information in different ways according to the application where the method is being employed. As an example a correct execution of the proposed method, Figure 5.4 presents one example of an input image and its resulting detection image.

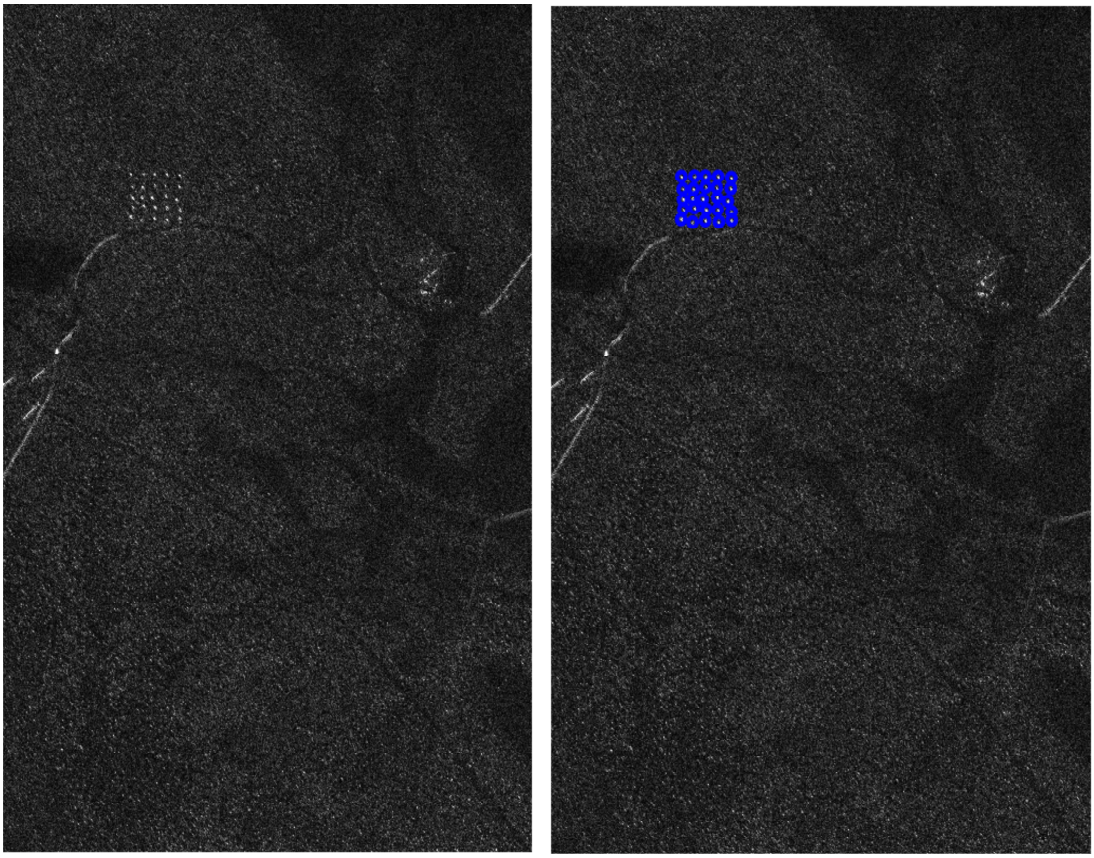

(a) (b)

Figure 5.4: Example of a detection using the proposed iterative method where (a) is the input surveillance image and (b) is the output image.

5.2 Study Case 1: Rayleigh Distribution

As mentioned in Section 5.1, the probability $P(\tilde{z}_s, \tilde{z}_r | s \not\equiv s_T)$ can be obtained by using an appropriate statistical model for the clutter-plus-noise, considering both reference and surveillance images. Among the statistical models mentioned in Section 5.1 for wavelength-resolution images, the Bivariate Rayleigh distribution is seen as the simplest one, since it belongs to a one-parameter family of probability distributions. This distribution has already been used for CARABAS-II data and presented a good performance for change detection applications [30, 48].

Hence, for an evaluation of the proposed change detection method using the Bayes theorem, the Bivariate Rayleigh distribution is selected as the case of study. The probability density

function of a Bivariate Rayleigh distribution can be written as [111]

$$p\left(z_s, z_r\right) = \frac{4 z_r z_s}{\Omega_r \Omega_s \left(1-\rho\right)} \times \exp\left\{-\frac{1}{1-\rho}\left(\frac{z_r^2}{\Omega_r} + \frac{z_s^2}{\Omega_s}\right)\right\} \times I_0\left(\frac{2\sqrt{\rho}}{1-\rho}\frac{z_r z_s}{\sqrt{\Omega_r \Omega_s}}\right), \tag{5.11}$$

where $\Omega_r = \overline{z_r^2}$, $\Omega_s = \overline{z_s^2}$, $I_0\left(c\right)$ is the modified Bessel function of the first kind with order zero, and ρ is the correlation coefficient, which can be estimated by [111]

$$\rho = \frac{\mathrm{cov}(z_s^2, z_r^2)}{\sqrt{\mathrm{var}(z_s^2)\mathrm{var}(z_r^2)}}. \tag{5.12}$$

where $\mathrm{cov}(\cdot,\cdot)$ and $\mathrm{var}(\cdot)$ represent the covariance and the variance of the random variables.

As can be observed, the selection of the clutter-plus-noise distribution is directly related to the statistical nature of the evaluated SAR Images. Also, considering the evaluated data and the specificity of each application, additional constraints can be used to improve the method performance. Thus, some application aspects regarding the evaluated CARABAS II data set are presented and discussed in Section 5.2.1.

5.2.1 Application Aspects

The proposed method is based on the probabilities $P\left(z_s, z_r | s \not\equiv s_T\right)$ and $P\left(z_s, z_r\right)$ obtained, respectively, from the selected distribution model and the data histogram. To evaluate the selection of the Bivariate Rayleigh distribution and provide useful information for application constraints, Figure 5.5 is presented. Figure 5.5 shows the theoretical Bivariate Rayleigh surface plot obtained from (5.11) and (5.12) and the three-dimensional histogram of the experimental data from the CARABAS II data set.

As can be observed, there is a mismatch between the selected bivariate distribution and the data histogram. For low amplitudes values of z_s and z_r, a candidate target pattern is observed, $P\left(z_s, z_r\right) > P\left(z_s, z_r | s \not\equiv s_T\right)$. However, this pattern is not expected for low amplitude values and tends to increase the false alarms. Another observed pattern is observed in the theoretical distribution curve decay where $P\left(z_s, z_r\right) < P\left(z_s, z_r | s \not\equiv s_T\right)$. This fact is related to the issue treated by (5.9), resulting in the impossibility of detecting any target for this range of amplitude values.

To further discuss the candidate distribution selection, the mismatch between the data histogram and a theoretical distribution for the surveillance image is evaluated. Under the

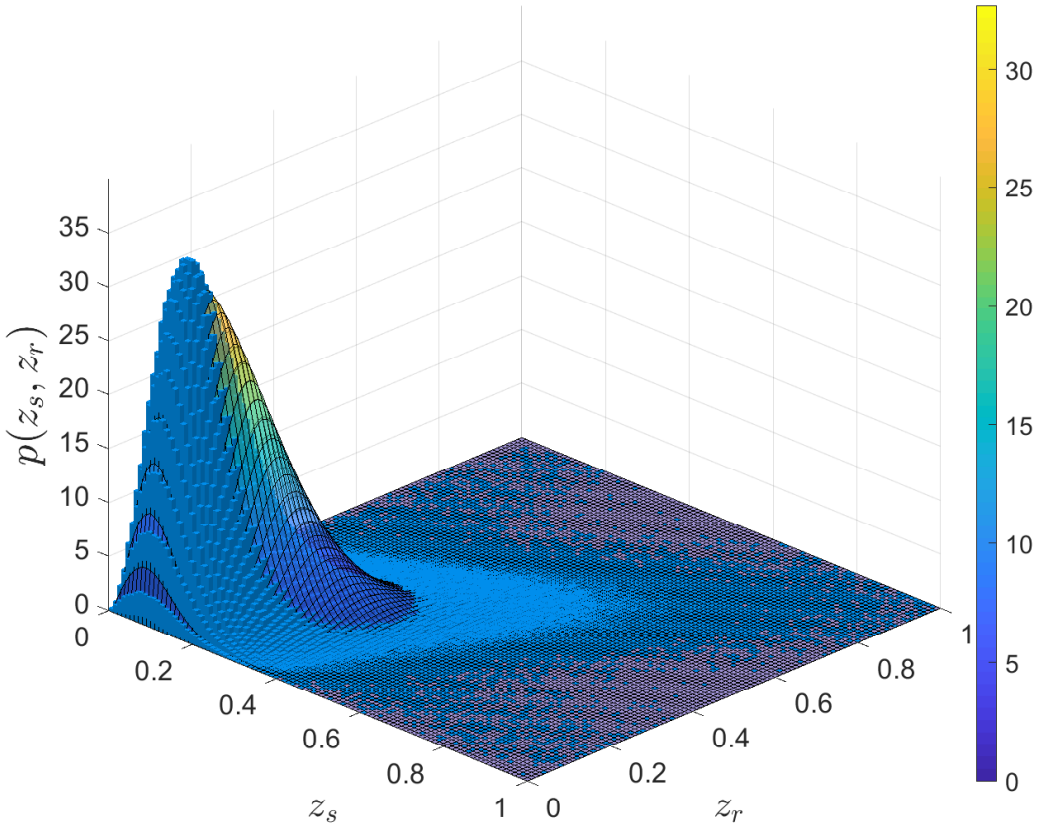

Figure 5.5: Surface plot of the theoretical Bivariate Rayleigh distribution and the three-dimensional histogram of the experimental data.

same assumption and considerations of [47, 48], the surveillance image is modeled as Rayleigh distributed. The shape parameter of the theoretical Rayleigh distribution, presented in (4.5), was obtained by using an MLE. Figure 5.6 shows the theoretical Rayleigh distribution and the histogram of the experimental data.

The patterns observed in Figure 5.5 are also observed in Figure 5.6. Also, the mismatch is more present in regions with lower values than, approximately, $z_s < 0.4$. Moreover, the proposed method detects changes in both surveillance and reference images, which could be an issue for some applications. It is possible to detect change only in the surveillance image by evaluating points only if $z_s > z_r$. Thus, to mitigate the mismatch-related false alarm occurrences, and to detect only changes in the surveillance image, one application constraint is applied in the processing chain, which consist in to set the probability $P\left(s \equiv s_T | z_u, z_r\right) = 0$ if

$$z_s < z_r + \nu, \tag{5.13}$$

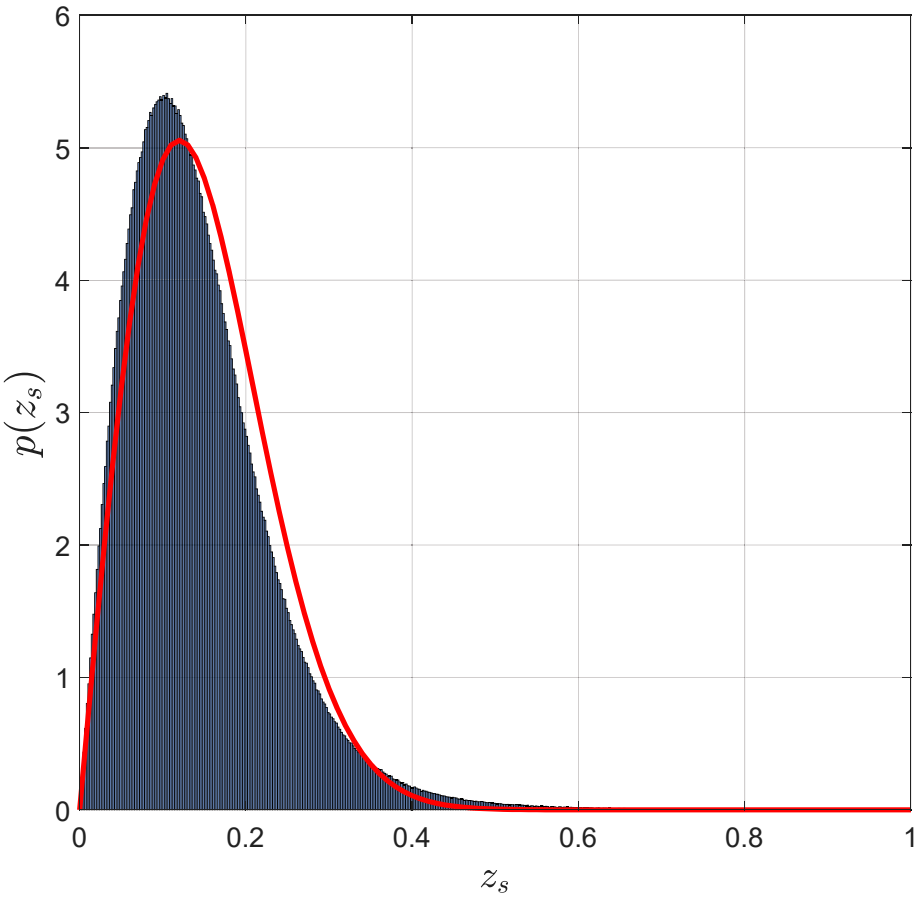

Figure 5.6: Theoretical Rayleigh distribution and surveillance image data histogram.

otherwise, the conditional probability is calculated using (5.9) for the non-iterative case or (5.10) for the iterative case. This constraint is based on a priori knowledge from the evaluated data, and it is similar to the one used in [47]. The approximation adopted in (5.13) is commonly used in change detection methods when the CARABAS II data set is considered [30, 46, 47]. Also, the same set of values $\nu \in [0.2, 0.3, 0.4]$ considered in [47] is used to guarantee a fair comparison between the evaluated methods. Additionally, other data sets may require other values for ν, including the situation with $\nu = 0$.

A fixed threshold is applied to all the results of the statistical tests. The threshold should be selected according to the characteristics of each specific application and should lie in the range $(0, 1)$. For this evaluation, a wide range of thresholds is considered to obtain the ROC curves.

For the iterative case, the values V = 30 pixels and a guard window of 31×31 pixels are considered, based on an extrapolation of the maximum test target size and the Kernel outer size for the Constant False Alarm Rate (CFAR) filter used in [76], respectively. Finally, the method is evaluated considering the same application constraint and the same set of thresholds used for the non-iterative case.

5.2.2 Experimental Results

The experimental evaluation of the proposed change detection method using the Bayes theorem considers all the 24 incoherent CARABAS II images from the data set presented in Chapter 3. The input image pairs were selected according to [76] to simplify the method evaluation. The 24 image pairs are presented in detail throughout this section.

Similarly to Section 4.2.3, the methods' performance is assessed in terms of the P_d and FAR. Moreover, the same decision criterion is considered regarding any object detected.

The first evaluation consists of the comparison of the ROC curve performances between the non-iterative proposed method and an existing change detection method, which uses CARABAS II images [61]. Figure 5.7 shows the proposed method outperforms the reference method for $\nu = 0.2$, $\nu = 0.3$, and $\nu = 0.4$.

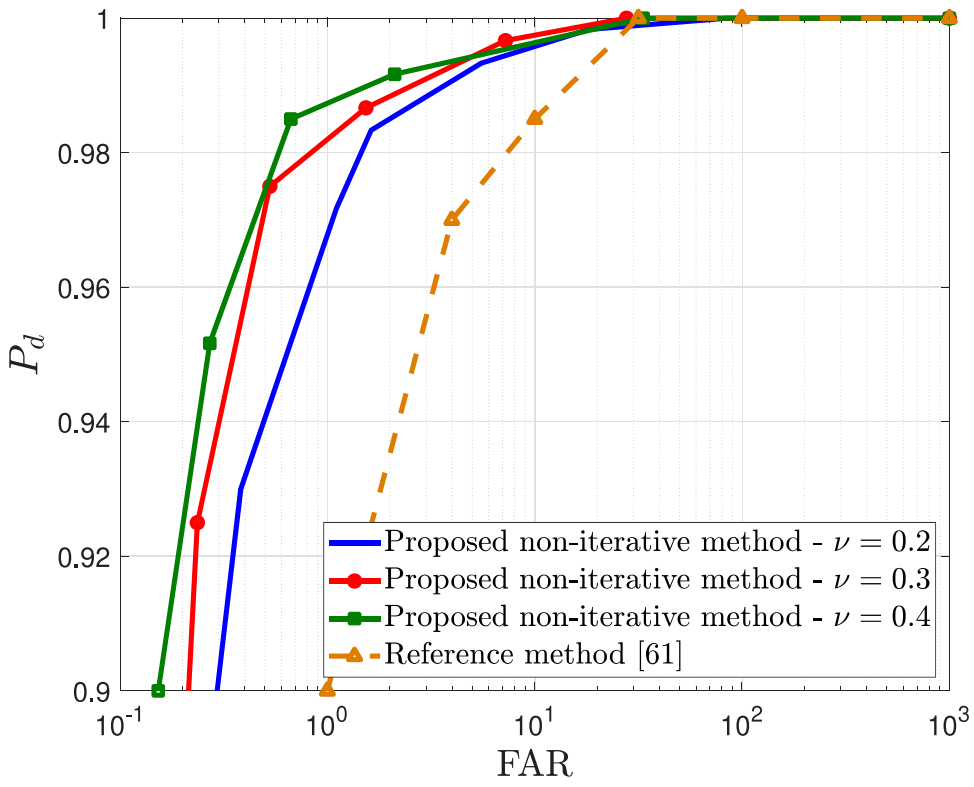

Figure 5.7: ROC performance comparison between the proposed non-iterative and the best curve of the reference method.

The use of higher values for the amplitude constraint reduces the impact of the mismatch between the data and the model distribution, reducing the occurrence of the false alarms. However, the combination of a high value of ν, and the erosion morphological operation could result in the erasure of some targets, making it impossible to obtain $P_d = 1.00$ with any threshold. Although this phenomenon has not been observed for the constraints used in Figure 5.7, it is

expected to occur for higher ν values. Finally, the possibility of occurrence of this phenomenon can be reduced by a selection of a better-matched distribution model or by using different signal processing schemes, such as the iterative approach.

Analyzing the results presented in Figure 5.7, for the points with FAR = 10^0, the following probabilities of detection are observable: $P_d \approx 0.90$ for the reference method; $P_d \approx 0.968$ for $\nu = 0.2$; $P_d \approx 0.982$ for $\nu = 0.3$; and $P_d \approx 0.98$ for $\nu = 0.4$. Thus, increasing ν improves the detection performance, but with diminishing returns. On the other hand, a large value of ν may have the detrimental effect of removing targets, as mentioned before. As can be observed, $\nu = 0.4$ is the best option tested for characterizing target-like pattern in this data set, although the intermediate value of $\nu = 0.3$ has also proved to be a good choice. Optimal values of ν could be achieved through an investigation about the statistics of the targets in the data set. So, based on the numerical results, prior knowledge about the targets in the data set can be incorporated into the application constraints to improve the performance of the proposed method.

The second evaluation consists of the comparison between the non-iterative method and the proposal in [47]. The technique published in [47] consists of a likelihood-based change detection method considering the clutter-plus-noise statistics modeled as a Bivariate Gamma distribution. Figure 5.8 shows the performance comparison between the evaluated methods. For visualization purposes, the curve for $\nu = 0.2$ was omitted, and only the two best ROC curves of the reference method [47] are presented.

From the results presented in Figure 5.8, the proposed method with $\nu = 0.4$ outperforms the reference method in all tested points with $s_1 = 0.3$, and outperforms the reference one with $s_1 = 0.4$ for $P_d > 0.95$. Moreover, the proposed method with $\nu = 0.3$ outperforms the reference method with $s_1 = 0.3$ and with $s_1 = 0.4$ for $P_d > 0.925$ and $P_d > 0.963$, respectively. However, for the reference method, when $s_1 = 0.4$ the algorithm was unable to detect some targets, resulting in a maximum $P_d < 1.00$. Finally, considering the points with FAR = 10^0, the following probabilities of detection were obtained for the method proposed in [47]: $P_d \approx 0.978$ for $s_1 = 0.3$; $P_d \approx 0.976$ for $s_1 = 0.4$. For the proposed non-iterative method, the following probabilities of detection were obtained: $P_d \approx 0.982$ for $\nu = 0.3$; and $P_d \approx 0.987$ for $\nu = 0.4$.

To further investigate the performance of the proposed detection method, Table 5.1 presents the experimental results for a specific test setup, where the gray highlighted rows refer to images that contain image formation issues. By comparison with the results presented in [76], Table 5.1 reveals that the proposed method presents better performance for both detection probability (585 target detections against 579) and false alarm rate (76 false alarms against 96). Furthermore,

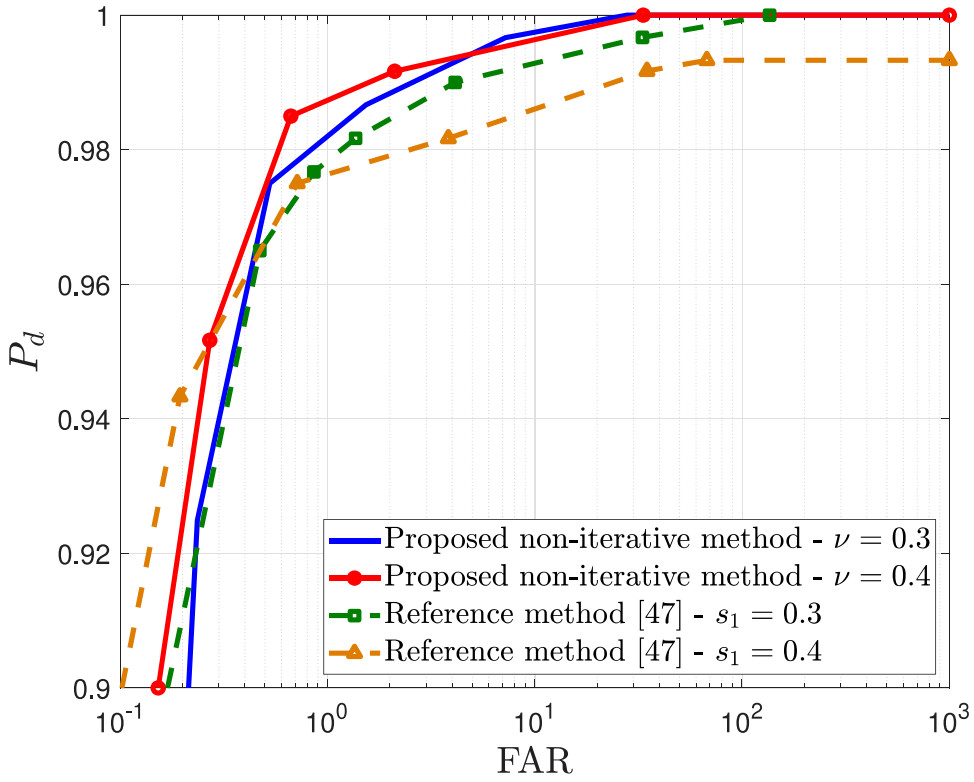

Figure 5.8: ROC performance comparison between the proposed non-iterative method and the best curves of the reference method.

Table 5.1 shows that the majority of false alarms 75% and a large number of the missed detections 46.66% are related to the pairs 18 and 20. These images were studied in [31] being characterized by the presence of some low amplitude targets and by high amplitude elongated structures, which may cause false alarms. Based on the study presented in [31], aiming to reduce false alarms in these image pairs, more sophisticated processing techniques would be required. However, the results in Table 5.1 show that the proposed method works satisfactorily with most of the experimental data without the aid of any other processing technique.

One possible cause for the image formation issues observed can be related to the leakage of side and back lobe signals, which can act as a source of error in the image formation process [112]. The structures generated by these issues tend to have a target-like pattern. Thus, detections related to these structures do not represent a method error and could not be counted as false alarms in our evaluation. By analyzing the results of the four image pairs, only two of the ten previously observed false alarms are not associated with this type of structure. Disregarding false alarms related to these structures, the presented false alarms numbers in Table 5.1 would drop to a total of 68, resulting in FAR 0.47. However, to guarantee a fair comparison among the evaluated methods, even these false alarms are counted in all other evaluations presented throughout this document.

Table 5.1: Performance results of the proposed non-iterative method for a probability threshold of 0.5 and $\nu = 0.3$[1].

Exp. No.	Surveillance image		Reference image		Number of detected targets	Detection probability	Number of false alarms	False alarm rate (km^{-2})
	Mission	Pass	Mission	Pass				
1	2	1	3	1	25	1.00	0	0.00
2	3	1	4	1	25	1.00	4	0.67
3	4	1	5	1	25	1.00	0	0.00
4	5	1	2	1	23	0.92	4	0.67
5	2	2	4	2	25	1.00	0	0.00
6	3	2	5	2	25	1.00	1	0.17
7	4	2	2	2	24	0.96	3	0.50
8	5	2	3	2	24	0.96	0	0.00
9	2	3	5	3	25	1.00	1	0.17
10	3	3	2	3	24	0.96	1	0.17
11	4	3	3	3	24	0.96	1	0.17
12	5	3	4	3	25	1.00	1	0.17
13	2	4	3	4	25	1.00	0	0.00
14	3	4	4	4	25	1.00	0	0.00
15	4	4	5	4	25	1.00	0	0.00
16	5	4	2	4	23	0.92	1	0.17
17	2	5	4	5	25	1.00	0	0.00
18	3	5	5	5	19	0.76	46	7.67
19	4	5	2	5	25	1.00	0	0.00
20	5	5	3	5	24	0.96	11	1.83
21	2	6	5	6	25	1.00	1	0.17
22	3	6	2	6	25	1.00	1	0.17
23	4	6	3	6	25	1.00	0	0.00
24	5	6	4	6	25	1.00	0	0.00
Total					585	0.97	76	0.53

[1]The gray highlighted rows are images that contain image formation issues.

The following evaluation consists of the comparison between the proposed non-iterative and iterative methods. Figure 5.9 shows the performance comparison between the evaluated methods.

From the results presented in Figure 5.9, the iterative method outperforms the non-iterative techniques for the application constraints of $\nu = 0.3$ and $\nu = 0.4$, mainly for the values of FAR < $10^{-0.5}$. However, the non-iterative method outperforms the iterative approach for $\nu = 0.2$. The pattern observed for $\nu = 0.2$ is related to the selection of false alarms as target candidates by the iterative method, which results in not accurately updated probabilities for the next iterations. As observed in Section 5.2.2, the distribution mismatch observed for low amplitude values tend to increase the occurrence of the false alarms, and this situation can be observed for amplitude values close to 0.2 in Figure 5.5. Thus, a bad selection of distribution or application constraint results in worse performances in the iterative approach than the non-iterative method. However,

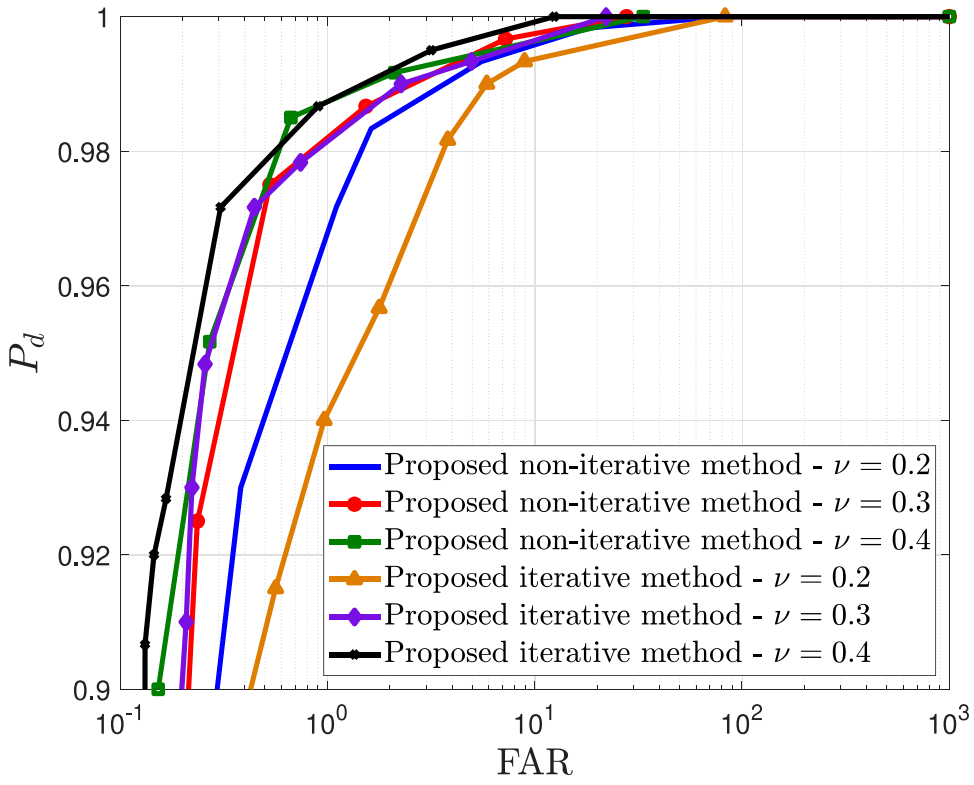

Figure 5.9: ROC performance comparison between the proposed non-iterative and iterative methods.

when more accurate information is provided to update the probabilities, better performance is observed.

Finally, as the last evaluation presented in this section, the iterative method performance is compared with the technique proposed in [47]. Figure 5.10 shows the performance comparison between the evaluated methods. For visualization purposes, the curve for $\nu = 0.2$ was omitted, and only the two best ROC curves of the reference method [47] are presented.

As can be observed in Figures 5.10, similar observations can be drawn about the proposed methods when compared with one of [47]. The iterative method using $\nu = 0.4$ outperforms the reference method in all tested points with $s_1 = 0.3$, and outperforms the reference one with $s_1 = 0.4$ for $P_d > 0.95$. Moreover, the proposed method with $\nu = 0.3$ outperforms the reference method with $s_1 = 0.3$ and with $s_1 = 0.4$ for $P_d > 0.92$ and $P_d > 0.963$, respectively.

Finally, the evaluated scenarios show that both proposed non-iterative and iterative methods present a competitive performance when compared with other techniques from the literature. It is important to emphasize that the Bivariate Rayleigh distribution is not the ideal selection. To evaluate the performance impact of a better-selected distribution model, a new study case is presented in Section 5.3.

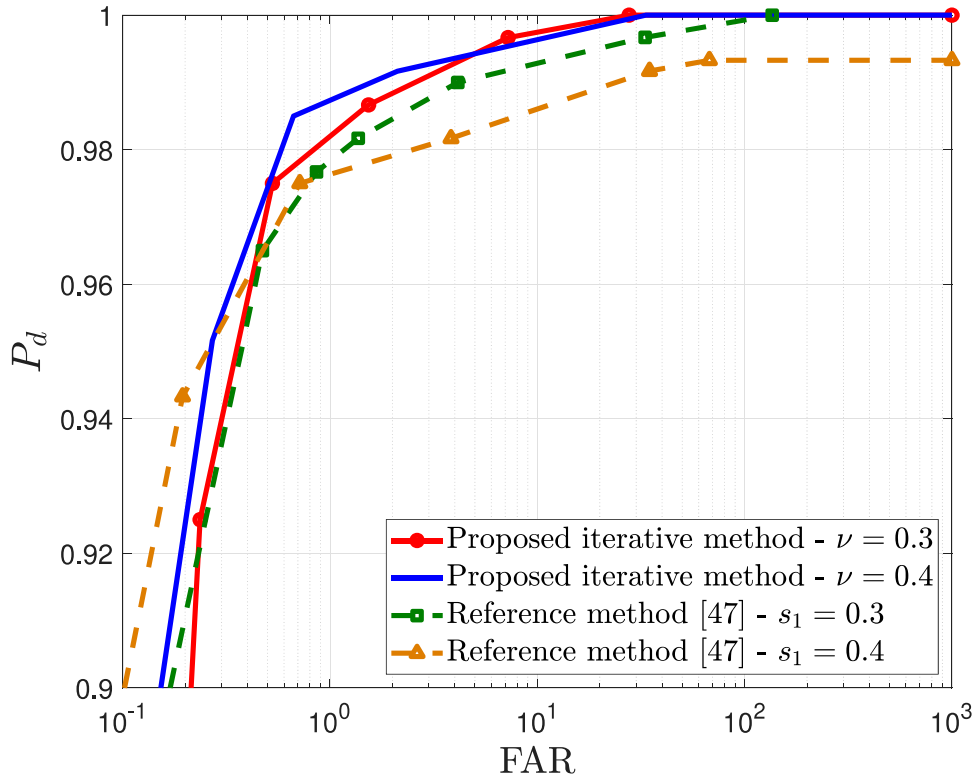

Figure 5.10: ROC performance comparison between the proposed iterative method and the best curves of the reference method.

5.3 Study Case 2: Gaussian Distribution

As previously observed in Section 5.2, the Bivariate Rayleigh distribution is not the ideal selection for the clutter-plus-noise model, considering the CARABAS II data set. Other bivariate distributions that were already used for this data set are the Bivariate Gaussian distribution [76, 61], the Bivariate Gamma distribution [47], and the K-distribution [48].

However, these three distributions have some particularities that jeopardize their selection for the method evaluation. According to [61], the Bivariate Gaussian distribution was used only due to its simplicity for the initial change detection tests in this data set, even knowing that the distribution does not provide a good fit for the images in the data set. On the other hand, the Bivariate Gamma distribution, and the K-distribution provided interesting results for change detection methods using wavelength-resolution images [48, 47]. However, these distributions are not good options for the evaluated scenario, especially for the iterative case, due to the computational complexity associated with them, which is mainly related to the estimation of the parameters. The estimation of these parameters can be a challenging problem and requires more sophisticated solutions than the one used for the Gaussian or the Rayleigh distribution,

resulting in higher computational complexity. Some examples of methods for the estimations of the parameters are presented in [113, 114].

Recently, the authors in [65] presented a study about the stability of wavelength-resolution SAR images considering images from the CARABAS II data set. According to [65], images obtained from the difference between two images with the same flight characteristics can be modeled as Gaussian distributed. Thus, under similar considerations than the ones made in [47, 48], a pair of wavelength-resolution SAR difference images can be modeled as Bivariate Gaussian distributed. To use the same notation adopted in Section 5.1, the difference image pairs used in this study can be written as

$$z_s = z_i - z_{r2}, \tag{5.14}$$

$$z_r = z_{r1} - z_{r2}, \tag{5.15}$$

where z_i is the image of interest, which is expected to contain the changes, and z_{r1} and z_{r2} are two reference images. Hence, for the evaluation of the proposed change detection method using two difference images as inputs, the Bivariate Gaussian distribution is selected as the case of study. The probability density function $p(z_s, z_r)$ is assumed to be Bivariate Gaussian distributed and can be written as [110]

$$\begin{aligned} p(z_s, z_r) = \frac{1}{2\pi\sigma_s\sigma_r\sqrt{1-\rho^2}} \exp\left(-\frac{1}{2(1-\rho^2)}\left[\frac{(z_s-\mu_s)^2}{\sigma_s^2}\right.\right. \\ \left.\left. +\frac{(z_r-\mu_r)^2}{\sigma_r^2} - \frac{2\rho(z_s-\mu_s)(z_r-\mu_r)}{\sigma_s\sigma_r}\right]\right), \end{aligned} \tag{5.16}$$

where μ_s, μ_r, σ_s and σ_r are, the mean values and standard deviations of the difference images z_s and z_r amplitudes, and ρ is the correlation coefficient that can be obtained by using (5.12).

5.3.1 Applications Aspects

The studied case presented throughout Section 5.2 consists of the use of the proposed method using the Bayes theorem with two difference images z_s and z_r as inputs. To evaluate the selection of the Bivariate Gaussian distribution and provide useful information for application constraints, Figure 5.11 is presented. Figure 5.11 shows the theoretical Bivariate Gaussian surface plot obtained from (5.16) and the three-dimensional histogram of the experimental data one difference image of the CARABAS II data set.

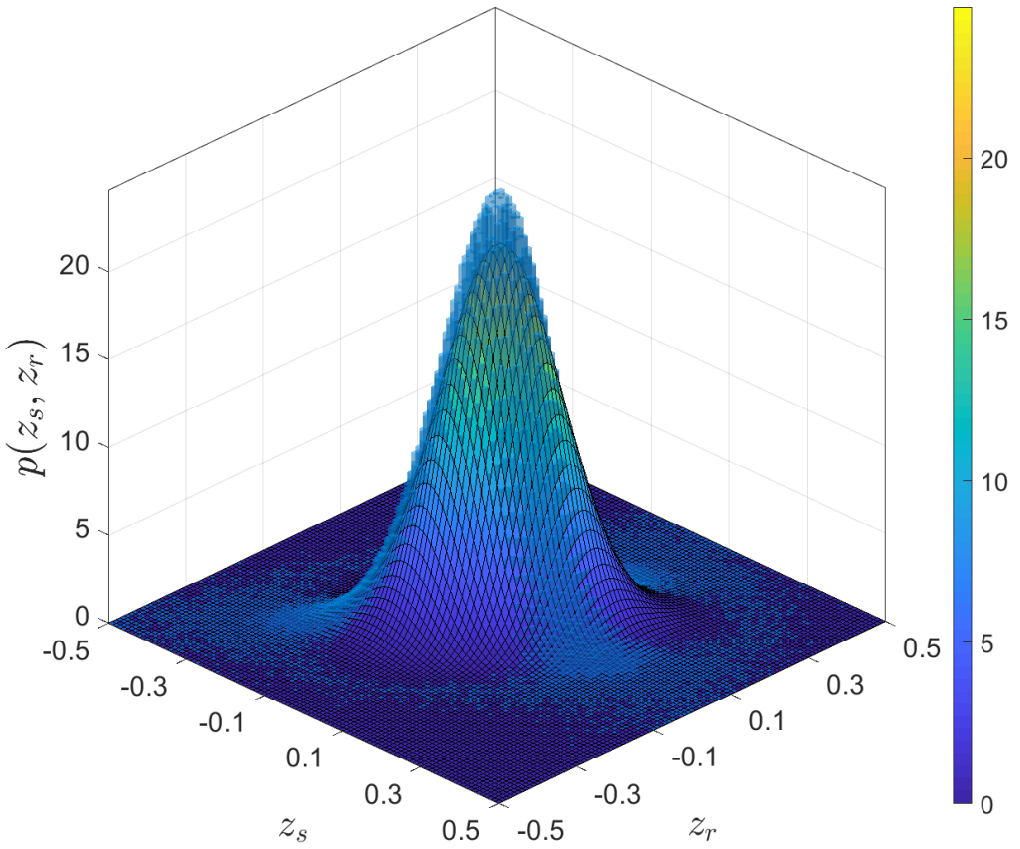

Figure 5.11: Surface plot of the theoretical Bivariate Gaussian distribution and the three-dimensional histogram of the difference images data.

As can be observed, there is a mismatch between the selected bivariate distribution and the data histogram. Similar mismatched-patterns as the ones observed in Section 5.2.1 are also detected for the Bivariate Gaussian distribution. Thus, similar conclusions and analysis can be drawn. However, it is possible to observe that the Bivariate Gaussian distribution provides a better match than the Bivariate Rayleigh distribution. This better-fit results in minor mismatch regions and minor discrepancies between the probabilities values when compared with the analysis presented in Section 5.2.1.

To further discuss the candidate distribution selection, the mismatch between the data histogram and a theoretical distribution is evaluated for one difference image. According to [65], the surveillance image used as input is modeled as Gaussian distributed. Figure 5.12 shows the theoretical Gaussian distribution plot and the histogram of the experimental data from the difference image. Also, the regions where mismatches were observed are highlighted.

The patterns observed in Figure 5.11 are also detected in Figure 5.12. The first detected pattern represented by sub-figure A) consists of a target-like pattern occurring for small

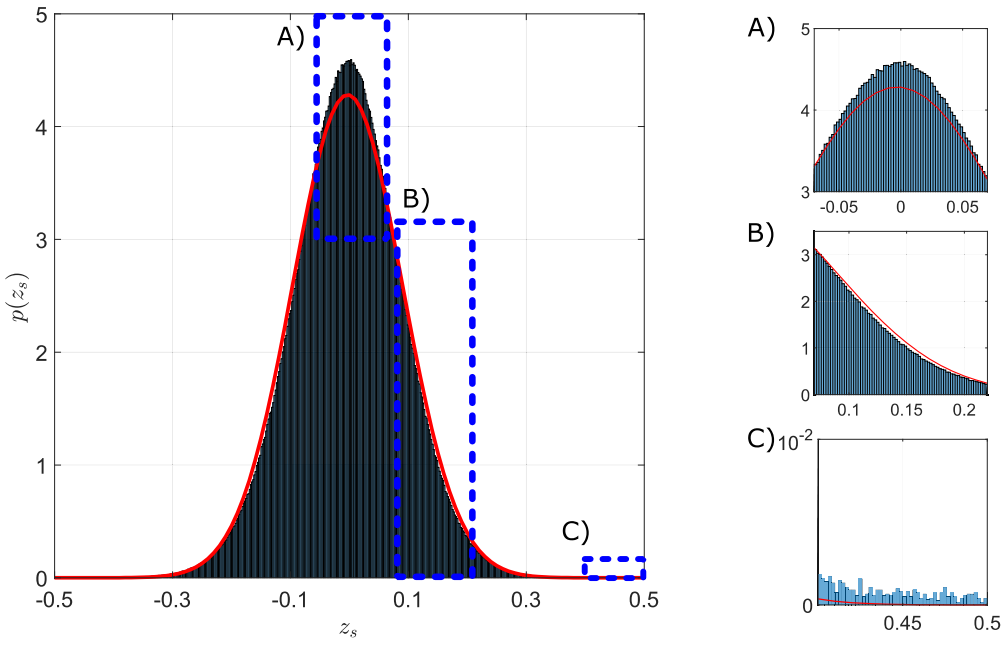

Figure 5.12: Theoretical Gaussian distribution and difference image data histogram. The regions where mismatches were observed are highlighted.

amplitudes values, i.e., $|z_s| < 0.05$. Since it is not expected that targets contain low-amplitude values, this situation tends to result in false alarms. However, due to the small values of discrepancies between the histogram and distribution model, these false alarms only will be an issue for low probability threshold values. The pattern of sub-figure B) consists of a region where no target can be detected due to the mismatch. Due to the region's low-amplitude values, this is not an issue for the application. Finally, sub-figure C) consists of the expected target-like pattern for adequate amplitude values. Thus, based on this analysis, there is no necessity of a minimum amplitude constraint like the one considered for the Bivariate Rayleigh distribution.

As mentioned in Section 5.2.1, the proposed method detects changes in both surveillance and reference image inputs. It is possible to detect changes only in the image of interest (z_i) by evaluating points only if $|z_s| \geq z_r$. Thus, to detect only changes in the image of interest, one application constraint is applied in the processing chain, which consists of setting the probability $P\left(s \equiv s_T | z_u, z_r\right) = 0$ if

$$|z_s| < |z_r|, \tag{5.17}$$

otherwise, the conditional probability is calculated using (5.9) for the non-iterative case or (5.10) for the iterative case.

Finally, the rest of the application setup for the non-iterative case, e.g., morphological operations, average filtering, and simulation parameters, follow the same configurations

discussed in Section 5.2.1. Similarly, the rest of the application setup for the iterative case, e.g., average filtering, and simulation parameters is the same as the one presented in Section 5.2.1.

5.3.2 Experimental Results

The experimental evaluation of the proposed change detection method using the Bayes theorem considers all the 24 incoherent CARABAS II images from the data set presented in Chapter 3. The image sets, which form the two difference image inputs used in the evaluation were selected according to the following criteria: i) The 24 images were selected once as the image of interest; ii) the sets were formed only by the same pass images; iii) the reference images pairs were always unique. This selection is presented in detail throughout this section.

Similarly to Section 4.2.3, the methods' performance is assessed in terms of the P_d and FAR. Moreover, the same decision criterion is considered regarding any object detected.

The first evaluation consists of the comparison of the ROC curve performances between the proposed method for both non-iterative and iterative approaches, and two already presented change detection methods from the literature [47, 61]. Figure 5.13 presents the performance of the proposed method and the best ROC curves presented in [47, 61].

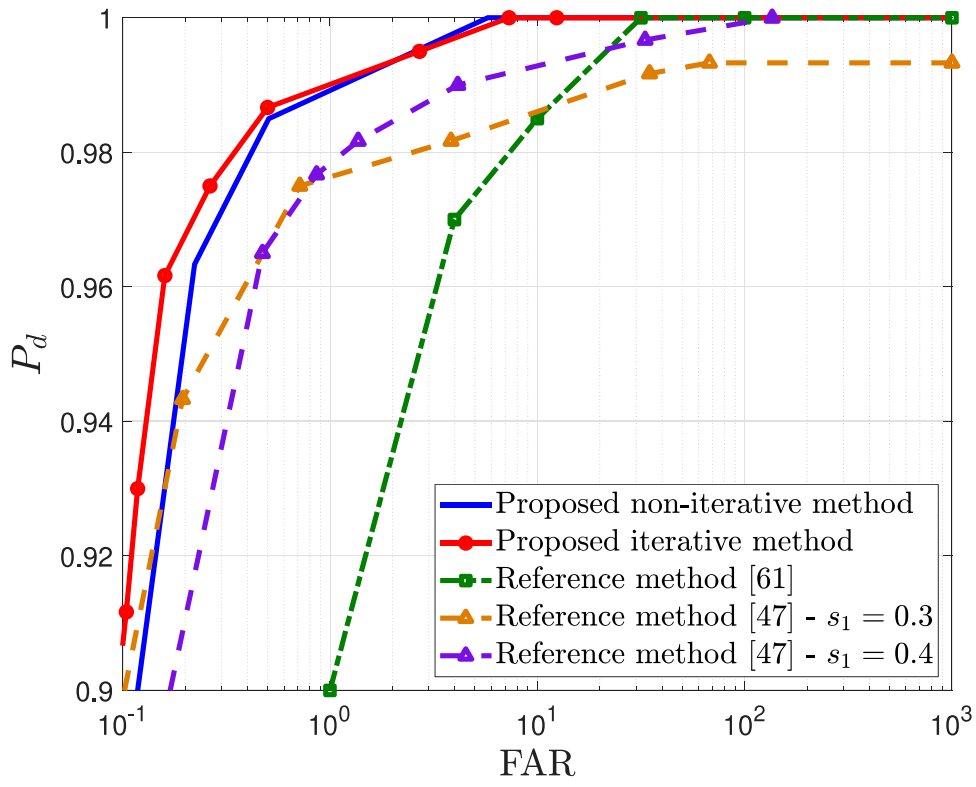

Figure 5.13: ROC performance comparison between the proposed method, for both non-iterative and iterative approaches, and the best curves of the reference methods.

From the results presented in Figure 5.13, it is possible to observe that the proposed iterative method outperforms all other methods for the majority of the tested points. Moreover, the non-iterative method outperforms the one presented in [61] for all the tested points and the one proposed in [47] with $s_1 = 0.4$ for $P_d > 0.93$. Also, considering the points with FAR = 10^0, the proposed method considering non-iterative and iterative approaches achieve the performance of $P_d \approx 0.99$. For the same evaluated point, the method presented in [61] has $P_d \approx 0.90$, and the method of [47] has $P_d \approx 0.978$ for $s_1 = 0.3$ and $P_d \approx 0.976$ for $s_1 = 0.4$.

The following evaluation consists of the comparison among the best results for both study cases considered in this document. These experimental results are presented in Figure 5.14. As it can be observed the techniques using the Bivariate Gaussian distribution outperforms the ones using the Bivariate Rayleigh distribution, for all the tested points. These results were expected due to the use of the difference images, which tend to remove some types of non-target-structures in the input images, and due to the use of a better-matched distribution selection.

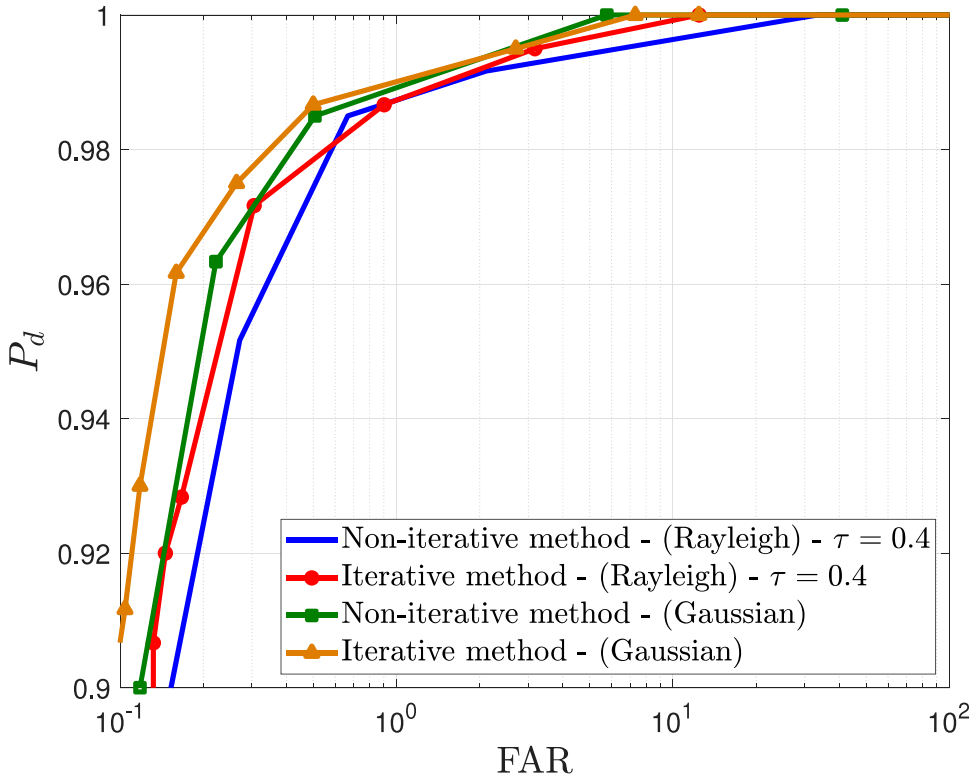

Figure 5.14: ROC performance comparison between the proposed method best ROC curves for both studied cases, considering both non-iterative and iterative approaches.

To further investigate the performance of the studied Case 2, Table 5.2 presents the results for a specific test setup. By comparison with the results presented in Table 5.1, Table 5.2 reveals

Table 5.2: Performance results of the proposed non-iterative method for a probability threshold of 0.5.

Exp. No.	Interest image		Reference image 1		Reference image 2		Number of detected targets	Detection probability	Number of false alarms	False alarm rate (km^{-2})
	Mission	Pass	Mission	Pass	Mission	Pass				
1	2	1	3	1	4	1	25	1.00	0	0.00
2	3	1	4	1	5	1	25	1.00	4	0.67
3	4	1	5	1	2	1	25	1.00	1	0.17
4	5	1	2	1	3	1	24	0.96	2	0.33
5	2	2	3	2	4	2	25	1.00	1	0.17
6	3	2	4	2	5	2	25	1.00	5	0.83
7	4	2	5	2	2	2	25	1.00	8	1.33
8	5	2	2	2	3	2	25	1.00	1	0.17
9	2	3	3	3	4	3	25	1.00	2	0.33
10	3	3	4	3	5	3	24	0.96	0	0.00
11	4	3	5	3	2	3	25	1.00	2	0.33
12	5	3	2	3	3	3	25	1.00	0	0.00
13	2	4	3	4	4	4	25	1.00	1	0.17
14	3	4	4	4	5	4	25	1.00	2	0.33
15	4	4	5	4	2	4	25	1.00	2	0.33
16	5	4	2	4	3	4	24	0.96	3	0.50
17	2	5	3	5	4	5	25	1.00	0	0.00
18	3	5	4	5	5	5	19	0.76	29	4.83
19	4	5	5	5	2	5	25	1.00	0	0.00
20	5	5	2	5	3	5	25	1.00	5	0.83
21	2	6	3	6	4	6	25	1.00	1	0.17
22	3	6	4	6	5	6	25	1.00	1	0.17
23	4	6	5	6	2	6	25	1.00	1	0.17
24	5	6	2	6	3	6	25	1.00	2	0.33
Total							591	0.985	73	0.51

that the proposed method presents better performance for both detection probability (591 target detections against 585) and false alarm rate (73 false alarms against 76).

Finally, the evaluated scenarios show that both proposed non-iterative and iterative methods present a competitive performance when compared with other techniques from the literature and with the study case presented in Section 5.2. Considering an adequate selection of the distribution and application constraints, the proposed method can be applied for other data sets and SAR images without losing generality.

5.4 Concluding Remarks

This chapter presented the proposal of a change detection method using the Bayes theorem for SAR images. Section 5.1 showed an analysis of the Bayes' theorem application in SAR change detection based on the use of different statistical models for the clutter-plus-noise. Moreover, two versions of the proposed change detection method are presented, i.e., iterative and non-iterative. An important feature of the proposed method is that it enables the change detection algorithm to consider different clutter-plus-noise distribution models in its formulation.

Sections 5.2 and 5.3 presented two distribution study cases for the proposed change detection method of Section 5.1, for both non-iterative and iterative approaches. The experimental results show that, for both study cases, the proposed change detection method is capable of achieving high detection probability values for low FAR scenarios, e.g., $P_d > 0.90$ and FAR $< 10^0$, considering an adequate selection of the distribution model and the application constraints. When compared to recently proposed change detection methods in the literature, the proposed technique provided competitive performance in terms of both evaluated metrics.

Finally, the results, discussions, and part of the text presented in Section 5.1 and 5.2 were already submitted to a journal, and it is currently under evaluation. Also, it is expected to submit for publication, shortly, the contributions presented in Section 5.3.

6

Concluding Remarks

In this dissertation, new change detection methods are proposed and studied for wavelength-resolution SAR images focusing on target detection applications. The contributions of this dissertation can be divided into the ones based on the use of SAR image stacks and the ones based on the implementation of the Bayes theorem into SAR change detection.

First, a statistical test analysis was performed for stacks of wavelength-resolution SAR images. The experimental results from this analysis indicated the best statistical distribution model, from a finite set of available distributions, that yields an adequate fit for the majority of the evaluated pixels. From these results, new change detection methods are proposed. They are divided into two classes, the NP criterion-based and the masking techniques based.

Second, a study regarding the implementation of the Bayesian detection methods is presented. Based on this study, a non-iterative version and an iterative version of a change detection method using the Bayes theorem are proposed. The proposed methods enable the use of different clutter-plus-noise distribution models and do not strictly require the assumption of a target model distribution. Moreover, the methods provide more information on the detected targets than traditional binary detection. Finally, two scenarios were studied considering two different clutter-plus-noise distribution models.

The performance of the proposed methods is evaluated in terms of detection probability and false alarm rate using real data from measurements made using the CARABAS II SAR system. The performance of the proposed change detection methods is compared with traditional and recent change detection methods from the literature. The results show that the proposed techniques provide better performance in terms of both metrics, i.e., P_d and FAR, under consideration for the majority of the evaluated cases.

Furthermore, comparing the proposed change detection methods performances and their requirements, it is possible to state that they are more suitable for different application scenarios. For instance, the use of image stacks tends to provide better performance in terms of the evaluated metrics than the methods using only two SAR images. However, these methods require the availability of multiple images with the same, or at least similar, measurement flight geometries. Additionally, some of these proposals, e.g., the masking based ones, require some information about the desired targets. Thus, given that their requirements are fulfilled, the stack-based methods tend to be a better selection for change detection applications than the traditional ones that use only two images. On the other hand, the change detection methods based on the Bayes theorem are adequate for scenarios where the clutter-plus-noise statistical distribution is well chosen. Applying well this Bayes approach, results for image pair tend to have similar performance than for some of the image stack proposed methods. Therefore, these methods can be used for a large set of detection applications, especially in scenarios where the requirements of the stack-based ones are not fulfilled. Moreover, the extra information regarding the detected targets can be further explored by the system operator in those applications.

Finally, based on this dissertation contributions, the following papers were submitted for publication:

1. D. I. Alves, B. G. Palm, M. I. Pettersson, V. T. Vu, R. Machado, B. F. Uchôa-Filho, P. Dammert, and H. Hellsten, "A statistical analysis for wavelength-resolution SAR image stacks," *IEEE Geoscience and Remote Sensing Letters*, vol. 17, no. 2, pp. 227-231, Feb. 2020.

2. D. I. Alves, B. G. Palm, H. Hellsten, V. T. Vu, M. I. Pettersson, R. Machado, B. F. Uchôa-Filho, and P. Dammert, "Wavelength-resolution SAR change detection using Bayes' theorem," *IEEE Journal of Selected Topics in Applied Earth Observations and Remote Sensing*, 2020. Submitted on February 13^{th} 2020. Current status: Under Review.

3. D. I. Alves, C. Muller, B. G. Palm, M. I. Pettersson, V. T. Vu, R. Machado, B. F. Uchôa-Filho, P. Dammert, and H. Hellsten, "Neyman-Pearson criterion-based change detection methods for wavelength-resolution SAR image stacks," *IEEE Transactions on Geoscience and Remote Sensing*, 2020. Submitted on January 17^{th} 2020. Current status: Under Review.

During the Ph.D. period, the author contributed as a collaborator with other researchers in projects that are related to the topics studied in this dissertation. These contributions resulted in the following papers:

4. V. T. Vu, D. I. Alves, B. G. Palm, N. R. Gomes and M. I. Pettersson, “Wavelength-resolution SAR change detection with changing flight heading during passes,” *in 2019 SEE Radar Conference*. Sep. 2019.

5. V. T. Vu, D. I. Alves, B. G. Palm, M. I. Pettersson, P. Dammert, and H. Hellsten, “A detector for wavelength resolution SAR incoherent change detection,” *in 2019 IEEE Radar Conference (RadarConf19)*. Apr. 2019.

6. L. P. Ramos, D. I. Alves, R. Machado, and B. F. Uchôa-Filho, “Influência de janelas internas em filtros CFAR para algoritmos de detecção de alvos em imagens SAR,” *in XXXVII Simpósio Brasileiro de Telecomunicações e Processamento de Sinais (SBrT 2019)*. Set. 2019.

7. B. G. Palm, D. I. Alves, V. T. Vu, M. I. Pettersson, F. M. Bayer, R. J. Cintra, R. Machado, P. Dammert, and H. Hellsten, “Autoregressive model for multi-pass SAR change detection based on image stacks,” *in SPIE Remote Sensing: Image and Signal Processing for Remote Sensing XXIV*. Oct. 2018.

8. L. P. Ramos, V. I. A. Medeiros, D. I. Alves, C. Muller, R. Machado, and B. F. Uchôa-Filho, “Influência de operações morfológicas em algoritmo de detecção de alvos para imagens SAR VHF UWB,” *in XXXVI Simpósio Brasileiro de Telecomunicações e Processamento de Sinais (SBrT 2018)*. Set. 2018.

9. L. P. Ramos, V. I. A. Medeiros, C. Muller, D. I. Alves, and R. Machado, “Estudo da influência de operações morfológicas em métodos de detecção de mudanças para imagens SAR de alta resolução,” *in XX Simpósio de Aplicações Operacionais em Áreas de Defesa (SIGE 2018)*. Set. 2018. pp. 190-194.

10. A. C. F. Fabrin, R. D. Molin Jr, D. I. Alves, R. Machado, F. M. Bayer, and M. I. Pettersson, “ A CFAR optimization for low frequency UWB SAR change detection algorithms,” *in 2017 IEEE International Geoscience and Remote Sensing Symposium (IGARSS)*. Jul. 2017, pp. 1071-1074.

11. R. D. Molin Jr, A. C. F. Fabrin, P. Sperotto, D. I. Alves, F. M. Bayer, R. Machado, and M. I. Pettersson, H. Hellsten, P. Dammert, and L. M H. Ulander, "Iterative change detection algorithm for low-frequency UWB SAR," *in XXXIV Simpósio Brasileiro de Telecomunicações e Processamento de Sinais (SBrT 2016)*. Set. 2016.

6.1 Future Works

There are still topics that can be further studied regarding the proposals presented in Chapters 4 and 5. Some topics regarding the proposals presented in Chapter 4 are:

- The evaluation of the performance impact of the use of Type I error control techniques in the mask formation process for the proposed masking change detection methods;
- The use of the obtained background statistics for image stacks in other decision criteria for target detection applications;
- Analytical performance metrics derivations for the proposed change detection methods;
- The evaluation of the proposed change detection methods for other data sets of SAR images.

Some topics regarding the proposals presented in Chapter 5 are:

- The evaluation of other clutter-plus-noise candidate distributions in the proposed techniques;
- To further study the presented Bayes' theorem implementation in SAR change detection to obtain analytical performance metrics derivations;
- The evaluation of the proposed change detection methods for other data sets of SAR images.

6.2 Financial Support

This work was partially supported by the Brazilian National Council for Scientific and Technological Development (CNPq) with scholarship 208402/2017-9 and by the Swedish-Brazilian Research and Innovation Centre (CISB) and SAAB with scholarships related to "*Chamada de Projetos* CISB SAAB 04/2016". Additionally, the author acknowledges the support of the *Universidade Federal do Pampa* granted in "*Portaria* 103/2018".

Bibliography

[1] O. Blumtritt, H. Petzold, and W. Aspray, *Tracking the History of Radar*, 1st ed. New Jersey, USA: IEEE-Rutgers Center for History of Electrical Engineering and Deutsches Museum, 1994.

[2] H. Hertz, *Electric waves: being researches on the propagation of electric action with finite velocity through space*, 1st ed. London, England: Dover Publications, 1893.

[3] J. L. Eaves and E. K. Reedy, *Principles of modern radar*, 1st ed. New York, USA: Chapman & Hall, 1987.

[4] A. O. Bauer, "Hülsmeyer's early radar commitments," in *2004 International Conference on Radar Systems (RADAR)*, Toulouse, France, Oct. 2004.

[5] M. I. Skolnik, *Introduction to radar systems*, 2nd ed. Singapure: McGraw-Hill, 1981.

[6] J. E. S. Fransson, F. Walter, and L. M. H. Ulander, "Estimation of forest parameters using CARABAS-II VHF SAR data," *IEEE Transactions on Geoscience and Remote Sensing*, vol. 38, no. 2, pp. 720–727, Mar. 2000.

[7] J. F. Vesecky and R. H. Stewart, "The observation of ocean surface phenomena using imagery from the SEASAT synthetic aperture radar: An assessment," *Journal of Geophysical Research*, vol. 87, no. C5, pp. 3397–3430, 1982.

[8] M. I. Pettersson, J. Askne, and D. J. Cavalieri, "SAR observations of arctic freeze-up compared to SSM/I during ARCTIC'91," *International Journal of Remote Sensing*, vol. 17, no. 13, pp. 2603–2624, 1996.

[9] E. Rignot, J. L. Bamber, M. R. van den Broeke, C. Davis, Y. Li, W. van den Berg, and E. van Meijgaard, "Recent antarctic ice mass loss from radar interferometry and regional climate modelling," *Nature Geoscience*, vol. 1, pp. 106–108, 2008.

[10] V. T. Vu, T. K. Sjogren, M. I. Pettersson, and P. A. C. Marques, "Application of the moving target detection by focusing technique in civil traffic monitoring," in *2010 IEEE International Geoscience and Remote Sensing Symposium (IGARSS)*, Honolulu, USA, Jul. 2010, pp. 4118–4121.

[11] V. Kotelnikov, A. Bogomolov, and O. Rzhiga, "Radar study of venus surface by VENERA-15 and -16 spacecraft," *Advances in Space Research*, vol. 5, no. 8, pp. 5–16, 1985.

[12] G. Galati, G. Perrotta, S. D. Girolamo, and R. Mura, "Space-based SSR constellation for global air traffic control," *IEEE Transactions on Aerospace and Electronic Systems*, vol. 32, no. 3, pp. 1088–1106, Jul. 1996.

[13] D. Parker, "Microwave industry outlook - defense applications," *IEEE Transactions on Microwave Theory and Techniques*, vol. 50, no. 3, pp. 1039–1041, Mar. 2002.

[14] J. C. Curlander and R. N. McDonough, *Synthetic aperture radar*, 1st ed. New York, USA: John Wiley & Sons New York, 1991.

[15] C. A. Wiey, "Pulsed Doppler radar methods and apparatus," Patent US 3 196 436, Jul. 20, 1965.

[16] A. Love, "In memory of carl a. wiley," *IEEE Antennas and Propagation Society Newsletter*, vol. 27, no. 3, pp. 17–18, Jun. 1985.

[17] M. A. Richards, J. A. Scheer, and W. A. Holm, *Principles of modern radar: volume I - basic principles*, 1st ed. Raleigh, USA: SciTech Publishing, 2010.

[18] M. Lazecky, I. Hlavacova, M. Bakon, J. J. Sousa, D. Perissin, and G. Patricio, "Bridge displacements monitoring using space-borne X-band SAR interferometry," *IEEE Journal of Selected Topics in Applied Earth Observations and Remote Sensing*, vol. 10, no. 1, pp. 205–210, Jan. 2017.

[19] S. Li, Y. Wang, P. Chen, X. Xu, C. Cheng, and B. Chen, "Spatiotemporal fuzzy clustering strategy for urban expansion monitoring based on time series of pixel-level optical and SAR images," *IEEE Journal of Selected Topics in Applied Earth Observations and Remote Sensing*, vol. 10, no. 5, pp. 1769–1779, May 2017.

[20] B. Snapir, T. W. Waine, R. Corstanje, S. Redfern, J. D. Silva, and C. Kirui, "Harvest monitoring of kenyan tea plantations with X-band SAR," *IEEE Journal of Selected Topics in Applied Earth Observations and Remote Sensing*, vol. 11, no. 3, pp. 930–938, Mar. 2018.

[21] H. Yan, R. Wang, F. Li, Y. Deng, and Y. Liu, "Ground moving target extraction in a multichannel wide-area surveillance SAR/GMTI system via the relaxed PCP," *IEEE Geoscience and Remote Sensing Letters*, vol. 10, no. 3, pp. 617–621, May 2013.

[22] M. Kirscht, J. Mietzner, B. Bickert, A. Dallinger, J. Hippler, J. Meyer-Hilberg, R. Zahn, and J. Boukamp, "An airborne radar sensor for maritime and ground surveillance and reconnaissance-algorithmic issues and exemplary results," *IEEE Journal of Selected Topics in Applied Earth Observations and Remote Sensing*, vol. 9, no. 3, pp. 971–979, Mar. 2016.

[23] Y. Wang, Z. Zhang, N. Li, F. Hong, H. Fan, and X. Wang, "Maritime surveillance with undersampled SAR," *IEEE Geoscience and Remote Sensing Letters*, vol. 14, no. 8, pp. 1423–1427, Aug. 2017.

[24] W. L. Melvin and J. A. Scheer, *Principles of Modern Radar: volume III - Radar Applications*, 1st ed. Edison, USA: SciTech Publishing, 2014.

[25] H. Hellsten, L. M. H. Ulande, A. Gustavsson, and B. Larsson, "Development of VHF CARABAS II SAR," in *Radar Sensor Technology*, vol. 2217, Orlando, USA, Apr. 1996, pp. 48–60.

[26] L. A. Bessette and S. Ayasli, "Ultra-wideband P-3 and CARABAS II foliage attenuation and backscatter analysis," in *2001 IEEE Radar Conference (RadarConf 2001)*, Atlanta, USA, May 2001, pp. 357–362.

[27] L. M. H. Ulander, P.-O. Froelind, A. Gustavsson, H. Hellsten, T. Jonsson, B. Larsson, and G. Stenstrom, "Performance of the CARABAS-II VHF-band synthetic aperture radar," in *2001 IEEE International Geoscience and Remote Sensing Symposium (IGARSS)*, vol. 1, Sydney, Australia, Aug. 2001, pp. 129–131.

[28] H. Hellsten, S. Sahlin, and P. Dammert, "Polarimetric subsurface SAR imaging outcome of theoretical development and CARABAS III tests," in *2014 IEEE International Radar Conference*, Lille, France, Oct. 2014, pp. 1–8.

[29] P.-O. Frolind and L. M. H. Ulander, "Motion compensation effects for repeat-pass processing in wavelength-resolution SAR," in *1998 IEEE International Geoscience and Remote Sensing Symposium (IGARSS)*, vol. 5, Seatle, USA, Jul. 1998, pp. 2637–2639.

[30] N. R. Gomes, M. I. Pettersson, V. T. Vu, P. Dammert, and H. Hellsten, "Likelihood ratio test for incoherent wavelength-resolution SAR change detection," in *2016 CIE International Conference on Radar (RADAR)*, Guangzhou, China, Oct. 2016, pp. 1–4.

[31] V. T. Vu, M. I. Pettersson, R. Machado, P. Dammert, and H. Hellsten, "False alarm reduction in wavelength-resolution SAR change detection using adaptive noise canceler," *IEEE Transactions on Geoscience and Remote Sensing*, vol. 55, no. 1, pp. 591–599, Jan. 2017.

[32] H. Israelsson, L. M. H. Ulander, J. L. H. Askne, J. E. S. Fransson, P.-O. Frolind, A. Gustavsson, and H. Hellsten, "Retrieval of forest stem volume using vhf SAR," *IEEE Transactions on Geoscience and Remote Sensing*, vol. 35, no. 1, pp. 36–40, Jan. 1997.

[33] P. Melon, J. M. Martinez, T. L. Toan, L. M. H. Ulander, and A. Beaudoin, "On the retrieving of forest stem volume from VHF SAR data: observation and modeling," *IEEE Transactions on Geoscience and Remote Sensing*, vol. 39, no. 11, pp. 2364–2372, Nov. 2001.

[34] K. Folkesson, G. Smith-Jonforsen, and L. M. H. Ulander, "Model-based compensation of topographic effects for improved stem-volume retrieval from CARABAS-II VHF-band SAR images," *IEEE Transactions on Geoscience and Remote Sensing*, vol. 47, no. 4, pp. 1045–1055, Apr. 2009.

[35] L. M. H. Ulander, W. E. Pierson, M. Lundberg, P. Follo, P.-O. Frolind, and A. Gustavsson, "Performance of VHF-band SAR change detection for wide-area surveillance of concealed ground targets," in *SPIE Defense and Security Symposium: Algorithms for Synthetic Aperture Radar Imagery XI*, vol. 5427, Orlando, USA, Sep. 2004, pp. 259–270.

[36] Z. Wei, G. Jian, and W. Jie, "Change detection of concealed targets using repeat-pass SAR images," in *1st Asian and Pacific Conference on Synthetic Aperture Radar*, Huangshan, China, Nov. 2007, pp. 275–278.

[37] L. M. H. Ulander, B. Flood, P.-O. Frolind, A. Gustavsson, T. Jonsson, B. Larsson, M. Lundberg, D. Murdin, and G. Stenstrom, "Change detection of vehicle-sized targets in forest concealment using VHF- and UHF-band SAR," *IEEE Aerospace and Electronic Systems Magazine*, vol. 26, no. 7, pp. 30–36, Jul. 2011.

[38] H. Hellsten, P.-O. Froelind, A. Gustavsson, T. Jonsson, B. Larsson, G. Stenstroem, B. T. Binder, M. Mirkin, and S. Ayasli, "Ultra-wideband VHF SAR - design and measurements," in *SPIE International Symposium on*

Optical Engineering and Photonics in Aerospace Sensing: Aerial Surveillance Sensing Including Obscured and Underground Object Detection, vol. 2217, Orlando, USA, Apr. 1994, pp. 16–25.

[39] K. N. L. Priya, R. Nagendran, and A. Sreedevi, "Detection of foliage covered immobile targets based on incoherent change detection and SURE," in *2012 International Conference on Communications, Devices and Intelligent Systems (CODIS)*, Kolkata, India, Dec. 2012, pp. 389–392.

[40] W. Ye, C. Paulson, D. O. Wu, and J. Li, "A target detection scheme for VHF SAR ground surveillance," in *SPIE Defense and Security Symposium: Algorithms for Synthetic Aperture Radar Imagery XV*, vol. 6970, Orlando, USA, Apr. 2008, pp. 270–281.

[41] Y. C. Liu, G. X. Wang, P. Li, and X. P. Yan, "Unsupervised sar change detection based on a new statistical model," in *IET International Radar Conference 2015*, Hangzhou, China, Oct. 2015, pp. 1–4.

[42] M. Liguori, A. Izzo, C. Clemente, C. Galdi, M. D. Bisceglie, and J. Soraghan, "A location scale based CFAR detection framework for FOPEN SAR images," in *2015 Sensor Signal Processing for Defence (SSPD)*, Edinburgh, UK, Sep. 2015, pp. 1–5.

[43] M. I. Pettersson, V. T. Vu, N. R. Gomes, P. Dammert, and H. Hellsten, "Incoherent detection of man-made objects obscured by foliage in forest area," in *2017 IEEE International Geoscience and Remote Sensing Symposium (IGARSS)*, Fort Worth, USA, Jul. 2017, pp. 1892–1895.

[44] V. T. Vu, "Wavelength-resolution SAR incoherent change detection based on image stack," *IEEE Geoscience and Remote Sensing Letters*, vol. 14, no. 7, pp. 1012–1016, Jul. 2017.

[45] R. Machado, M. I. Pettersson, V. T. Vu, P. Dammert, and H. Hellsten, "Empirical-statistical analysis of amplitude SAR images for change detection algorithms," in *2015 IEEE International Geoscience and Remote Sensing Symposium (IGARSS)*, Milan, Italy, Jul. 2015, pp. 365–368.

[46] H. Hellsten, R. Machado, M. I. Pettersson, V. T. Vu, and P. Dammert, "Experimental results on change detection based on bayes probability theorem," in *2015 IEEE International Geoscience and Remote Sensing Symposium (IGARSS)*, Milan, Italy, Jul. 2015, pp. 318–321.

[47] V. T. Vu, N. R. Gomes, M. I. Pettersson, P. Dammert, and H. Hellsten, "Bivariate gamma distribution for wavelength-resolution SAR change detection," *IEEE Transactions on Geoscience and Remote Sensing*, vol. 57, no. 1, pp. 473–481, Jan. 2019.

[48] N. R. Gomes, P. Dammert, M. I. Pettersson, V. T. Vu, and H. Hellsten, "Comparison of the rayleigh and K-distributions for application in incoherent change detection," *IEEE Geoscience and Remote Sensing Letters*, vol. 16, no. 5, pp. 756–760, May 2019.

[49] A. Moreira, P. Prats-Iraola, M. Younis, G. Krieger, I. Hajnsek, and K. P. Papathanassiou, "A tutorial on synthetic aperture radar," *IEEE Geoscience and Remote Sensing Magazine*, vol. 1, no. 1, pp. 6–43, Mar. 2013.

[50] T. K. Sjoegren, A. Gustavsson, P.-O. Froelind, T. Jonsson, G. Stenstroem, and L. M. H. Ulander, "Experimental results for human detection in UHF UWB SAR," in *10th European Conference on Synthetic Aperture Radar (EUSAR 2014)*, Berlin, Germany, Jun. 2014, pp. 1–4.

[51] K. Tomiyasu, "Tutorial review of synthetic-aperture radar (SAR) with applications to imaging of the ocean surface," *Proceedings of the IEEE*, vol. 66, no. 5, pp. 563–583, May 1978.

[52] C. Oliver and S. Quegan, *Understanding Synthetic Aperture Radar Images*, 1st ed. Boston, USA: SciTech Publishing, 2004.

[53] R. N. McDonough, B. E. Raff, and J. L. Kerr, "Image formation from spaceborne synthetic aperture radar signals," *Johns Hopkins APL Technical Digest*, vol. 6, no. 4, pp. 300–312, Oct. 1985.

[54] R. Wu, J. Li, Z. Bi, and P. Stoica, "SAR image formation via semiparametric spectral estimation," *IEEE Transactions on Aerospace and Electronic Systems*, vol. 35, no. 4, pp. 1318–1333, Oct. 1999.

[55] M. Antoniou, R. Saini, and M. Cherniakov, "Results of a space-surface bistatic SAR image formation algorithm," *IEEE Transactions on Geoscience and Remote Sensing*, vol. 45, no. 11, pp. 3359–3371, Nov. 2007.

[56] B. Rigling, W. Garber, R. Hawley, and L. Gorham, "Wide-area, persistent SAR imaging: Algorithm tradeoffs," *IEEE Aerospace and Electronic Systems Magazine*, vol. 29, no. 1, pp. 14–20, Jan. 2014.

[57] H. Xie, S. Shi, D. An, G. Wang, G. Wang, H. Xiao, X. Huang, Z. Zhou, C. Xie, F. Wang, and Q. Fang, "Fast factorized backprojection algorithm for one-stationary bistatic spotlight circular SAR image formation," *IEEE Journal of Selected Topics in Applied Earth Observations and Remote Sensing*, vol. 10, no. 4, pp. 1494–1510, Apr. 2017.

[58] H.Maitre, *Processing of Synthetic Aperture Radar (SAR) Images*, 1st ed. New Jersey,USA: Wiley-ISTE, 2008.

[59] S. M.Kay, *Fundamentals of Statistical Signal Processing. Detection Theory*, 1st ed. New Jersey, USA: Prentice-Hall, 1989.

[60] J. Neyman and E. S. Pearson, "On the problem of the most efficient tests of statistical hypotheses," *Philosophical Transactions of the Royal Society of London. Series A, Containing Papers of a Mathematical or Physical Character*, vol. 231, pp. 289–337, Feb. 1933.

[61] L. M. H. Ulander, M. Lundberg, W. Pierson, and A. Gustavsson, "Change detection for low-frequency SAR ground surveillance," *IEE Proceedings - Radar, Sonar and Navigation*, vol. 152, no. 6, pp. 413–420, Dec. 2005.

[62] L. M. H. Ulander, H. Hellsten, and G. Stenstrom, "Synthetic-aperture radar processing using fast factorized back-projection," *IEEE Transactions on Aerospace and Electronic Systems*, vol. 39, no. 3, pp. 760–776, Jul. 2003.

[63] L. M. H. Ulander, "VHF-band SAR for detection of concealed ground targets," in *RTO SCI Symposium on Sensors and Sensor Denial by Camouflage, Concealment and Deception*, Brussels, Belgium, Apr. 2004, pp. 1–11.

[64] G. Smith and L. M. H. Ulander, "A model relating VHF-band backscatter to stem volume of coniferous boreal forest," *IEEE Transactions on Geoscience and Remote Sensing*, vol. 38, no. 2, pp. 728–740, Mar. 2000.

[65] R. Machado, V. T. Vu, M. I. Pettersson, P. Dammert, and H. Hellsten, "The stability of UWB low-frequency SAR images," *IEEE Geoscience and Remote Sensing Letters*, vol. 13, no. 8, pp. 1114–1118, Aug. 2016.

[66] B. T. Binder, M. F. Toups, S. Ayasli, and E. M. Adams, "SAR foliage penetration phenomenology of tropical rain forest and northern us forest," in *1995 IEEE International Radar Conference*, Alexandria, USA, May 1995, pp. 158–163.

[67] J. R. Rasmusson, M. Blom, B. Flood, P.-O. Frolind, A. Gustavsson, T. Jonsson, B. Larsson, G. Stenstrom, and L. M. H. Ulander, "Bistatic VHF and UHF SAR for urban environments," in *SPIE Defense and Security Symposium: Radar Sensor Technology XI*, vol. 6547, Orlando, USA, 2007, pp. 40–51.

[68] L. M. H. Ulander, M. Blom, B. Flood, P. Follo, P.-O. Frolind, A. Gustavsson, T. Jonsson, B. Larsson, D. Murdin, M. Pettersson, U. Raaf, and G. Stenstrom, "Development of the ultra-wideband LORA SAR operating in the VHF/UHF-band," in *2003 IEEE International Geoscience and Remote Sensing Symposium (IGARSS)*, vol. 7, Toulouse, France, Jul. 2003, pp. 4268–4270.

[69] *TRACER Airborne Counter-concealment Radar - MSAZ13-118*, Lockheed Martin's, USA.

[70] J. E. Simms, "Applications of synthetic aperture radar (SAR) to unexploded ordnance (UXO) delineation," U.S. Army Engineer Research and Development Center, Vicksburg, USA, Tech. Rep., Aug. 2003.

[71] "The sensor data management system - SDMS," U.S. Air Force. [Online]. Available: https://www.sdms.afrl.af.mil/

[72] A. Gustavsson, P.-O. Frolind, H. Hellsten, T. Jonsson, B. Larsson, and G. Stenstrom, "The airborne VHF SAR system CARABAS," in *1993 IEEE International Geoscience and Remote Sensing Symposium (IGARSS)*, vol. 2, Tokyo, Japan, Aug. 1993, pp. 558–562.

[73] H. Hellsten, "CARABAS-an UWB low frequency SAR," in *1992 IEEE MTT-S Microwave Symposium Digest*, vol. 3, Albuquerque, USA, Jun. 1992, pp. 1495–1498.

[74] *CARABAS Foliage penetration radar - EN/LZTM1100003 R4*, SAAB AB, Gothenburg, Sweden.

[75] L. M. H. Ulander, M. Blom, B. Flood, P. Follo, P.-O. Frolind, A. Gustavsson, T. Jonsson, B. Larsson, M. Lundberg, W. Pierson, and G. Stenstrom, "Flight campaign vidsel 2002 CARABAS-II change detection analysis," Swedish Defence Research Agency - FOI, Linköping, Sweden, Tech. Rep., Nov. 2003.

[76] M. Lundberg, L. M. H. Ulander, W. E. Pierson, and A. Gustavsson, "A challenge problem for detection of targets in foliage," in *SPIE Defense and Security Symposium: Algorithms for Synthetic Aperture Radar Imagery XIII*, vol. 6237, Orlando, USA, May 2006.

[77] L. M. H. Ulander, P.-O.Frolind, and T. Martin, "Processing and calibration of ultra-wideband SAR data from CARABAS-II," in *SAR workshop: CEOS Committee on Earth Observation Satellites*, vol. 450, Toulouse, France, Oct. 1999, p. 273.

[78] F. Walter, J. E. S. Fransson, and P.-O. Frolind, "Fully automatic geo-coding of CARABAS-II VHF SAR images," in *1999 IEEE International Geoscience and Remote Sensing Symposium (IGARSS)*, vol. 1, Hamburg, Germany, Jun. 1999, pp. 569–573.

[79] N. VandenBerg, D. R. Sheen, S. Shackman, and D. L. Wiseman, "P-3 ultrawideband SAR: system applications to foliage penetration," in *SPIE Aerospace/Defense Sensing and Controls: Algorithms for Synthetic Aperture Radar Imagery III*, vol. 2757, Orlando, USA, Jun. 1996, pp. 130–135.

[80] M. A. Sletten and J. Brozena, "FOPEN target detection via joint space/angle variation," *IEEE Geoscience and Remote Sensing Letters*, vol. 13, no. 6, pp. 762–766, Jun. 2016.

[81] L. M. Ulander, P.-O. Froelind, A. Gustavsson, H. Hellsten, and B. Larsson, "Detection of concealed ground targets in carabas sar images using change detection," in *SPIE AeroSense'99: Algorithms for Synthetic Aperture Radar Imagery VI*, vol. 3721, Orlando, USA, Aug. 1999, pp. 243–252.

[82] H. Hellsten and R. Machado, "Bayesian change analysis for finding vehicle size targets in vhf foliage penetration SAR data," in *2015 IEEE Radar Conference (RadarConf 2015)*, Johannesburg, South Africa, Oct 2015, pp. 510–515.

[83] J. W. Wood, R. G. White, and C. J. Oliver, "Distortion free SAR imagery and change detection," in *1988 IEEE National Radar Conference*, Ann Arbor, USA, Apr. 1988, pp. 95–99.

[84] F. Baselice, G. Ferraioli, and V. Pascazio, "Markovian change detection of urban areas using very high resolution complex SAR images," *IEEE Geoscience and Remote Sensing Letters*, vol. 11, no. 5, pp. 995–999, May 2014.

[85] Y. Wang, X. X. Zhu, and R. Bamler, "An efficient tomographic inversion approach for urban mapping using meter resolution SAR image stacks," *IEEE Geoscience and Remote Sensing Letters*, vol. 11, no. 7, pp. 1250–1254, Jul. 2014.

[86] S. N. Anfinsen, A. P. Doulgeris, and T. Eltoft, "Goodness-of-fit tests for multilook polarimetric radar data based on the mellin transform," *IEEE Transactions on Geoscience and Remote Sensing*, vol. 49, no. 7, pp. 2764–2781, Jul. 2011.

[87] M. D. DeVore and J. A. O'Sullivan, "Statistical assessment of model fit for synthetic aperture radar data," in *SPIE Aerospace/Defense Sensing, Simulation, and Controls: Algorithms for Synthetic Aperture Radar Imagery VIII*, vol. 4382, Orlando, USA, Aug. 2001.

[88] D. Teguig, V. L. Nir, and B. Scheers, "Spectrum sensing method based on likelihood ratio goodness-of-fit test," *Electronics Letters*, vol. 51, no. 3, pp. 253–255, Feb. 2015.

[89] H. Wang, E. H. Yang, Z. Zhao, and W. Zhang, "Spectrum sensing in cognitive radio using goodness of fit testing," *IEEE Transactions on Wireless Communications*, vol. 8, no. 11, pp. 5427–5430, Nov. 2009.

[90] N. M. Razali and Y. B. Wah, "Power comparisons of shapiro-wilk, kolmogorov-smirnov, lilliefors and anderson-darling tests," *Journal of statistical modeling and analytics*, vol. 2, no. 1, pp. 21–33, Jan. 2011.

[91] Y. Wang, Y. Deng, W. Fei, R. Wang, H. Song, J. Wang, and N. Li, "Modified statistically homogeneous pixels' selection with multitemporal SAR images," *IEEE Geoscience and Remote Sensing Letters*, vol. 13, no. 12, pp. 1930–1934, Dec. 2016.

[92] C. Brekke and S. N. Anfinsen, "Ship detection in ice-infested waters based on dual-polarization SAR imagery," *IEEE Geoscience and Remote Sensing Letters*, vol. 8, no. 3, pp. 391–395, May 2011.

[93] T. W. Anderson and D. A. Darling, "Asymptotic theory of certain "goodness of fit" criteria based on stochastic processes," *Annals of Mathematical Statistics*, vol. 23, no. 02, pp. 193–212, Jun. 1952.

[94] R. B. D'Agostino and M. A. Stephens, *Goodness-of-fit techniques*, 1st ed. New Yor, USA: CRC Press, 1986.

[95] G. Marsaglia and J. C. W. Marsaglia, "Evaluating the anderson-darling distribution," *Journal of Statistical Software*, vol. 9, no. 2, pp. 1–5, Feb. 2004.

[96] M. Migliaccio, G. Ferrara, A. Gambardella, F. Nunziata, and A. Sorrentino, "A physically consistent speckle model for marine SLC SAR Images," *IEEE Journal of Oceanic Engineering*, vol. 32, no. 4, pp. 839–847, Oct. 2007.

[97] J. A. Jackson and R. L. Moses, "Clutter model for VHF SAR imagery," in *SPIE Defense and Security Symposium: Algorithms for Synthetic Aperture Radar Imagery XI*, vol. 5427, Orlando, USA, Sep. 2004.

[98] R. A. Fisher, *Statistical methods for research workers*, 5th ed. Edinburgh, ISA: Oliver and Boyd Ltd., 1934.

[99] B. Yoav and H. Yosef, "Controlling the false discovery rate: A practical and powerful approach to multiple testing," *Journal of the Royal Statistical Society. Series B (Methodological)*, vol. 57, no. 1, pp. 289–300, Aug. 1995.

[100] V. A. Krylov, G. Moser, S. B. Serpico, and J. Zerubia, "False discovery rate approach to unsupervised image change detection," *IEEE Transactions on Image Processing*, vol. 25, no. 10, pp. 4704–4718, Oct. 2016.

[101] S. Nakagawa, "A farewell to bonferroni: the problems of low statistical power and publication bias," *Behavioral ecology*, vol. 15, no. 6, pp. 1044–1045, Nov. 2004.

[102] R. M. Haralick and L. G. Shapiro, "Glossary of computer vision terms," *Pattern recognition*, vol. 24, no. 1, pp. 69–93, Mar. 1991.

[103] G. Srinivasa, M. C. Fickus, Y. Guo, A. D. Linstedt, and J. Kovacevic, "Active mask segmentation of fluorescence microscope images," *IEEE Transactions on Image Processing*, vol. 18, no. 8, pp. 1817–1829, Aug. 2009.

[104] H. Dadkhahi and M. F. Duarte, "Masking strategies for image manifolds," *IEEE Transactions on Image Processing*, vol. 25, no. 9, pp. 4314–4328, Sep. 2016.

[105] T. D. Nguyen, A. Shinya, T. Harada, and R. Thawonmas, "Segmentation mask refinement using image transformations," *IEEE Access*, vol. 5, pp. 26 409–26 418, Nov. 2017.

[106] G. P. H. Styan, "Hadamard products and multivariate statistical analysis," *Linear algebra and its applications*, vol. 6, pp. 217–240, May 1973.

[107] D. I. Alves, B. G. Palm, M. I. Pettersson, V. T. Vu, R. Machado, B. F. Uchôa-Filho, P. Dammert, and H. Hellsten, "A statistical analysis for wavelength-resolution SAR image stacks," *IEEE Geoscience and Remote Sensing Letters*, vol. 17, no. 2, pp. 227–231, Feb. 2020.

[108] F. Wang, Y. Wu, Q. Zhang, P. Zhang, M. Li, and Y. Lu, "Unsupervised change detection on SAR images using triplet markov field model," *IEEE Geoscience and Remote Sensing Letters*, vol. 10, no. 4, pp. 697–701, Jul. 2013.

[109] M. N. Sumaiya and R. S. S. Kumari, "Unsupervised change detection of flood affected areas in SAR images using rayleigh-based bayesian thresholding," *IET Radar, Sonar Navigation*, vol. 12, no. 5, pp. 515–522, Apr. 2018.

[110] A. Papoulis, *Probability, random variables, and stochastic processes*, 4th ed. Boston, USA: McGraw-Hill, 2002.

[111] M. K. Simon and M.-S. Alouini, "A simple single integral representation of the bivariate Rayleigh distribution," *IEEE Communications Letters*, vol. 2, no. 5, pp. 128–130, May 1998.

[112] F. Hong, R. Wang, Z. Zhang, P. Lu, and T. Balz, "Integrated time and phase synchronization strategy for a multichannel spaceborne-stationary bistatic SAR system," *Remote Sensing*, vol. 8, no. 8, 2016.

[113] I. Chalabi and A. Mezache, "Estimating the K-distribution parameters based on fractional negative moments," in *12th IEEE International Multi-Conference on Systems, Signals Devices ((SSD15)*, Mahdia, Tunisia, 2015, pp. 1–5.

[114] V. S. Vaidyanathan and R. V. Lakshmi, "Parameter estimation in multivariate gamma distribution," *Statistics, Optimization & Information Computing*, vol. 3, no. 2, pp. 147–159, 2015.